Università degli Studi di Cagliari

DOTTORATO DI RICERCA IN DIFESA E CONSERVAZIONE DEL SUOLO, VULNERABILITÀ AMBIENTALE E PROTEZIONE IDROGEOLOGICA

Ciclo XXIII

GIS AND MATHEMATICAL GROUNDWATER SIMULATION AS TOOLS FOR HYDROGEOLOGICAL CONCEPTUAL MODELING AND VULNERABILITY ASSESSMENT OF PORTO TORRES INDUSTRIAL ZONE AQUIFER (NW SARDINIA)

SSd GEO/05

Presentata da: Dott.ssa Monica Casu

Coordinatore Dottorato: Prof. Felice Di Gregorio

Tutor: Prof. Giulio Barbieri

Esame finale anno accademico 2010 – 2011

Acknowledgements

I would like to thank all people that, in different ways, have helped me during this PhD, providing me the opportunity to deepen and expand my understanding of the subject treated.

First of all, I would like to thank my tutor Prof. Giulio Barbieri, who patiently supported my work throughout the years in the effort to overcome difficulties, in defining and remarking crucial direction and, at the same time, giving me great freedom to pursue independent work. I also want to thank him for suggesting and organizing my stage at Barcelona, that was a great chance for me to acquire important knowledge on dual porosity modeling.

My sincere thanks to those that supported me during my stage at Barcelona. Thanks to Professor Lurdes Martínez Landa for her helpfulness, for suggestions in modeling approaches and for reporting about significant experiences done by her research group in fractured aquifer mathematical modeling. I'm also very grateful to Silvia Aranda for her precious support in administrative matter and especially for her kindness. Thanks also to Khadijetou El Moustapha for her delicious friendship and for the pleasant time passed together.

I would like to acknowledge Professor Giacomo Oggiano for providing me the indispensable hydrogeological information necessary to implement the conceptual model and Eng. Nicoletta Sannio of Sardinian Regional Administration to provide me access to environmental data of the study area.

Many thanks also to those geologists that have always been willing to collaborate with me, sharing ideas and knowledge, despite of the commonplace antagonism with engineers. Thanks to Marco Pusceddu and Andrea Serreli for their continuous support and to Piercarlo Ciabatti and Giorgio Madau to be always available to provide useful and productive suggestions.

I'm also grateful to Rajandrea Sethi for our last encouraging and constructive discussion.

Finally, I would like to thank my family and all my friends that have always seconded my aims.

Abstract

The object of this study has been to develop an integrated technique of GIS and groundwater modeling program to improve hydrogeological setting understanding of Porto Torres industrial zone and to perform intrinsic vulnerability evaluation of the aquifer to contamination. To reach this purpose, GIS interfaced to the hydrogeological software GMS has been used to efficiently manage a wide range of geographical information and data. Hydrogeological understanding has been facilitated by a tree-dimensional schematization of aquifer domain and by numerical modeling, that has been finalized to provide proof to support or dismiss assumptions made on conceptual model implementation. Finally, based on GIS elaborations and groundwater simulation, SINTACS method has been applied to evaluate vulnerability degree of the Mesozoic aquifer.

Table of contents

1 Introduction

The industrial zone of Porto Torres is included in the National Priority List Sites, which encompasses those polluted sites that, because of extension and type of contamination, can be considered of national interest and their cleanup procedures are verified and validated by the Italian Ministry of the Environment.

The Porto Torres industrial production started in sixties years of the last century, when the first chemical and petrochemical plants were built. Later, in eighties years, the Fiumesanto electric power plant raised up on the West of the petrochemical area, beyond the Fiume Santo stream, operating on fuel oil. Due to the processes, feedstock and waste management, illegal waste storage and dumping related to these activities (that were not subject to appropriate rules on environmental protection in the past) soils and groundwater of the industrial zone have been contaminated and thus they are currently subject to remediation activities.

According to the Italian Legislative Decree n. 152/06, cleanup activities are in charge of the responsible for contamination. However, if the responsible party cannot be found or it doesn't act, then the property owner must carry out the remediation procedure. Since the costs required for polluted site remediation are usually very high, legal actions occur frequently in those cases where pollution responsibility is not well defined.

The present study was first motivated to understand the hydrogeology of the Fiumesanto power station, where chlorinated compounds were found in groundwater. Since chlorinate compounds are not included in the feedstock processed at the power station, the owner company decided to investigate whether contamination occurred in the neighboring industrial plants could be transported to the site. Consequently, the company hired consultants to perform geological, geochemical and hydrogeological surveys sought to understand contamination fate and transport. The present work is part of this study as it has been aimed to firstly investigate and determine the hydrogeological setting of the site and of the surrounding area, in order to provide the necessary support to improve a contamination conceptual model needed for the intended purposes.

The hydrogeological setting of the power station area is very complex due to aquifer system features, consisting in heterogeneous Miocene-Quaternary sediments characterized by a variable primary permeability that overlies the even more complex Mesozoic carbonate aquifer permeable due to fracturing and karst.

The proposed task, finalized to better understand the complex hydrogeological system in a site where pollution problems, environmental issues and employment pressure have gained increasing attention over the last years, gave the opportunity to perform this PhD thesis applying GIS technologies and mathematical modeling to reach the intended objectives.

The overall purposes of the present work are:

- to identify the hydrogeological conceptual model;
- to assess aquifer vulnerability.

To reach these main goals, the specific objectives of this research, regarding method development, are the following:

- development of GIS and associated database, aimed to store all environmental data collected, to easily handle attribute data in conjunction to spatial information and to compute different parameters distribution map;
- development of a GIS-based modeling approach as to simplify data management and computations needed for mathematical modeling and vulnerability assessment;
- hydrogeological conceptual model delineation of the study area;
- mathematical modeling implementation, aimed to improve and verify hydrogeological assumptions made;
- aquifer vulnerability assessment, based on an integrated approach that takes into account of mathematical modeling results.

Those specific objectives were pursued after a research that analysed state of the art on the methodologies applied to study the particular hydrogeological settings of the study area.

Figure 1 and Figure 2 show orthophotos of industrial area in 1954 and in 2008.

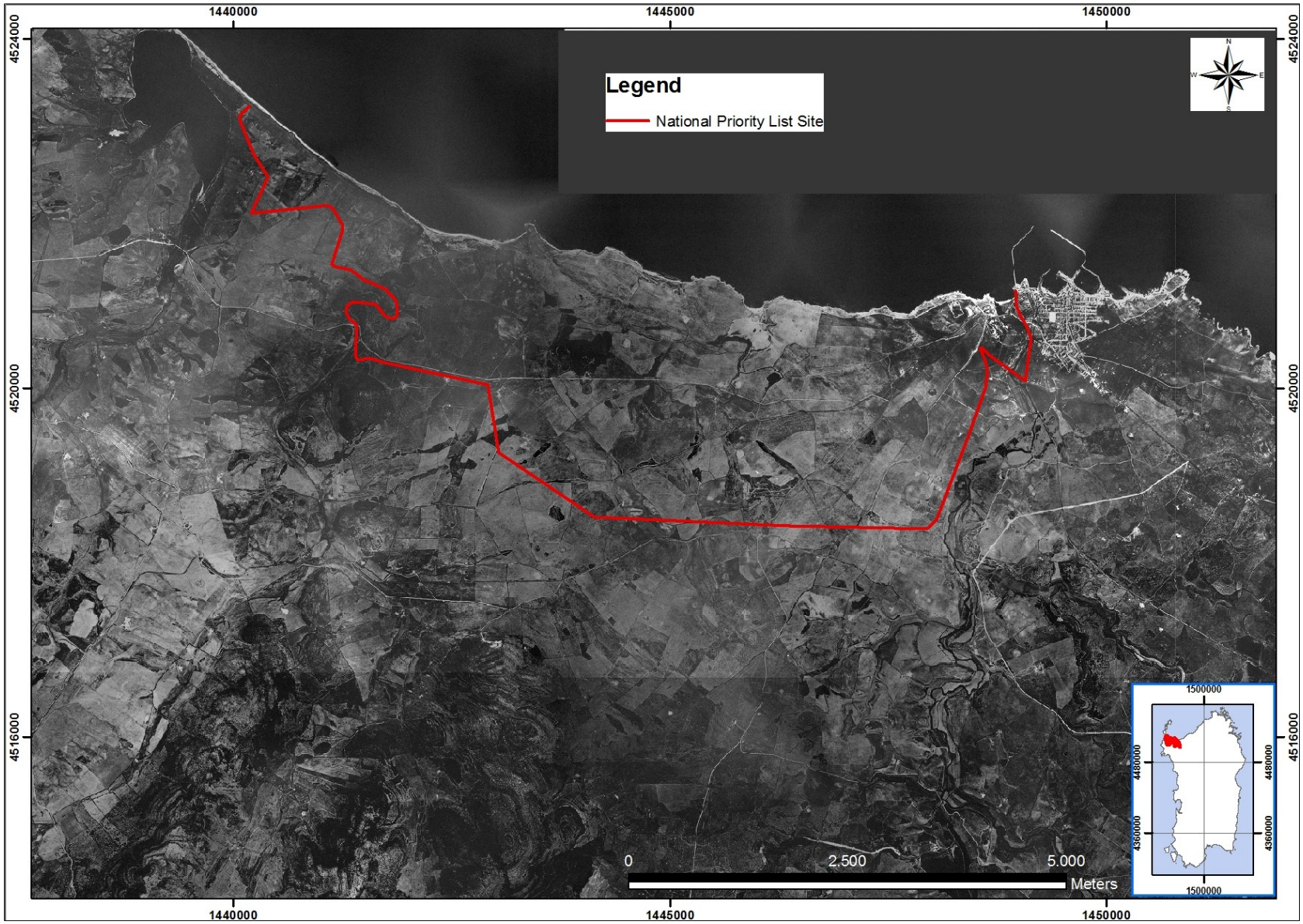

Figure 1. Porto Torres in 1954, before industrial activity started (source: WEBGIS of Sardinian Regional Administration).

Figure 2. Porto Torres industrial zone in 2008 (source: WEBGIS of Sardinian Regional Administration).

2 Methodology outline

Data management and parameters distribution calculation were handled using GIS software (ESRI ArcGis 9.2). Afterwards, the groundwater modeling software GMS 6.0 (Environmental Modeling Systems, 2006) allowed interfacing to GIS and to perform mathematical modeling using the code MODFLOW-2000 (McDonald and Harbaugh, 1988). The steps followed can be briefly summarized as:

- environmental data collection;
- GIS database implementation (data acquirement, management and elaboration);
- GIS database conversion to GMS input data;
- aquifer modeling schematization using GMS;
- groundwater flow mathematical modeling using MODFLOW GMS;
- vulnerability assessment using GIS and aquifer modeling results.

Data stored into the geodatabase include environmental and hydrogeological information relevant to aquifer conceptual model characterization, mathematical model implementation and vulnerability assessment.

Firstly, previous studies related to the area and dealing with geology, hydrogeology, hydrology, meteorology, soils and other environmental information were analyzed. In particular, the main available works are:

- the RIADE project (Ghiglieri et al., 2007), that presents a multidisciplinary approach to analyze water resource in Southern Nurra;
- the environmental impact assessment study of the Fiumesanto power station, performed in 1985 by ENEL company;
- the Porto Torres industrial zone environmental survey, carried out by the Sardinian Regional Administration in 2007 to characterize contamination in the industrial zone and to develop a groundwater pollution monitoring network;
- the “POS 25” project (Pietracaprina et al., 1985), finalized to perform an hydrogeological study of Sardinia.
- the environmental characterization plan of Fiumesanto power station that, according to Legislative Decree n. 152/06, was performed to examine the site pollution status.

Moreover, all digital data available were recovered from external source:

- aerial photography;
- satellite images;
- topographical datasets, including elevation contours;
- numerical cartography;
- digitized maps.

Nowadays, Geographic Information Systems (GIS) offer new abilities and tools for the collection, storage, management, analysis and display of spatially distributed environmental data. In particular, data analysis may includes database operations, time and spatial analysis functions and image elaboration, while display tools permit map realization and efficiently data presentation.

The objects in a GIS are defined by their location and by multiple attributes related to different objects characteristics. Therefore, due to the spatial attribute of the object, GIS can handle geographically-referenced data. Furthermore, computer files containing GIS information can be related to each other in a "spatially-aware" database.

GIS capabilities let the user to implement geographic data more efficiently for hydrogeological analysis, management and modeling. Moreover, GIS interfaced to hydrogeological models, enhances this usefulness by permitting to powerfully manage a wide range of environmental information and data.

GIS tools were useful to the purposes of this study as were applied to:

- describe aquifer basin characteristics;
- derive input distributed parameters to model processes and vulnerability assessment;
- display and represent results.

GMS software was applied to reproduce the complex hydrogeological system of the aquifer basin within a GIS framework, to estimate groundwater head for each cell of the model, to compute water balance and to represent the spatial distribution of hydrogeological variables at the catchment scale. In fact, GMS includes a GIS interface that is useful to integrate all environmental data so that hydrogeological basin characteristics, needed to understand the conceptual model, were easily stored and handled in a user-friendly interface.

3 Study area description

3.1 Site location

The study area was first analyzed at the catchment scale, before defining the groundwater divides needed to delimitate the aquifer domain to be modeled.

The Porto Torres industrial zone is located within the Northern Nurra district, on the North-West coast of Sardinia, in the Sassari Province. It is placed along the coast, on the west side of the homonymous village, at a distance of 20 km from Sassari city (on the East) and 30 km from Alghero (on the South).

The Northern Nurra lays within the municipalities of Sassari, Porto Torres and Stintino. It is bounded to the North by the Asinara Gulf, to the East by the Turritano district reliefs, to the South by the Alghero plain (Southern Nurra) and to the West by the Sardinian Sea.

The area is mainly flat but it also comprises some North-South striking hills that lay on the South and South-West part of the industrial zone (see Figure 3), where the maximum altitude occurs at Monte Alvaro peak (342 m a.m.s.l.).

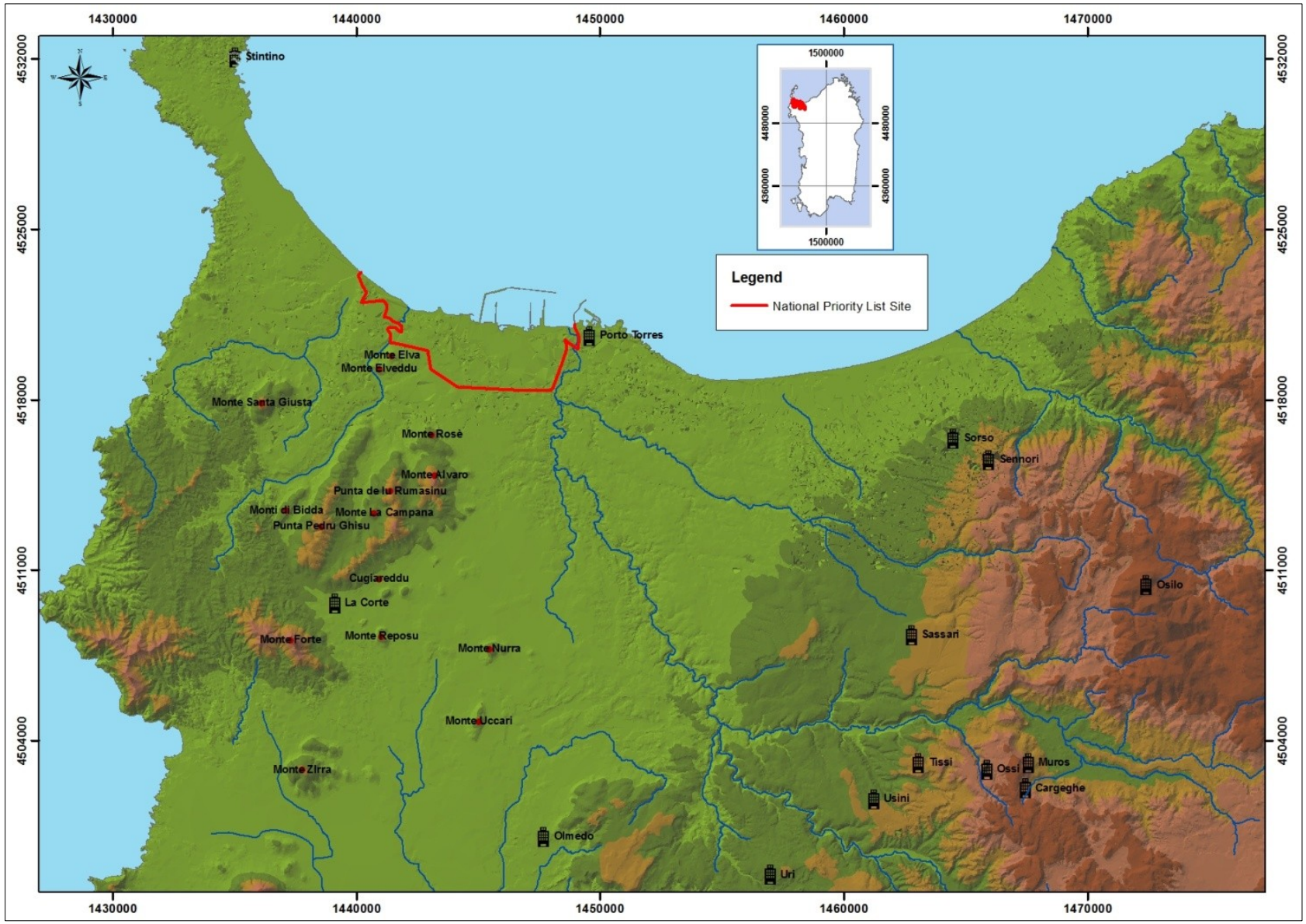

Figure 3. Study area location.

3.2 Climate

Sardinia has a typical Mediterranean climate, with hot dry summers and mild wet winters. Based on Köppen climate classification, Nurra climate can be defined as warm-temperate (see Figure 4, average annual temperatures between 14.5 and 16.9 °C; coldest month average temperatures between 6 and 9.9 °C; at least four months averaging above 20 °C; annual temperatures range between 15 and 17 °C).

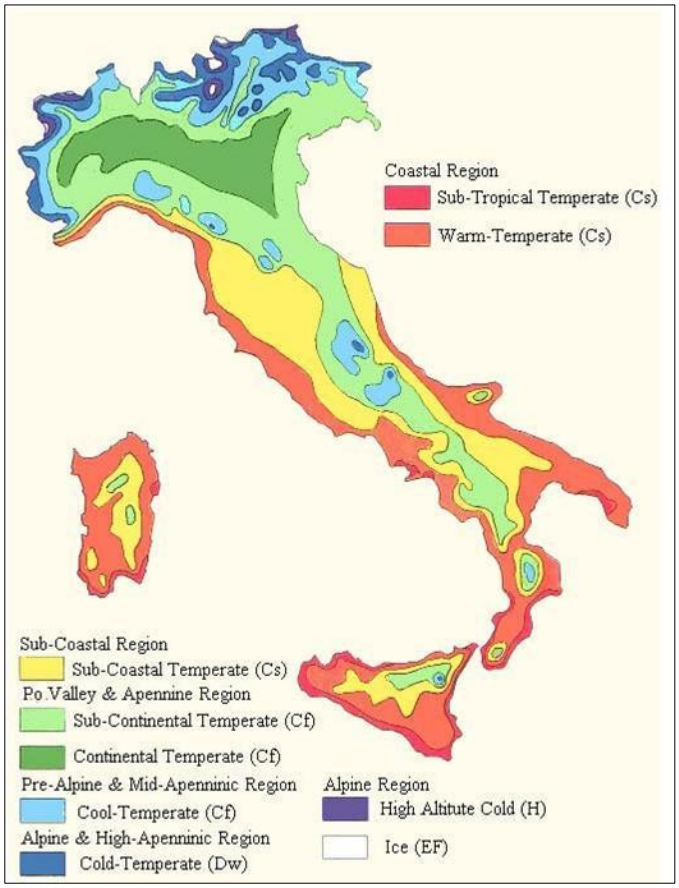

Figure 4. Italian climatic map (Pinna, 1978).

The following information about temperatures and precipitations of Nurra region derives from the study on superficial water resources of the Sardinia Island (SISS, 1998) made by the Regional Administration of Sardinia and by the Autonomous Management Body of Flumendosa Basin. Data coming from different meteorological stations located in the study area are analyzed in the following paragraphs.

3.2.1 Meteorological stations

Meteorological gauge stations located in the nearness of the industrial zone were identified and georeferenced and their recorded measurements were acquired and loaded into the Geodatabase as to allow meteorological data management for hydrological analysis and calculations required to fulfill the purposes of the present work.

Station name	X coordinate	Y coordinate	Ground elevation [m a.m.s.l.]	Measurement instruments
Alghero	1441800	4490000	7	temperature and rainfall
Olmedo	1447400	4500210	52	rainfll
Asinara	1434170	4538570	6	rainfall
Stintino	1435050	4532110	9	rainfall
Sassari	1463250	4507600	224	temperature and rainfall
Macciadosa	1449610	4509010	74	rainfall
Porto Torres	1449670	4520660	2	rainfall

Table 1. Meteorological stations data and coordinates (Gauss-Boaga system).

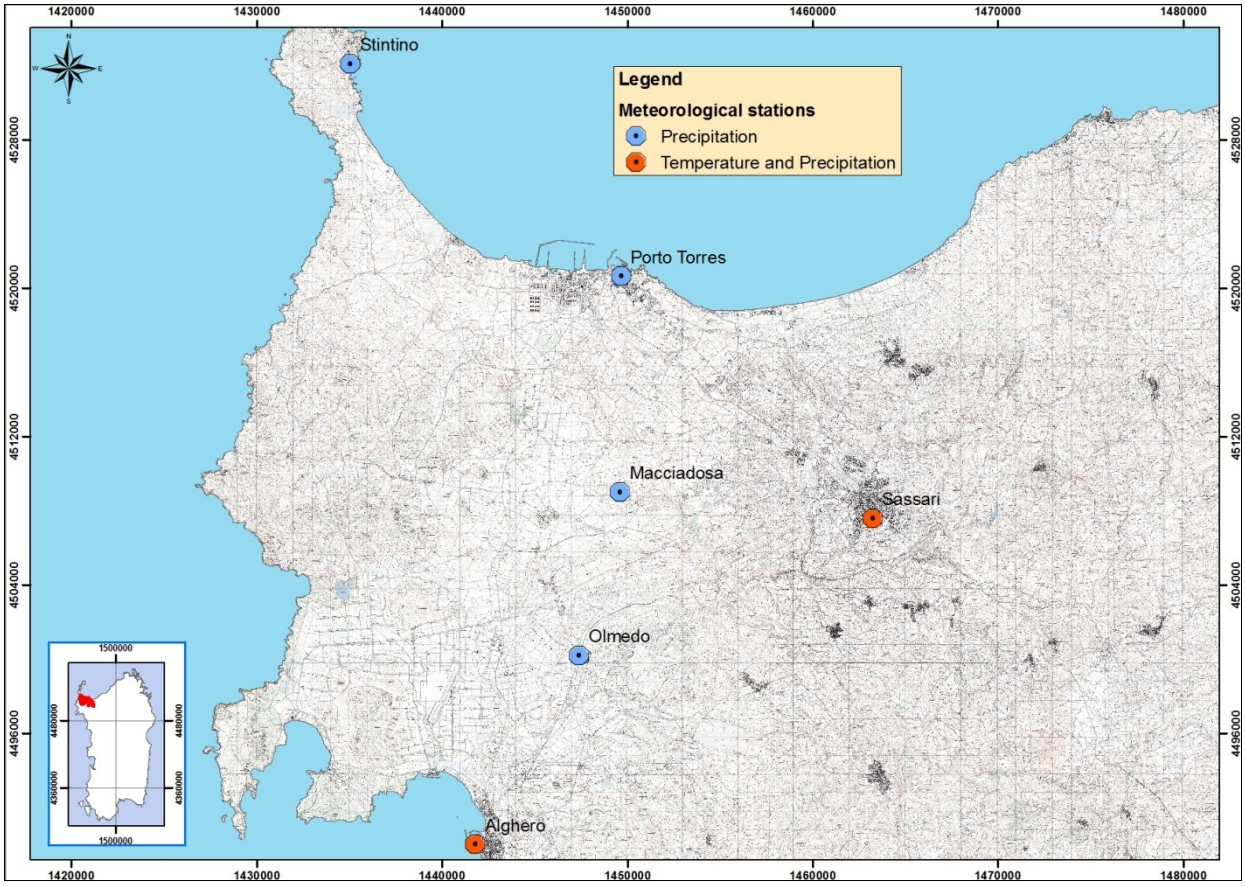

Figure 5. Meteorological stations location.

The climate dataset available by SISS Study contains monthly temperature and precipitation measurements collected from the meteorological stations listed in Table 1 over the period 1922-1992, where the continuous series was obtained after homogenization procedure and multivariate linear regression analysis as to estimate lacking values coming from missing station observations or instrumental errors (RAS and EAF, 1998).

3.2.2 Temperature

Temperature in Sardinia is characterized by two transition periods, before winter (September-November) and before summer (March- April), and its variability depends

mainly on orography and altitude. Moreover, winter temperatures are principally influenced by the distance from the sea, therefore coastal areas are characterized by the stabilizing effect of the sea (whereas the inner areas show a continental behavior), while summer temperatures variability in the island is determined by the stabilizing effect of anticyclonic cells and a North-South gradient can be seen (SAR, 1997).

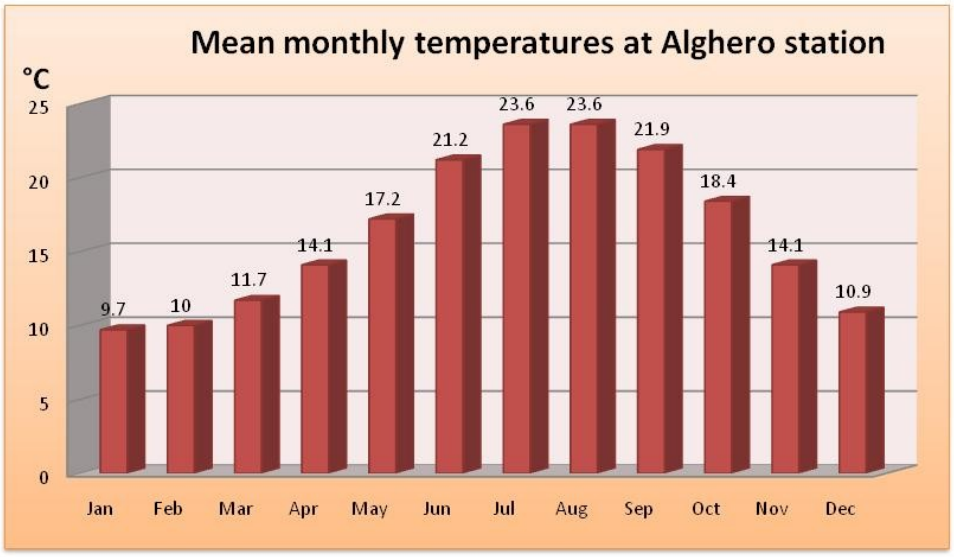

Figure 6. Mean monthly temperatures at Alghero station (SISS, 1998).

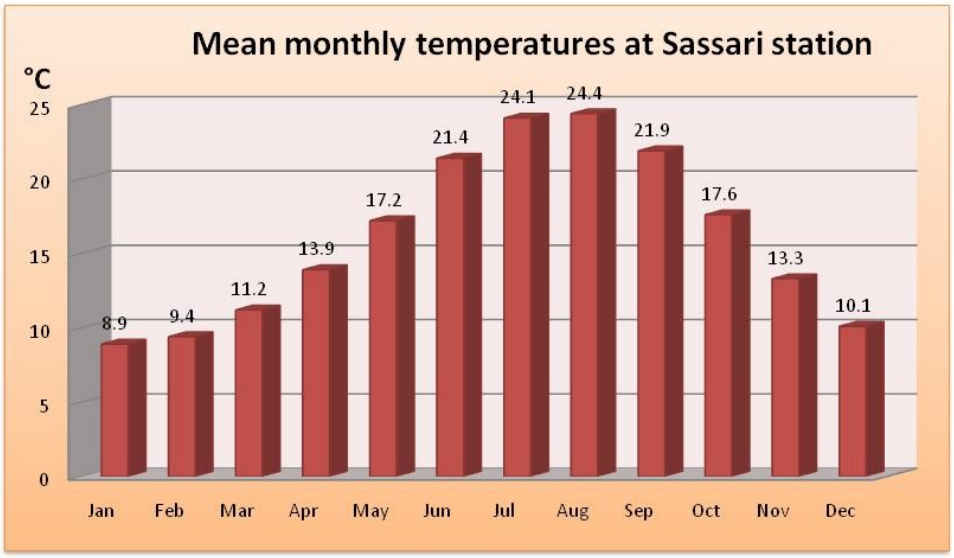

Figure 7. Mean monthly temperatures at Sassari station (SISS, 1998).

Temperature measurements are available only for two of the six meteorological stations located in the area: Sassari and Alghero (see Appendix A). Based on data measurements over the analyzed period of time, mean monthly and annual values were computed and reported in Figure 6 and in Figure 7. Mean annual temperature over the entire period of time is 16.2 °C at Sassari station and 16.4 °C at Alghero station. Inter-annual variability of temperatures is similar for the two stations, maximum values occur in July and August and minimum values in January and February (see Figure 8).

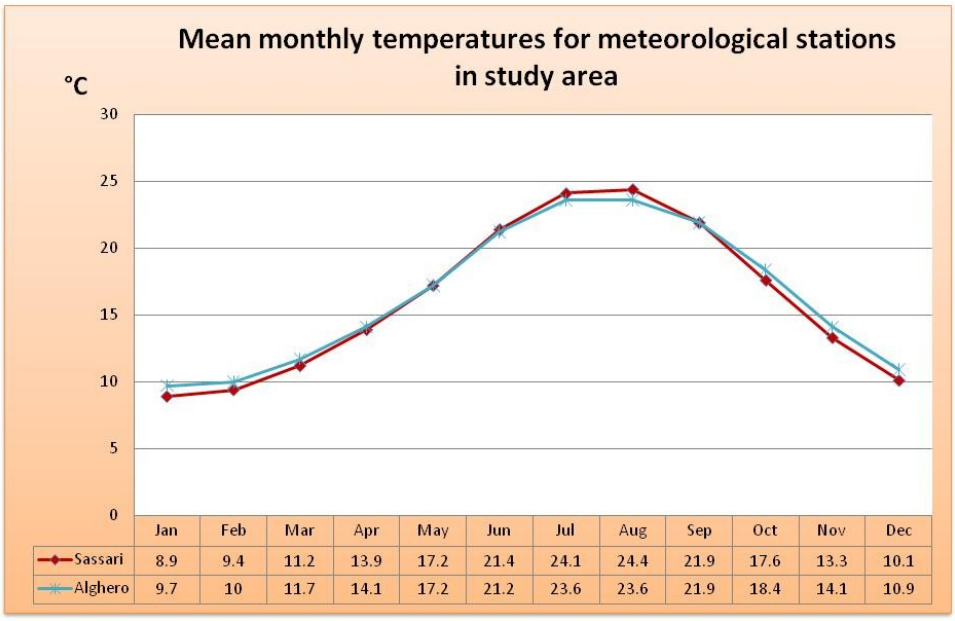

Figure 8. Mean monthly temperatures comparison for meteorological stations in study area.

3.2.3 Rainfall

Nurra is one of the three Sardinian dry regions (together with Campidano and Central-North Sardinia) since mean annual rainfall is less than 700 mm, whereas the maximum value of the mean annual rainfall for the island is about 1200-1300 mm, occurring in mountain areas (SAR, 1997).

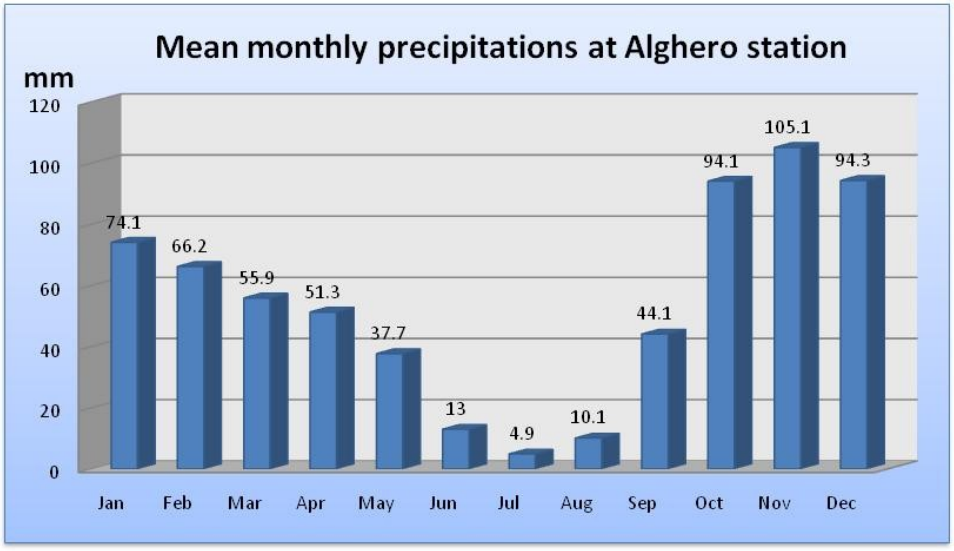

Figure 9. Mean monthly precipitations at Alghero station (SISS, 1998).

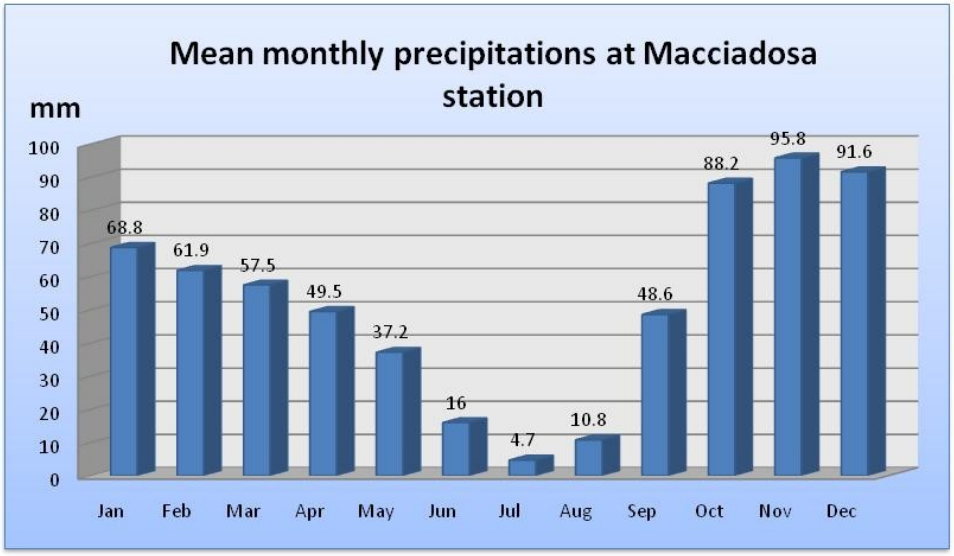

Figure 10. Mean monthly precipitations at Bancali (ex Macciadosa) station (SISS, 1998).

Precipitation values analyzed in this paragraph were observed in the period 1922-1992 in six meteorological stations located in the surroundings of the study area: Alghero, Bancali (ex Macciadosa), Olmedo, Porto Torres, Sassari e Stintino (see Figure 5).

The mean monthly rainfall values for the different meteorological stations are represented in Figure 9, Figure 10, Figure 11, Figure 12, Figure 13 and Figure 14, showing the presence of two different seasons during a year: the wet season, that occurs between October and April, and the dry season between May and September. The transition from one season to the other one is more marked between September and October, when rainfall almost doubles, than between April and May.

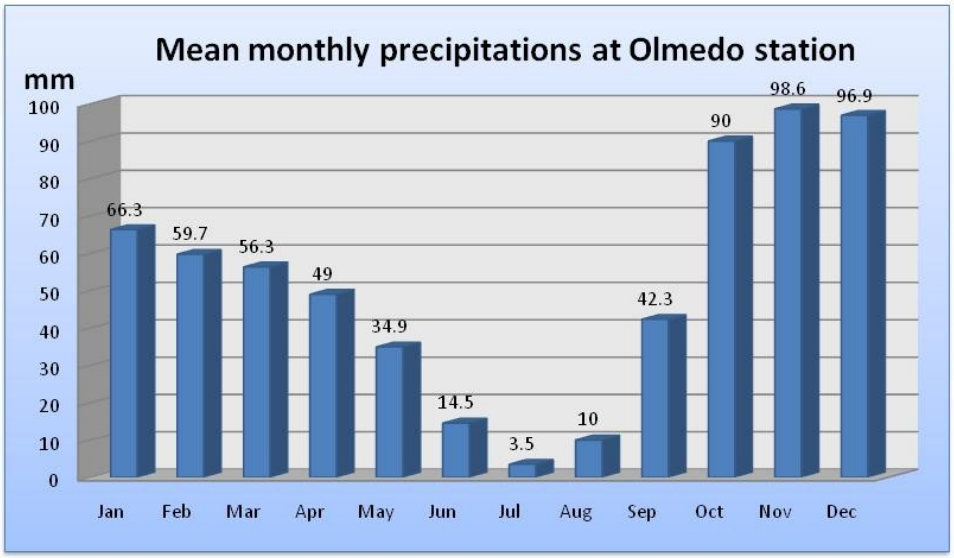

Figure 11. Mean monthly precipitations at Olmedo station (SISS, 1998).

Rainfall inter-annual variability is similar for the six meteorological stations analyzed (see Figure 15), however higher differences in mean monthly values can be observed during

the wet season than during the dry season: Alghero station recorded the highest and Stintino station the lowest precipitation values.

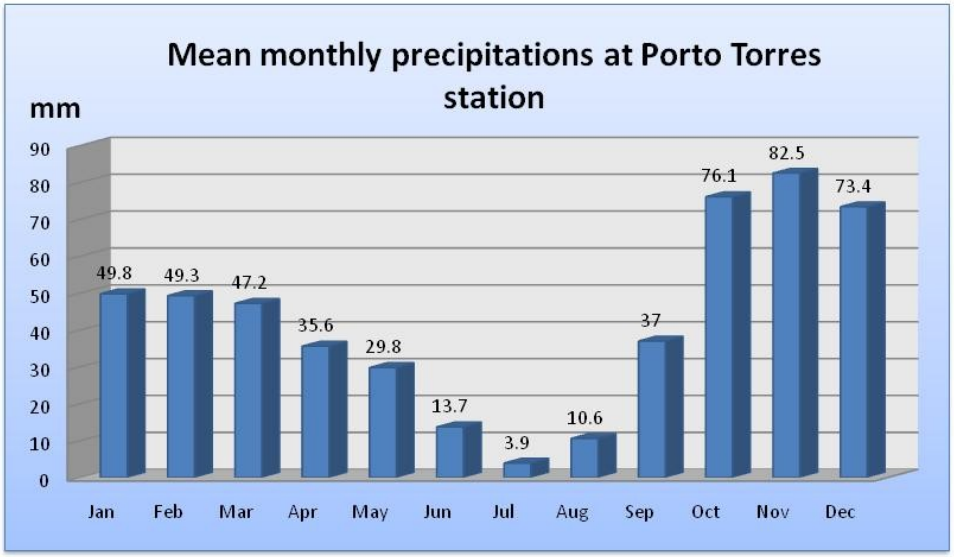

Figure 12. Mean monthly precipitations at Porto Torres station (SISS, 1998).

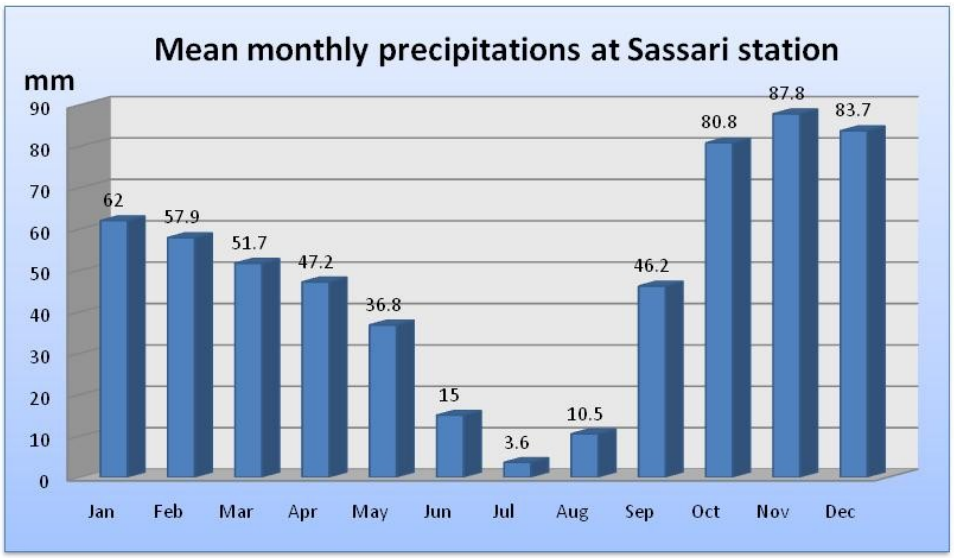

Figure 13. Mean monthly precipitations at Sassari station (SISS, 1998).

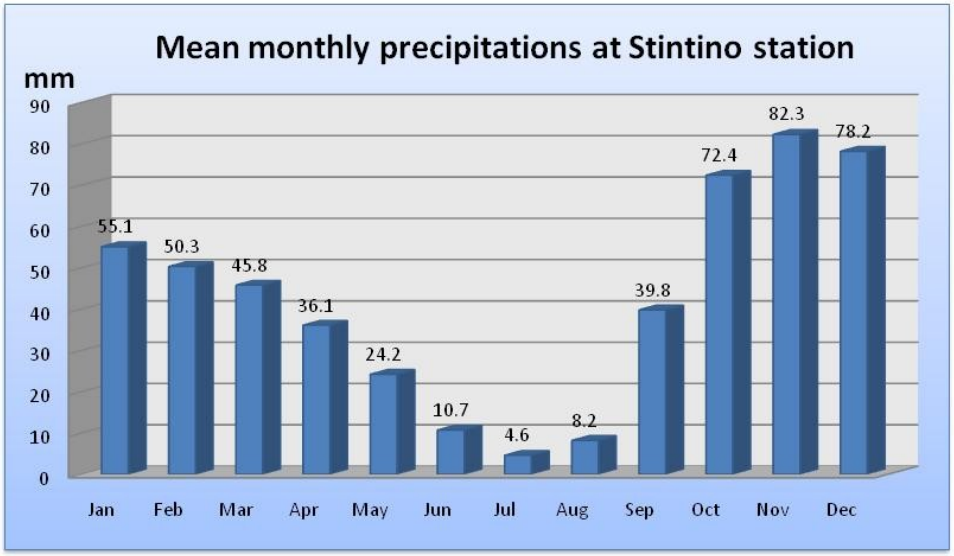

Figure 14. Mean monthly precipitations at Stintino station (SISS, 1998).

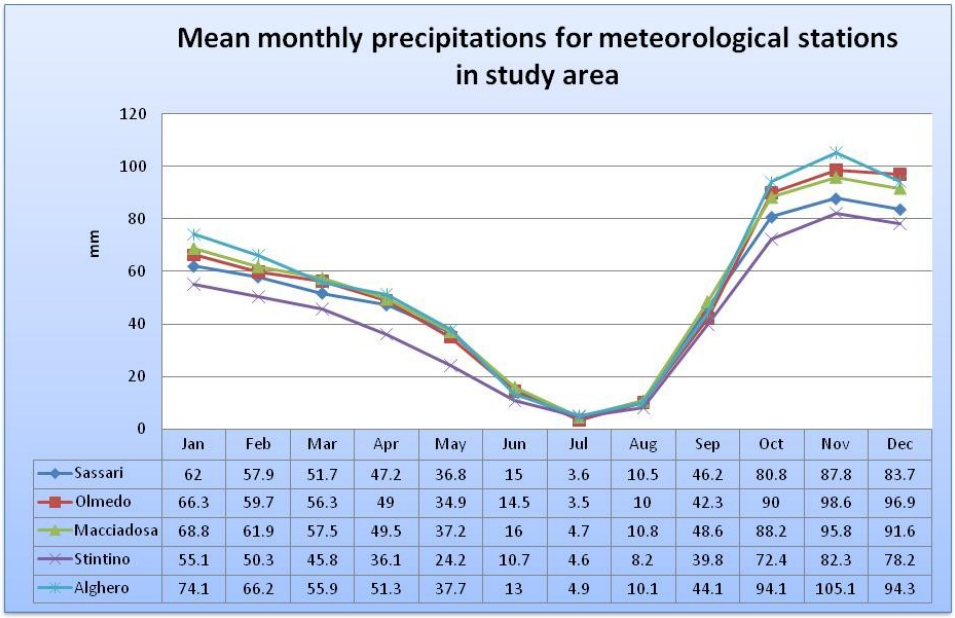

	Jan	Feb	Mar	Apr	May	Jun	Jul	Aug	Sep	Oct	Nov	Dec
Sassari	62	57.9	51.7	47.2	36.8	15	3.6	10.5	46.2	80.8	87.8	83.7
Olmedo	66.3	59.7	56.3	49	34.9	14.5	3.5	10	42.3	90	98.6	96.9
Macciadosa	68.8	61.9	57.5	49.5	37.2	16	4.7	10.8	48.6	88.2	95.8	91.6
Stintino	55.1	50.3	45.8	36.1	24.2	10.7	4.6	8.2	39.8	72.4	82.3	78.2
Alghero	74.1	66.2	55.9	51.3	37.7	13	4.9	10.1	44.1	94.1	105.1	94.3

Figure 15. Mean monthly precipitation comparison for meteorological stations in study area.

Monthly precipitation values for the different meteorological stations are shown in Appendix B.

3.3 Geology

The main geological events that involved Sardinia are briefly summarized in the following (see Barca et al., 2001; Ghiglieri et al., 2006; Ghiglieri et al., 2008).

Sardinian geological history started in the Paleozoic Era (570-250 Million years ago). During the Cambrian period the island was submerged and marine sedimentation took place under mostly shallow water conditions, except for a temporary emersion between the Early and the Middle Cambrian (this is the "Caledonian Sedimentary Cycle").

Under the Ordovician period, while Northern Europe was involved into the Caledonian Orogeny, Sardinia was implicated in a mild tectonic phase, the so called "Sardinian Phase" transpression folding (middle Ordovician), characterized also by a marine regression period when some areas emerged (mainly in Sulcis-Iglesiente).

A marine transgression occurred in the Late Ordovician and therefore a new deposition period took place, the so called "Hercynian Sedimentary Cycle".

The Caledonian and Hercynian sedimentary cycles determined the formation of those marine deposits that were subsequently subjected to metamorphism in the Hercynian Orogeny, resulting in the formation of the Sardinian Basement.

The Hercynian (or Variscan) Orogeny, occurred in the Late Paleozoic, affected the whole Sardinian Basement with varying degrees of deformation and metamorphism followed by important and extended post-collisional magmatism. As mentioned before, this orogeny resulted in compression, folding and thrusting of Paleozoic deposits.

During the Middle Carboniferous, Sardinia was completely emerged as part of Hercynian Chain, constituted by mountains that started to be strongly eroded up to the Permian Period and consequently, at the end of the Paleozoic Era, it resulted as a low relief plain.

Post-collisional events of Variscan Orogeney caused extensional tectonics that led granite intrusion (Late Carboniferous - Permian).

The Mesozoic Era (250-67 Million years ago) was characterized by marine transgression that caused a long deposition period along a wide area, although Sardinia was probably totally submerged only for a short period of time during Jurassic Period. Nurra is one of the main Sardinian regions involved into this sedimentary cycle so that marine transgression occurred from the Middle Triassic almost continuously up to the Aptian-Albian time under shallow marine water in a carbonate platform environment. During the Aptian-Albian time an important tectonic phase (Bedoulian movement, see Oggiano et al., 1987) took place in the region causing marine regression and Jurassic deposits partial erosion. During the Coniacian Age a new transgression led to land submersion and thus to carbonate-terrigenous sedimentation up to the Maastrichtian Age.

During Cenozoic Era (66.7-1.8 Million years ago) Sardinia moved into its current position. In fact, as a consequence of Alpine Orogeny, Sardinia-Corsica block was part of mainland Europe until rifting began in Miocene and subsequent counter-clockwise rotation resulted in the actual location. This rotation of the Sardinia-Corsica block was contemporaneous with volcanic episodes that, together with marine sedimentation, filled the Sardinian Rift. The Nurra region represents a structural high developed in this Era and since the Paleocene it encountered weathering, erosion, widespread calcalkaline volcanism and

two tectonic events related to the Prenaic and to the North Apennine Orogeny. Volcanic episodes, that involved the whole Northern Sardinia since Oligocene up to Early Miocene, area mainly characterized by pyroclastic flow that evolved in a sequence of active eruptive phase with some pauses in between. Whereas, during deposition periods, the sedimentation process in Nurra region was characterized by continental deposition environment (alluvial fan and alluvial plane) and transitional environment (river delta) that passed to marine platform environment.

During Quaternary Era (1.8 Million years ago up to now) the island was subject mainly to continental sedimentation and second to marine deposition.

The lithostratigraphy of the different geological formations occurring in the study area is given in the next paragraph following the time periods in which they were formed (see Barca et al., 2001; Ghiglieri et al., 2006; Ghiglieri et al., 2008).

3.3.1 Variscan Basement

In the structural high represented by the Nurra region, Paleozoic rocks constituting the Variscan metamorphic basement are progressively exposed westward and outcrop in the western part of the study area along the coast.

The Variscan basement consists of metamorphic rocks, described briefly as following:

- quartzites and meta-sandstones containing phyllites and meta-conglomerates intercalations (?Cambrian – Ordovician). These rocks outcrop extends from the South of Argentiera to Monte Forte;
- metagreywackes and meta-volcanic rocks (meta-dolerites and alkaline meta-basalts), with rare meta-rhyolites intercalated (Late Ordovician), that outcrop at La Pietraia and at Monte Rugginosu;
- oolitic ironstones (Late Ordovician) that outcrop from Canaglia to the coast;
- graphitic phyllites (Silurian) as meta-argillites composed by fine grains full of graphite;
- paragneisses and micaschists, under greenschists and anphibolite facies conditions, that, among Nurra region, outcrop only in Asinara island.

3.3.2 Paleozoic and Mesozoic covers

The Paleo-Mesozoic succession overlies the Variscan basement. Late Paleozoic deposits are made up of continental rudites and sandstones intercalated with acid volcanic rocks that passes up into Triassic sandstones and rudites. During this deposition period, the sedimentation processes changed from fluvial continental environment (alluvial fan and alluvial plane) to transitional environment (lagoonal). These deposits are grouped into the so called Buntsandstein Formation (SGI – CARG) that in Nurra region consists of:

- clastic rocks and variegated sandstones and clays that on the whole are about 60 m thick (outcropping in Cala Viola and Torre del Porticciolo);
- chalky clays alternating with sandstones intercalated to marlstones and dolostones with chalk or dolostones intercalation, 40 m thick (outcropping in Monte Santa Giusta).

First marine transgression deposits of Nurra region are of the Middle Trias and include Muschelkalk Formation (Middle Triassic) that consists of the following lithotypes:

- grey, green or rose, nodular, stratified or structureless, marly or dolomitic limestones;
- dolostones;
- marly argillites;

The thickness of Muschelkalk deposits is about 50 m in Monte Santa Giusta, whereas a full succession occur only in the underground of Nurra region and it is about 140 m thick (SGI – CARG).

The overlying Triassic deposits are included into the Keuper Formation (Middle-Late Triassic) that, according to borehole data carried out in Cugiareddu and Monte Santa Giusta, encompasses marine sediments made by (SGI – CARG):

- dolomitic limestones and laminated dolostones with flint layers and sulfate pseudomorphs;
- yellow, stratified and laminated dolomitic marls;
- vuggy and brecciated dolostones, with limonitic nodules;
- green and/or red clays intercalated with gypsum.

The thickness of the Keuper formation is not known due to ductile behaviour of evaporitic deposits, however it was estimated to be 50-100 m thick. These deposits are strongly folded, this is the case of Cugiareddu anticline where they were crossed for 287 m (SGI - CARG).

The base of the Jurassic system lies on the Triassic evaporites constituting the Campanedda formation (Lias), that consists of:

- oolitic, oncoid and bioclastic limestones, marls and marly limestones;
- grey and blue limestones with flint lenses.

The most widely outcropping Mesozoic formation of the study area is the Monte Nurra Formation (Dogger), that encompasses the following litotypes:

- quartzy sandstones;
- dolostones and dolomitic limestones, bioclastic limestones, flinty limestones, marly limestones and marls, with quartzy sandstones intercalations.

The upper Mesozoic formation of Northern Nurra is the Monte Uccari Formation (Malm), since younger deposits, that are outcropping in Southern Nurra, have being eroded. Monte Uccari formation consists of:

- grey and white, micritic and bioclastic limestones well stratified;
- grey dolostones and oolitic limestones lenses with cobbles.

3.3.3 Cenozoic covers

The Cenozoic geological succession is made out of two different complexes: the volcanic and the sedimentary.

Volcanic complex consists of pyroclastic flows that were deposited during the Lower Miocene. Pyroclastic deposits can be seen in Southern Nurra forming a volcanic plateau, whereas they outcrop slightly over Northern Nurra. The different volcanic units are divided by palaeosols and they have a variable thickness from a few to a hundred of meters. They consist of ignimbrites, lava domes and rare lava flows of rhyolitic, rhyodacitic, dacitic and locally comenditic composition with fall and surge deposits, with intercalations of sedimentary and epiclastic deposits (Late Oligocene – Middle Miocene). Bentonite deposits, deriving from the hydrothermal alterations of feldspar and glassy material, generally seal the bottom of the pyroclastic complex.

The sedimentary complex is made up of marine and continental sediments. Fluvial deposits consist mainly of monogenic (calcareous, dolomitic or volcanic) to polygenic conglomerates of different grain size and with bioclastic or volcaniclastic matrix, that are intercalated to volcanic layers. Alluvial deposits consist of fine to medium sized sands and yellow sandy clays intercalated to coarse sands and conglomerates. Marine deposits are make by nodular limestons, calcarenites and marls.

The Cenozoic covers that interest study area are described in the followings.

The Oppia Nuova Formation is made of quartz-feldspathic sands and conglomerates of different grain size, with elements of Variscan Basement, Oligo-Miocenic volcanites and Mesozoic limestons. This formation outcrop on the south of Petrochemical plants.

The Mores Formation consists of different lithofacies, two of that outcrop in Northern Nurra:

- calcarenites, bioclastic fossiliferous limestones and nodular limestones;
- sandstones and conglomerates with carbonate fossiliferous and bioturbated matrix, with intercalations of sandy-arenaceous, quartz-feldspathic, medium-coarse sized deposits.

Finally, the Fiume Santo Formation, consists of red clays with intercalations and lenses of conglomerates made by cobbles coming from the Variscan Basement, volcanites and Mesozoic limestones.

3.3.4 Quaternary covers

Quaternary covers encompass alluvial deposits, mainly with cobbles, located along the main streams, characterized by limited thickness. These sediments are made of:

- conglomerates, sands, clays (Plio-Pleistocene);
- gravels and sands, silts and clays (Olocene), that form main streams deposits, dunes and beaches.

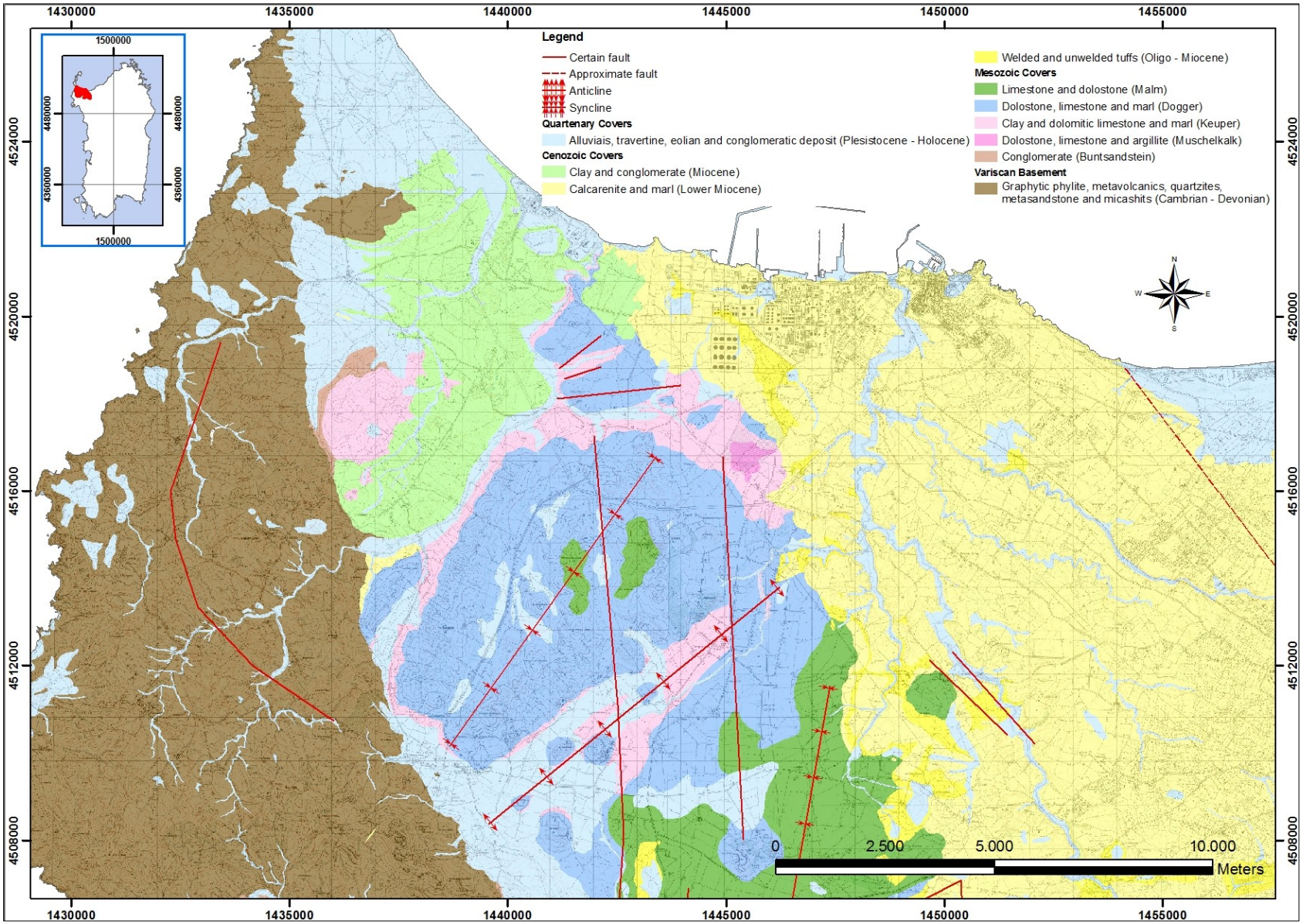

Figure 16. Geology of the study area (source: GIS of Sardinian Regional Administration).

3.4 Structural geology

Structural setting of Nurra region is the effect of the major deformation events mostly occurred in the Cenozoic Era and secondly in the Mesozoic Era. Variscan tectonic events are important only in Western Nurra, where Variscan basement outcrops. Structural setting is described in the following paragraphs (see Barca et al., 2001; Ghiglieri et al., 2006; Ghiglieri et al., 2008).

3.4.1 Variscan tectonics

Variscan orogeny, that influenced Basement tectonics, is characterized by a polyphase evolution that can be summarized into different deformation phases. The first deformation stage determined isoclinals folds that show a South-Westward overturning; the main basement schistosity is a result of this folding. Other deformation phases followed, developing new schistosity and transposing the previous one. The whole basement forms a synform dipping eastward (the fold dipping seems to be caused by Miocene tectonic events).

3.4.2 Mesozoic tectonics

Mesozoic tectonic events can be briefly summarized in the phases described as following.

The first Mesozoic deformational phase, developed in an extensional tectonic environment (Middle Cretaceous), was linked the so called Bedoulian movements (Oggiano et al., 1987), that caused carbonate platform to emerge. These deformation movements led to normal faults, having East-North-East striking, and reactivated Variscan Basement faults. Moreover, this tectonic phase determined the North-Western part of carbonate platform to uplift so that it has being eroding since Middle Cretaceous. This is the reason for which Mesozoic deposits evidence a decreasing thickness in a North-Westward direction.

A transpressive regime characterized the next phase, causing sinistral strike slip faults accompanied by mild folding (North-North-West direction) and normal faults (North-East direction).

The last tectonic phase caused the emersion of the whole Mesozoic carbonate platform (Late Cretaceous). Tectonic structures related to this phase are not recognized.

3.4.3 Cenozoic tectonics

Also Cenozoic tectonics events can be divided into different phases, described as following.

Different tectonic events took place between the Late Cretaceous and the Middle Miocene that can be referred to the Eocene Pyrenaic phase and to the Oligocene Appenninic collision. This events mainly caused East-North-East folds.

Extensional events, related to Sardinia-Corsica block rotation and consequent Balearic basin opening, had an important role in performing the final tectonic setting of Nurra region. Those movements caused the current tilting in the North-East direction, as can be seen in folded deposits located between Fiumesanto mouth and Monte Nurra (Miocene-Pliocene).

The last tectonic phase (Pliocene) caused normal faults and block uplifting. These faults are characterized by mainly East striking axis and sometimes were responsible of pre-existing faults reactivation.

3.5 Hydrogeology

The most important aquifer of Nurra region is lying in Mesozoic covers. In the following paragraphs a description of the main aquifers of the study area is given (see Ghiglieri et al., 2006; Ghiglieri et al., 2008). The lithostratigraphic formations are grouped into four hydrogeological units that may be composed of different aquifers.

3.5.1 The Paleozoic hydrogeological unit

While phyllites inhibit vertical infiltration (among all Variscan lithotypes, the graphitic phyllites are the less permeable), the only rock with very low secondary permeability ($1 \cdot 10^{-7}$ m/s) is the quartzite, which is jointed due to its brittle nature. Meta-volcanic rocks, especially meta-dolerites, evidenced a fair permeability due to fractures (Ghiglieri et al., 2006).

Infiltration that occurs in metamorphic rocks is small and, therefore, most groundwater flow is shallow. Moreover, the structural setting of the Paleozoic Basement is determined by the latest Variscan folding phase that generated a wider synform with an east striking and dipping axis. Consequently, water that incomes the metamorphic hydrogeological unit flows laterally into Mesozoic limestones in a eastward direction. The main hydraulic conductivity of the whole hydrogeological unit can be estimated as $1 \cdot 10^{-11}$ m/s (Ghiglieri et al., 2006).

3.5.2 The Mesozoic hydrogeological unit

As mentioned before, the Mesozoic deposits play the main role in Nurra hydrogeologic system as carbonate lithology enhances infiltration in those areas where limestones outcrop and leads to higher aquifer storage capacity. The most important Hydrogeological features are given in this paragraph (Ghiglieri et al., 2006).

Three main hydrogeological aquifers can be recognized in the Mesozoic succession:

- the Triassic aquifer, lying in the Buntsandstein, Muschelkalk and Keuper formations;
- the Jurassic aquifer, included in the Dogger Formation;
- the Cretaceous aquifer, of limited interest for the study area as its deposits have been almost entirely eroded.

Among the Triassic aquifer deposits, Buntsandstein formation (composed by arenite-conglomerate deposit) shows highly variable thickness and medium permeability, especially because of silt intercalation typical of the older deposits. The other Triassic deposits have an high permeability, as are made by soluble rocks, except for argillites of Keuper formation. The main hydraulic conductivity value of the Triassic aquifer is in the range of $1 \cdot 10^{-6}$ m/s.

The most permeable aquifer is the Jurassic one, mainly consisting in limestones, due to fractures and karst conduits, with an hydraulic conductivity value of about $1 \cdot 10^{-4}$ m/s.

The Cretaceous deposits that, as already said, are limited and scanty in the Nothern Nurra and therefore can't be considered hydrogeologically relevant, have an hydraulic conductivity of $1 \cdot 10^{-5}$ m/s.

Deformation events that involved carbonate deposits influence the hydrogeological setting as a consequences of different factors that should be taken into account in defining the conceptual model of the study area:

- tectonic activities that caused land emersion and erosion influence the deposit thickness. That's the reason why the Mesozoic covers thickness decreases in the North-West direction;
- deformation episodes involving permeable and impermeable layers can results in locally perched aquifer conditions;
- compressive deformations can lead to a local increase in deposits thickness;
- some faults formed in the past can behave as vertical impermeable layer or, oppositely, as discontinuities that acts as drains.

The main aquifer reservoir of Northern Nurra is given by Jurassic deposits around Monte Alvaro peak, that are folded in a syncline striking in the North-East direction and therefore draining groundwater to the industrial zone underneath the Miocene carbonates.

3.5.3 The Tertiary volcanic hydrogeological unit

The Tertiary volcanic unit hosts a multilayer aquifer as a result of the presence of alternated weakly welded and deeply fractured high grade ignimbrites. Each permeable layer is confined by clay-rich paleosols or by pumice and ash flows converted into bentonite. The welded tuffs that overlie volcanic complex are intensively fractured favoring vertical infiltration, whereas bentonite deposits at the bottom constitute an impermeable barrier between volcanic rocks and Mesozoic deposits. The main hydraulic conductivity of the whole hydrogeological unit can be estimated as $1 \cdot 10^{-8}$ m/s (Ghiglieri et al., 2006).

3.5.4 The Miocene hydrogeological unit

The Miocene covers increase in thickness Eastward, therefore this complex is hydrogeological relevant only for Eastern Nurra, where the thickness is considerable (some hundred meters), whereas it is of less importance for the study area, where these deposits occur only in the industrial zone, overlying the Mesozoic limestones with higher thickness eastward. The main hydraulic conductivity of the whole hydrogeological unit is about $1 \cdot 10^{-8}$ m/s (Ghiglieri et al., 2006).

3.5.5 The Quaternary hydrogeological unit

The Quaternary deposits that overlie the Miocene or the Mesozoic formations are usually limited to a few meters depth and always less than 10 m. The hydraulic conductivity of this hydrogeological unit is variable due to lithological eterogeneity and ranges between $1 \cdot 10^{-6}$ m/s and $1 \cdot 10^{-4}$ m/s (Ghiglieri et al., 2006).

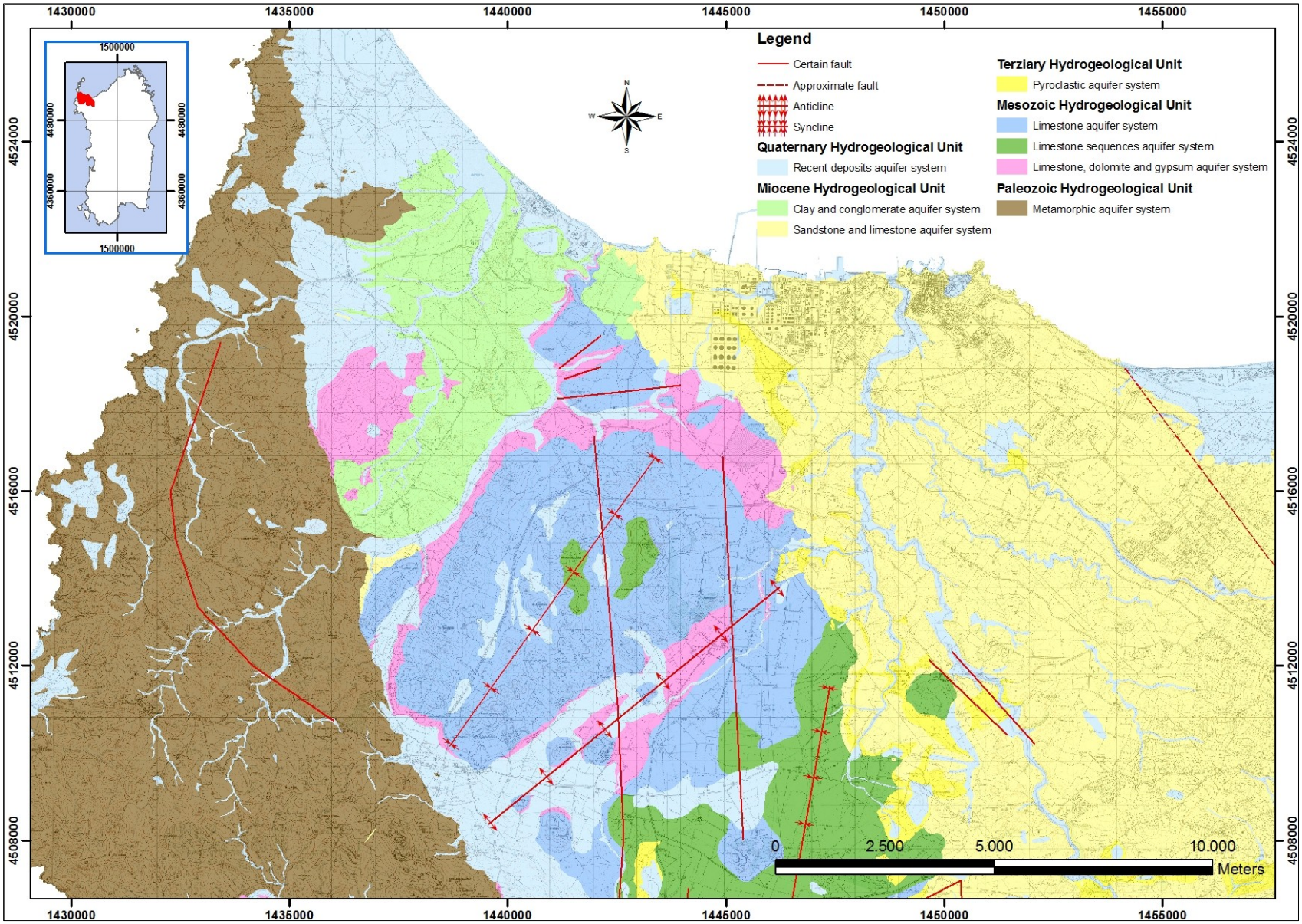

Figure 17. Hydrogeological units of the study area (source: GIS of Sardinian Regional Administration).

3.6 Surface water

Surface water bodies in the study area are given by three main streams and a coastal pond. The main streams are Fiume Santo, Riu San Nicola e Riu Mannu.

The Fiume Santo stream flows from Serra de Li Sambinzi (222 m s.l.m.) to the Asinara Gulf in a main North-East direction. The total length of the main stream course is about 18 km. The upstream of its basin consists of Paleozoic rocks while the lower course flows through the Fiume Santo Formation. Due to the very low permeability of this formation, downward leakage from the stream into the aquifer can be considered slight. The discharge is maximum during winter, starts decreasing during Spring season and goes dry during the Summer, except for its final course in the nearness of the mouth where the presence of some springs leads to a base flow occurring also in the dry season. Nevertheless, groundwater exploitation for industrial uses caused the springs to dry up in the last decades.

Similarly, Riu san Nicola stream runs down the Paleozoic relief on the Western Nurra and flows into the Stagno di Pilo on the West of Fiumesanto power plants.

As mentioned in the last chapters, the latest Variscan folding phase generated a wide synform with an East striking and dipping axis that controls the superficial drainage in the upper course basin of Fiume Santo and San Nicola basin, resulting in water flow eastward.

Riu Mannu stream flows in the Eastern Nurra and its headwaters lay out of the study area. The main stream course has a total length of about 65 km, flowing mostly through the Miocene covers. The mouth is on the East of the industrial zone nearby Porto Torres village.

The Stagno di Pilo is a coastal pond mainly fed by Riu San Nicola stream and by some other brooks. Its mouth tends to be closed to the sea preventing water turnover and causing nutrients accumulation.

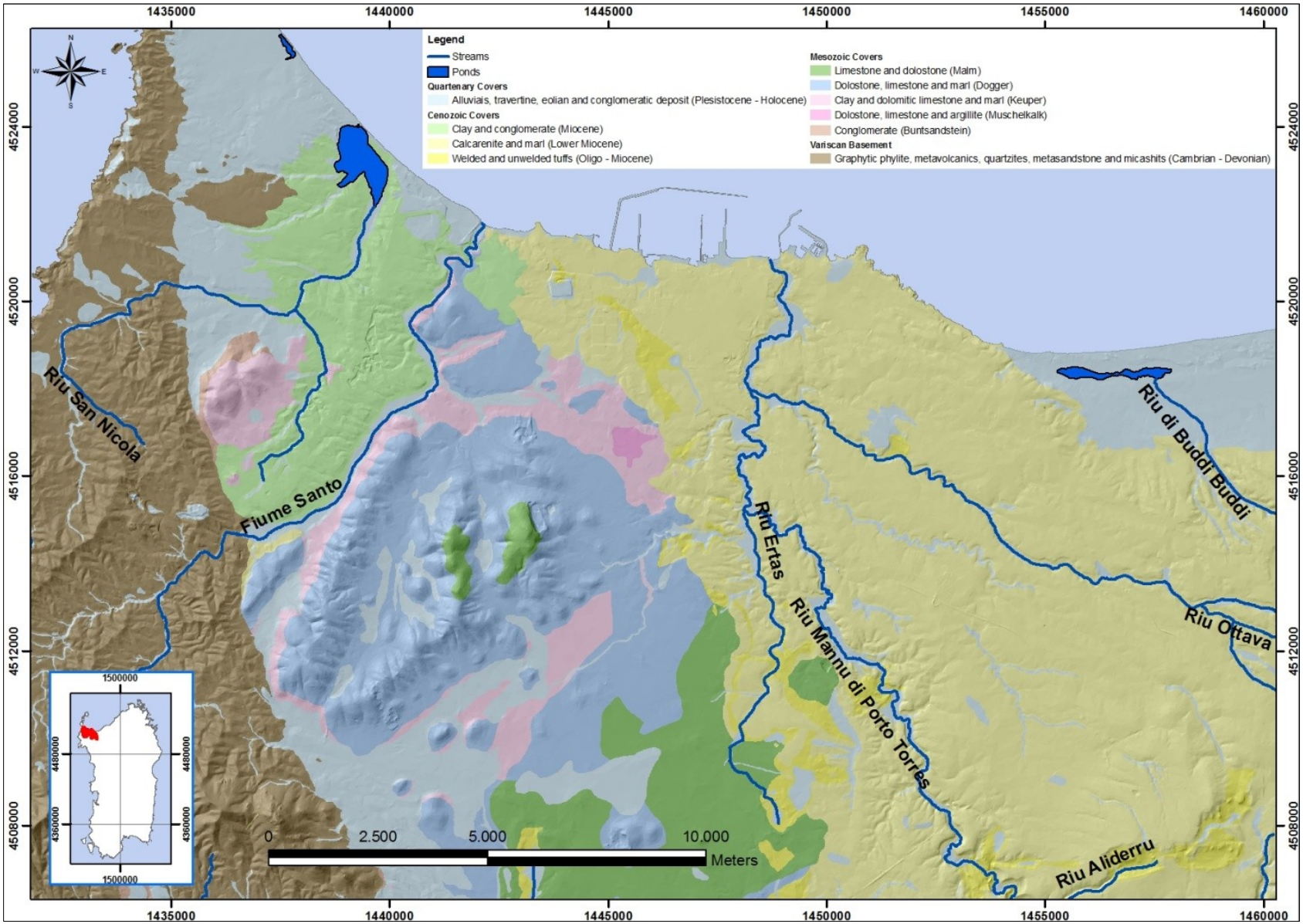

Figure 18. Surface waters of study area.

3.7 Soil

Soli map of the study area is shown in Figure 19 and the following description of soil tassonomy labels is given here:

- A1: rock outcrop, lithic xerorthents, subordinately rhodoxeralfs, haploxerolls;
- A2: lithic and typic xerorthents, lithic and typic rhodoxeralfs, lithic and typic xerochrepts, rock outcrop subordinately haploxerolls;
- B1: rock outcrop, lithic, typic, and dystric xerorthents, subordinately xerochrepts;
- B2: typic, dystric, lithic xerorthents and typic, dystric, lithic xerochrepts, subordinately palexeralfs and haploxeralfs, rock outcrop, xerofluvents;
- D3: rock outcrop, lithic xerorthents, subordinately xerochrepts;
- D4: typic, vertic, lithic xerochrepts, typic, lithic xerorthents, subordinately rock outcrop, haploxerolls, chromoxererts;
- F1: rock outcrop, lithic, typic xerorthents, lithic, typic rhodoxeralfs, subordinately xerofluvents;
- F2: typic, lithic xerorthents, typic, lithic xerochrepts, typic rhodoxeralfs, subordinately rock outcrop, arents, xerofluvents;
- F2: typic, lithic xerorthents, typic, lithic xerochrepts, typic rhodoxeralfs, subordinately rock outcrop, arents, xerofluvents;
- G3: typic pelloxerert, entic pelloxererts, subordinately xerofluvents;
- I1: typic, aquic, ultic palexeralfs, subordinately xerofluvent, ochraqualfs;
- I2: calcic and petrocalcic palexeralfs, subordinately xerofluvents;
- L1: typic, vertic, aquic and mollic xerofluvents, subordinately xerochrepts;
- M1: typic xeropsamments, aquic xeropsamment, subordinately xerochrepts, quartzipsamments;
- N1: typic salorthids, subordinately fluvaquents;
- O: Artificial fill.

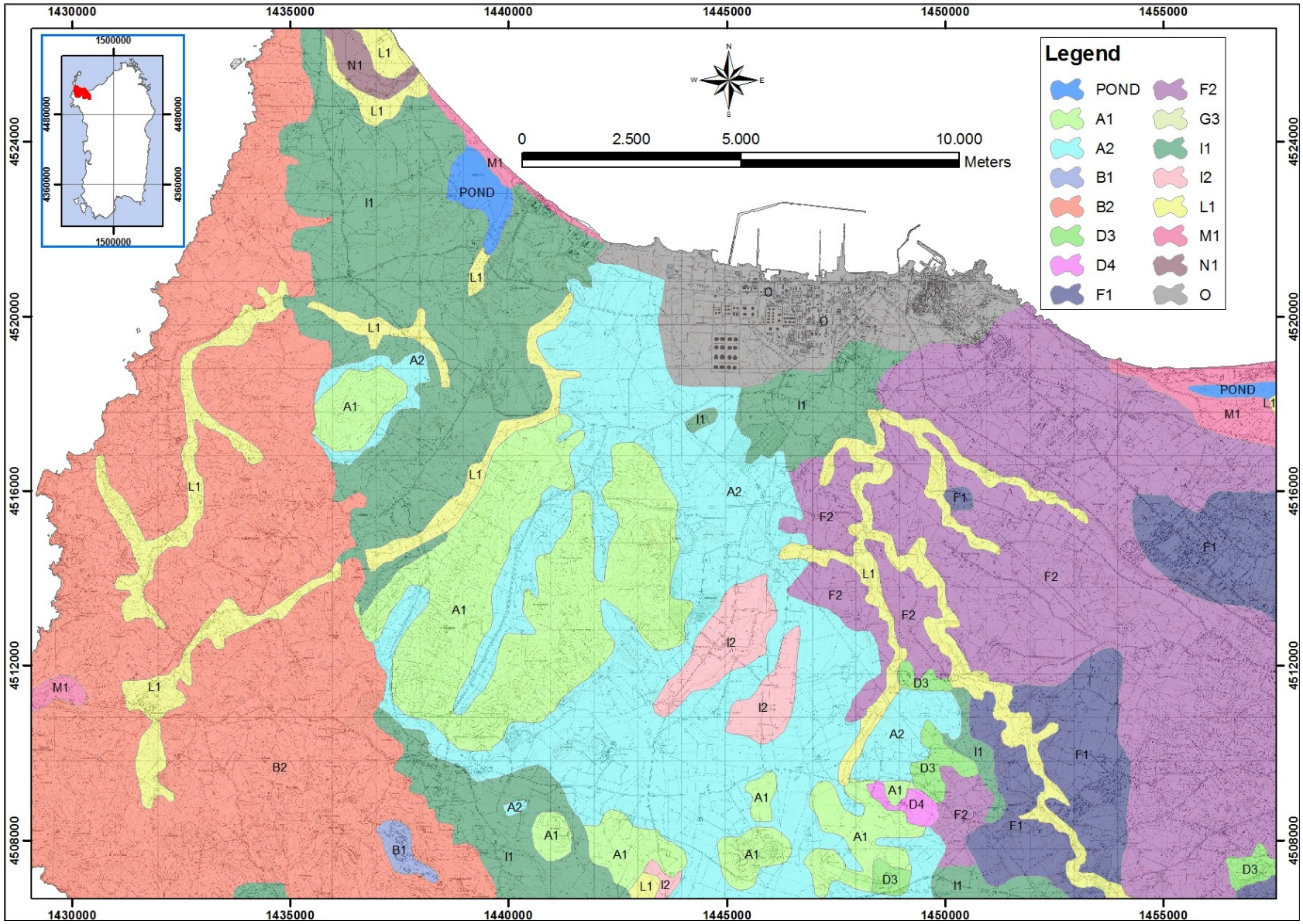

Figure 19. Soil map (source: GIS of Sardinian Regional Administration).

4 Conceptual model

4.1 Introduction

Hydrogeological conceptual model understanding of the study area results to be quite difficult due to aquifer complexity, hosted in a karst medium. This complexity in characterizing karst aquifer features is owing to discontinuities and anisotropy of hydraulic parameters that lead to a flow pattern occurring in conduits, fractures and/or in the matrix medium. Also recharge processes may vary spatially inside the hydrogeological basin and are sometimes difficult to identify and to evaluate properly.

All the available data were integrated into a reasoned and logical structure supported by user-friendly softwares that assured a proper management and interpretation, simplifying the hydrogeological conceptual model understanding.

The topographic dataset and its derived elaboration allow firstly to analyze different information like morphometric and hydrographic aspects and secondly to arrange input data for successive elaborations of this work (like aquifer three-dimensional schematization and mathematical modeling). Topographical data used come from the DB 10k database (scale 1:10.000), created by Sardinian Regional Administration as shape files. Starting from terrain elevation data two derived datasets were created:

- the Digital Terrain Model (DTM) in raster format;
- the DTM in vector-based format, i.e. the Triangular Irregular network (TIN).

Other digital data acquired are:

- geological dataset (SITR – Sardinian Regional Administration, scale 1:25.000);
- pedological dataset (Aru at al., scale 1:100.000);
- several environmental datasets (coming mainly from the SITR, that is a GIS developed by Sardinian Regional Administration, scale 1:25.000).

Moreover, further datasets were produced to include different kind of information not available in digital format, for example:

- karst sinkholes information coming from speleological data;
- springs localization and related data;
- lithological data coming from borehole logs;
- well data and hydraulic head measurements.

All these datasets were arranged in a geodatabase that constituted a useful tool designed firstly to store, query and manage quite all geographic information and spatial data collected and secondly to create distributed parameters maps needed for mathematical modeling input and aquifer vulnerability assessment.

4.2 Aquifer basin limits

Based on hydrogeological information acquired, the first step in implementing conceptual model was to define aquifer boundaries in order to identify the area subject to mathematical modeling and vulnerability assessment.

In this case, study area borders consist of impermeable divides, flow line and constant head boundary, that are (see Figure 20):

- the sea on the North side (the Asinara Gulf);
- the Paleozoic outcrops on the Western and South_Western side;
- the Riu Mannu stream on the East;
- the flow line that runs from La Corte, through Cugiareddu anticline, already defined by RIADE project (Ghiglieri et al., 2006).

The area defined does not coincide with surface water catchment. In fact, Fiumesanto and Riu Mannu stream basins extends beyond the study area. The former crosses Paleozoic outcrops on the South-West of the study area and the latter crosses Miocene sediment on the Eastern Nurra.

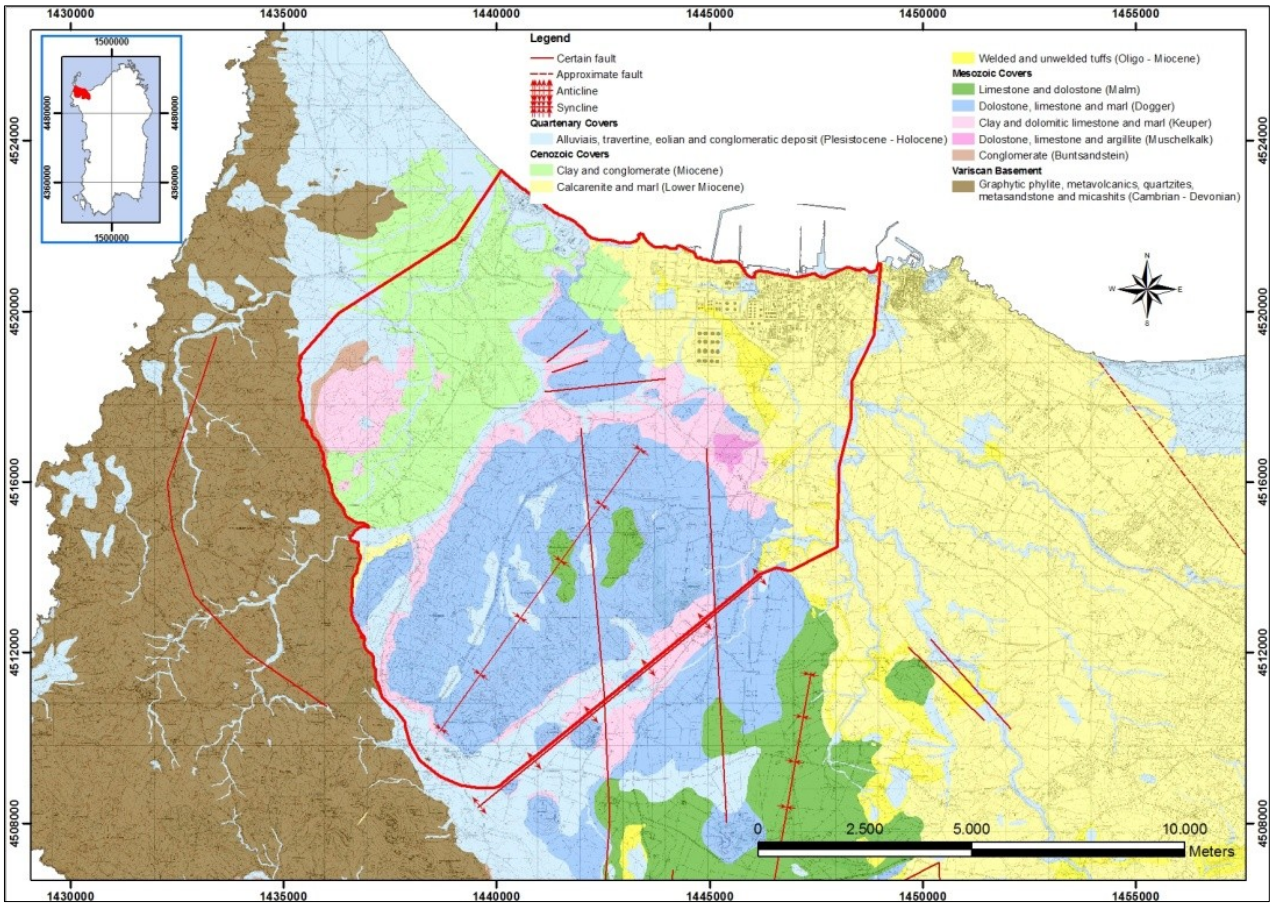

Figure 20. Boundaries of modeled domain (red polygon).

4.3 Three-dimensional schematization

Lithological data were stored in a geospatial database using a structure that could be easily exported in GMS environment as to be handled in the tree-dimensional schematization process of aquifer domain. Indeed, using the borehole module of GMS, lithological data could be quickly imported and three-dimensionally visualized in order to simplify the spatial reconstruction of the different aquifer layers. Moreover, geological schematization coming from previous studies and referred to the study area were included as to improve aquifer setting comprehension.

Available stratigraphic log description come from:

- groundwater abstraction licences (Regional Administration);
- the Porto Torres industrial zone characterization study (Regional Administration);
- the "POS 25" project on hydrogeological study of Nurra region;
- the environmental characterization plan of Fiumesanto power station (according to Legislative Decree n. 152/06);
- other studies or surveys.

The three-dimensional schematization process concerned first the Fiumesanto power plant site, thus the Miocene-Quaternary covers were reconstructed and represented through geological profiles. Secondly, the Mesozoic system was analyzed at the aquifer basin scale.

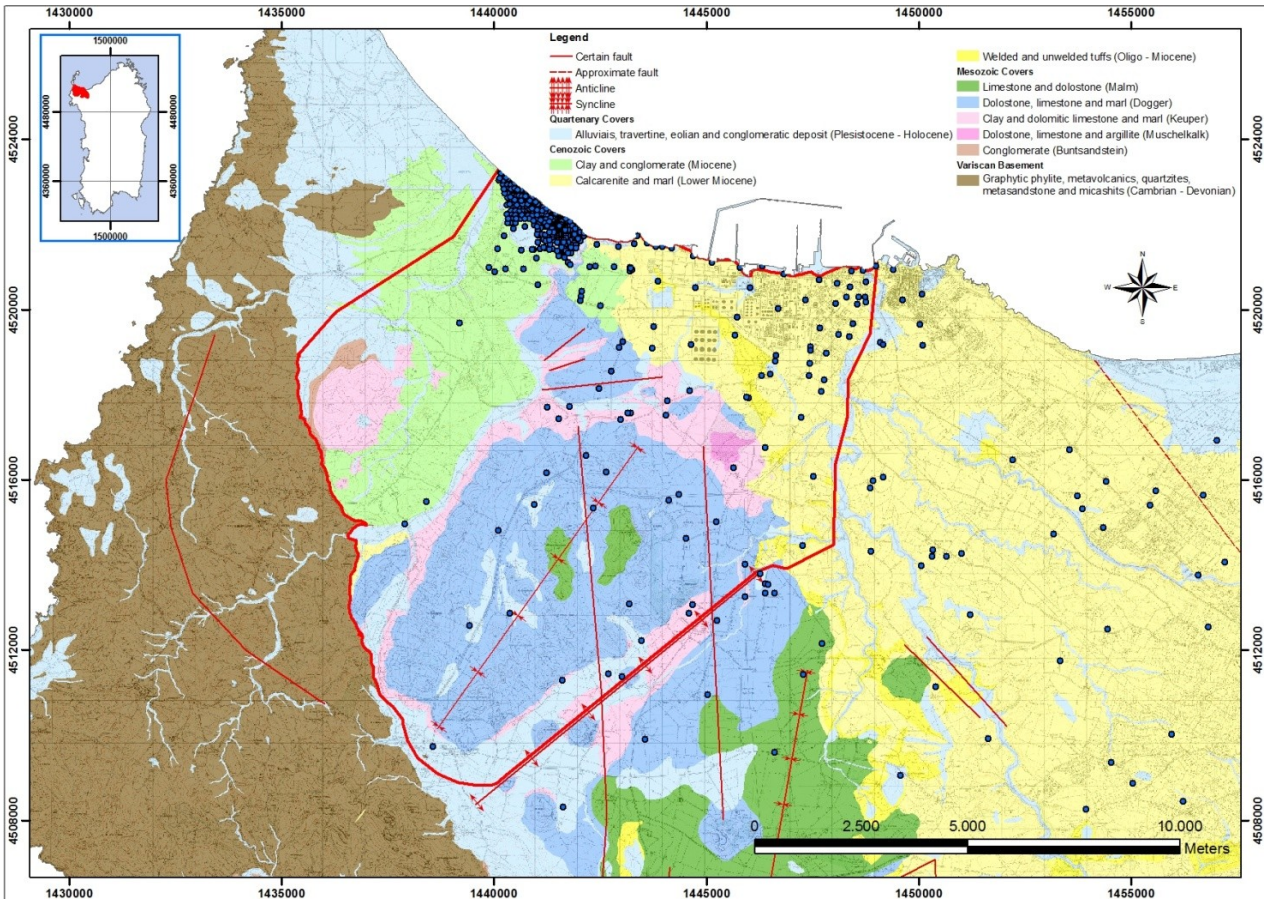

Figure 21. Boreholes and wells location.

4.3.1 Miocene-Quaternary covers

The Miocene-Quaternary covers schematization was reconstructed mainly based on borehole data coming from the environmental characterization plan of Fiumesanto power station, performed according to the Legislative Decree n. 152/06. Moreover, field activities were carried out within this study finalized to acquire piezometric measurement and well tests.

Geological data analysis led to understand the hydrogeological setting of sedimentary covers occurring at the Fiumesanto power station. Lithological cross sections created (see Figure 22) show an high heterogeneity and spatial variability of sedimentary covers, that consist mainly of a stratified clay/silt with sand and gravel layers intercalated. Moreover, sand and gravel layers are not continuous and act as permeable lenses included into impermeable sediments.

Hydraulic head measurements, performed on wells and piezometers located at the power station site, show a strong spatial variability of groundwater levels (also on the order of tens of meters) among neighboring piezometers. Moreover, aquifers hosted in these permeable layers are generally not under pressure and, on the contrary, show a small saturated thickness suggesting to be scarcely fed.

Therefore, both lithological cross section and field measurements confirm that permeable layers are not connected together and instead evidence the presence of aquifer lenses barely fed due to continuous overlying impermeable layer.

An exception are permeable lenses located on the Eastern part of the power station site, close to the Fiumesanto mouth, where those sediments enter into contact with the underlying Mesozoic carbonate formations and are under pressure.

Aquifer saturation decreases in the westward direction, so in western part of the site groundwater flow occur in clay and silt layers that, anyway, can be considered aquitards rather than aquifers. This is confirmed by simple slug test performed in piezometers located in this area: after a quick water removal, the head recovery time was considerable long.

4.3.2 Mesozoic covers

Based on geological cross section, borehole logs and various information coming from other geological studies (Caboi et al., 1982, Dettori et al., 1982, Ghiglieri et al., 2006), a three-dimensional scheme of Mesozoic sediment was done, shown in Figure 23.

The main groundwater reservoir of the study area basin occur in the syncline on the South of the industrial zone, located in the Campu Chelvaggiu area, where more recent Mesozoic deposits constituted by Dogger formation widely outcrop; whereas, syncline fold limbs are present on the boundary of Dogger outcrops and are given by Keuper and, secondly, by Muschelkalk formations (Ghiglieri et al., 2006; Caboi et al., 1982; Dettori et al., 1982).

On the North of this area, other smaller synclines occur at Monte Elva and Monte Elveddu.

Mesozoic deposits underlying Fiumesanto formation consists mainly of Triassic rocks, as Dogger carbonate has been almost totally eroded. The Fiumesanto formation constitutes

the confining unit of Mesozoic formations and its thickness increases in the North direction and decreases in the West and South direction. Moreover its thickness varies as following:

- it is higher than 70 m on the west of Fiumesanto power station;
- it is about 40 meters at Scala Erre area;
- it is about 100 meters at Sa Cazzalarga place.

In the petrochemical industrial area, Mesozoic succession lies under Miocene sediments, whose thickness increases in the East direction, varying between few meters in Minciaredda area (on the West side) to one hundred meters near Rio Mannu mouth (on the East side). Miocene deposits are divided from Mesozoic carbonate by the volcanic formations that act as an impermeable layer.

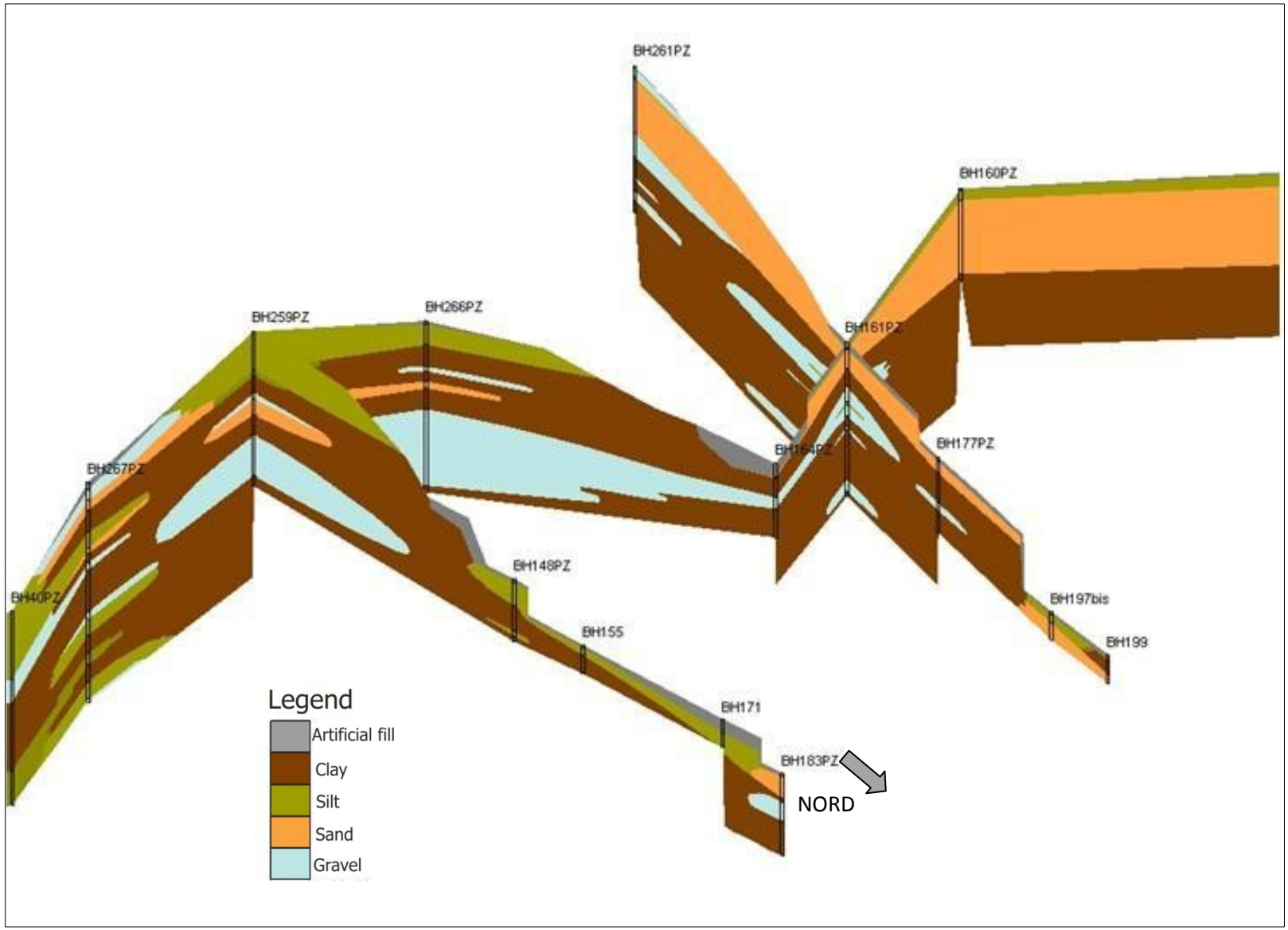

Figure 22. Three-dimensional schematization of Miocene-Quaternary sediments of Fiumesanto power station.

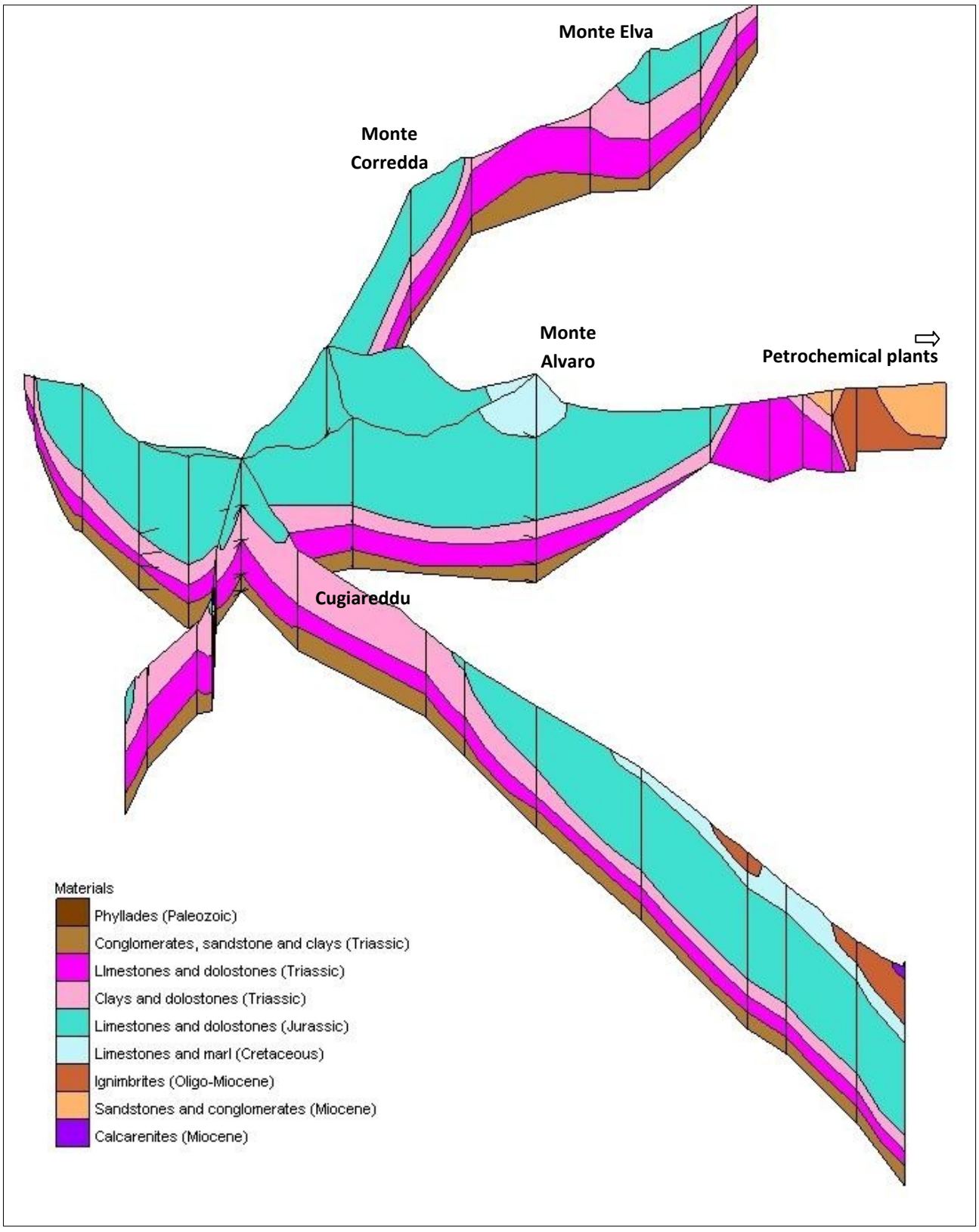

Figure 23. Three-dimensional schematization of Mesozoic covers in the study area (vertical magnification set as 7).

4.4 Recharge

Recharge main components, occurring into the study area drainage basin, can be distinguished as:

- diffuse infiltration: rainfall entering the aquifer through the soil, the fractures and matrix permeability of the carbonate rock;
- internal runoff: water enters the aquifer quickly through sinkholes.

Both diffuse infiltration and internal runoff take place in Mesozoic outcropping inside the study area, where also sinkhole are present (like vertical shafts or sub-superficial caves).

Sinkholes information come from surveys done by the Speleological Group of Sassari, that identifies some vertical shafts and caves, shown in Figure 24 and Figure 25. The sinkholes are:

- two caves at Monte Santa Giusta;
- a vertical shift at Monte Santa Giusta;
- four vertical shifts in the nearness of Monte Alvaro, Punta Rumasinu and Pedru Ghisu peacks.

Diffuse infiltration can be estimated taking into account the effective rainfall and the potential infiltration coefficient χ, which was evaluated by the RIADE project (Ghiglieri et al., 2006) based on hydrogeological properties of outcropping formations (see Figure 25):

- χ=0.8 for Jurassic carbonate sediments (Dogger formation);
- χ=0.5for Triassic sediments (Muschelkalk, Keuper and Buntsandstein formations);
- χ=0.4 for Miocene marls and limestones;
- χ=0.1 for Miocene clays and sands (Fiumesanto Formation).

Diffuse infiltration estimation is shown in paragraph 6.3..

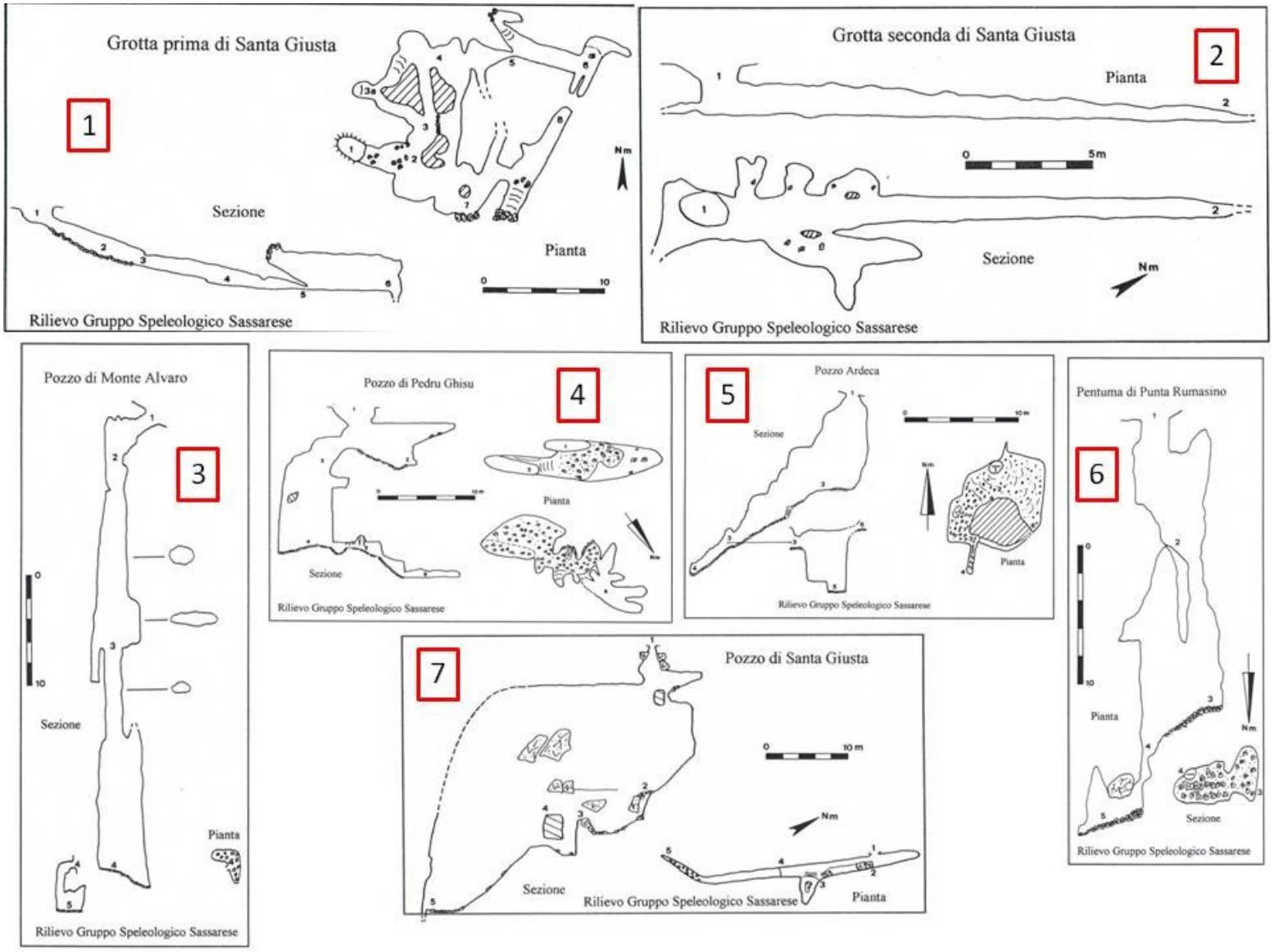

Figure 24. Plant and cross sectional view of sinkholes: Santa Giusta caves (1 and 2), Monte Alvaro (3), Pedru Ghisu (4), Ardeca (5), Punta Rumasino (6) and Santa Giusta vertical shifts (7) (Mucedda, 1998).

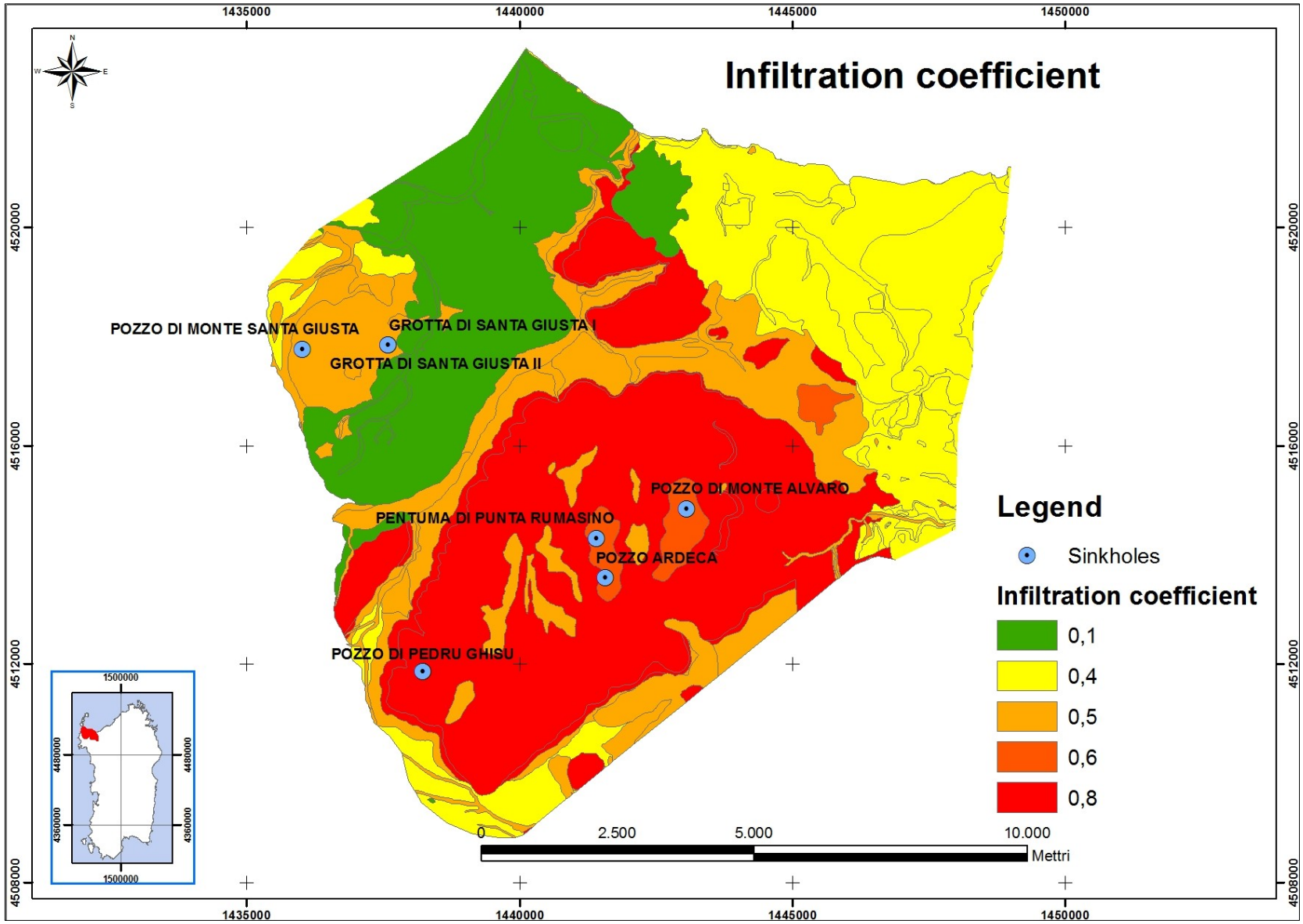

Figure 25. Infiltration coefficinet and sinkholes.

4.5 Springs

The most important springs of the study area, located near Fiumesanto mouth, could guarantee an high amount of discharge in seventies years, while nowadays are almost completely dried out because of groundwater abstraction.

Discharge rates, measured in the springs between 1968 and 1970, show nearly constant values during the year and were giving the followings average values (ENEL, 1985 and Pietracaprina, 1971):

- Voltino spring: 55 l/s;
- S'Oggiastru spring: 41 l/s;
- Costone spring: 38 l/s.

Other springs located in the aquifer basin are characterized by lower discharges values (about 1-2 l/s) and occurr in Quaternary sediments on the western part of the study area (Lunestas, Pozzo San Nicola and Mancinu, see Dettori, 1972).

Finally, Bitichesu spring discharges only after significant rain events from a sub-superficial cave in Mesozoic limestones (see Figure 26).

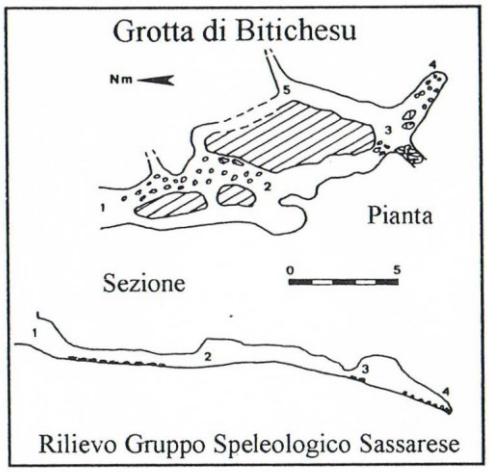

Figure 26. Plan and cross sectional view of Bitichesu cave (Mucedda, 1998).

4.6 Groundwater abstraction

According to Water Resource Plan of Sardinia (2006), most groundwater extracted from wells in the study area is used for industrial purposes (authorized discharge of 678 l/s) while there is only one well registered for irrigational use (1.4 l/s). Anyway, it is known that some other wells are present, probably mainly for domestic use, whose overall discharge amount is not available.

The Fiumesanto power station utilizes water coming from two wells drilled close to Fiumesanto springs. Those wells are about 30 m deep and are authorized to discharge 23 l/s each.

Also the Petrochemical plant uses groundwater coming from different wells drilled in Mesozoic limestones:

- three wells located around Monte Elva, having a total authorized discharge of 112 l/s (RAS, 2006);
- six wells located at Businco place (North-East of Monte Alvaro), in the Triassic outcrop, four of them with authorized discharges of 41.7 l/s each and two with 27.8 l/s. The depth of those wells ranges from 200 m to 300 m.

4.7 Flow system

Karst flow system is characterized by a combination of highly anisotropic pathways that occur through three possible ways:

- matrix permeability, due to the intergranular permeability of the bedrock itself (without fractures);
- fracture permeability, that are also subject to enlargement caused by dissolution processes;
- conduit permability due to karstification.

Hydrogeological site information analysis lead to make some assumptions regarding the flow system in the karst aquifer of the study area.

According to piezometric measurements, the main amount of groundwater flows from the recharge zone in Campu Chelvaggiu syncline to the Fiumesanto Spring; secondly, a smaller amount flows to the petrochemical zone and to the Western sector of aquifer domain.

Three-dimensional lithological schematization confirms that most permeable layers converge to the Fiumesanto river mouth direction. In fact, Fiumesanto formation that overlies the karst aquifer and constitutes an almost impermeable barrier, increases its thickness in the West direction (this is known by boreholes data performed in the Western part of the power station, where silt and clay deposits were crossed for about seventies meters without reaching Mesozoic deposits). Moreover, Miocene deposits below the petrochemical area increases their thickness in the East direction, reaching a depth of about one hundred meters at the Riu Mannu mouth. The inflow from Mesozoic into Miocene aquifer should be low due to the volcanic layer that isolate the two hydrogeological complexes.

Western sector groundwater flow occurs below the Fiumesanto formation through an high fractured karst medium, constituted by almost only Triassic deposits and confined by the overlying impermeable unit.

Karst conduits and fractures distribution and geometry are not well known. Anyway, the presence of very high productive wells, drilled for industrial uses in seventies years, let to assume the localization of the higher conductive zone (see paragraph 4.6).

The most uncertain element of hydrogeological conceptual model is given by the difficulties to dismiss hypothesis regarding a possible inflow to the study area coming from Eastern Nurra. A support to the possibility of an East inflow come from discharge amounts authorized for industrial wells and from discharge values of Fiumesanto springs foregoing

the industrial utilization, that seem not comprehensible whether inflow to the aquifer came only by infiltration evaluated inside the study area.

Therefore, numerical modeling was finalized to provide proof to support or dismiss assumptions made on conceptual model implementation. Therefore, two different conceptual models were tested by simulating groundwater system both with and without the East inflow and thus comparing water flow balance.

5 Groundwater flow simulation

5.1 Groundwater flow modeling theory

5.1.1 Modeling approaches

A model is a tool designed to represent a simplified version of reality. The models that have been used to study groundwater flow can be divided into three categories: physical, analogue and mathematical:

- physical model is a physical representation of a larger, more complex, system. It is a scale model, which simulates groundwater flow directly;
- analogue model uses some other physical phenomenon (for example electric phenomena) or the same phenomenon in some other area to describe the groundwater flow;
- mathematical model, that can be divided into two subcategories:
    - analytical model is a mathematical representation of a physical system, which describes groundwater flow by means of partial differential equations. Usually, the assumptions necessary to solve an analytical model are fairly restrictive. For instance, many analytical solutions require homogeneous and isotropic conditions;
    - numerical model is a discretized representation of a physical system, in which flow equations are solved numerically to give approximative results. The calculations are based on partial differential equations, which are replaced by approximations easier to solve. Numerical models are not subject to many of the restrictive assumptions required for analytical solutions (Bear, 1979).

Among numerical models, several solution techniques are available, the most significant of them are the Finite Difference Method (FDM) and the Finite Element Method (FEM).

In the FDM method a rectangular grid is established and the system is divided into many elements called grid blocks or cells. As it is used a rectangular grid, it is important to place the grid in such a way to minimize the number of nodes that fall outside the boundary of the area to model. These nodes are called inactive nodes, while the nodes that fall inside the modeled area are called active nodes.

The most common types of grid used in the FDM method are the mesh-centered grid and the block-centered grid (Figure 27). In the block-centered grid the nodes lie in the centre of cells. This grid is suitable when the flux across the boundary is specified. Whereas in the mesh-centred grid the nodes lie at the intersections of the grid lines, this grid is typical of problems in which values of the hydraulic head are specified at the boundary.

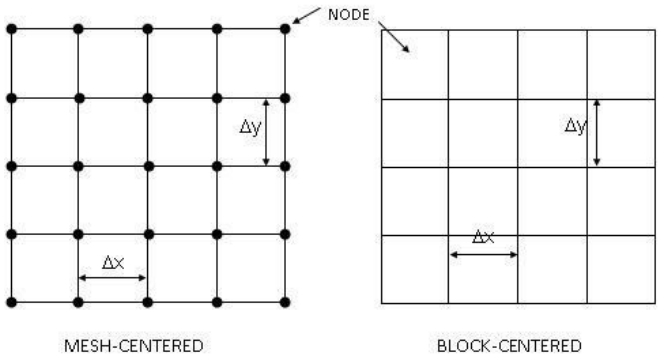

Figure 27. Mash centered and block centered grid in the Finite Difference method (modified from Mercer and Faust, 1981).

The FEM divides the system into a mesh of node points that form polygonal cells (which are usually triangles). The shape and the size of these cells can vary to reflect the changing value of parameters (or a complex geometry). For this reason the FEM is more suitable than the FDM when the system is heterogeneous and anisotropic.

As mentioned above, numerical methods replace the continuous differential equations, that describe groundwater flow, with a finite number of algebraic equations which calculates the hydraulic head at each node of the grid. These algebraic equations can be solved numerically in two ways: using a direct method or an iterative method. In the former case, the solution is reached by performing only one sequence of arithmetic operations and the solution found is exact, except for round-off error. Nevertheless when large system have to be solved, the direct method leads to accumulation of round-off error and the results obtained could be unacceptable. The latter method provides an alternative approach. It starts with an approximate solution and then an iterative process is performed until an error criterion is attained. In this case the solution is obtained by successive approximations (Mercer and Faust, 1981).

5.1.2 Governing equation of saturated groundwater flow

The mathematical description of groundwater flow is governed by the laws of physics. In deriving governing equations, the laws of conservation for mass and energy are employed. These principles require that the net quantity (mass and energy) leaving or entering a specified volume of an aquifer during a given time interval should be equal to the change in the amount of that quantity stored in the volume. In order to derive the governing equation of saturated groundwater flow a small part of the aquifer, called representative elementary volume (REV), is considered. The size of the REV is chosen to be large enough to contain many typical pore spaces and, at the same time, small enough so that the aquifer properties are approximately constant within the element (see, for example, Mercer and Faust, 1981).

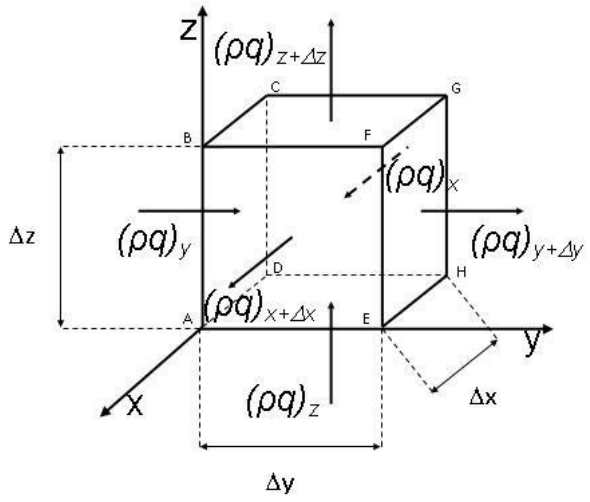

Figure 28. Control volume (adapted from Fetter, 2001).

If M_{out} and M_{in} are, respectively, the mass of water flowing out and flowing into the control volume [M], the mass balance equation for the control volume represented in Figure 28 over a small time interval ΔT is given by:

$$M_{out} - M_{in} = \Delta M \tag{1}$$

where ΔM is the chance in mass storage [M]. Considering the component of flow parallel to x-axis, qx+Δx and qx are respectively the flow volume leaving and entering the REV along x-axis (which have dimensions of [L^3 T^{-1}]). Therefore the difference between the mass leaving through the face EFGH and the mass entering the face ABCD is given by:

$$\left[(\rho q)_{x+\Delta x} - (\rho q)_x\right]\Delta t \tag{2}$$

Where ρ is the fluid density [M L^{-3}]. Similar terms can be determined for the other two directions y and z. Combining the three terms, the left side of equation 1 can be written as:

$$\left\{\left[(\rho q)_{x+\Delta x} - (\rho q)_x\right] + \left[(\rho q)_{y+\Delta y} - (\rho q)_y\right] + \left[(\rho q)_{z+\Delta z} - (\rho q)_z\right]\right\}\Delta t \tag{3}$$

Expression 3 is equal to the change in storage in the REV over time interval ΔT. As the mass of water in the REV is equal to nρΔxΔyΔz, where n is the porosity (dimensionless), equation 1 can be rewritten as:

$$\left\{\left[(\rho q)_{x+\Delta x} - (\rho q)_x\right] + \left[(\rho q)_{y+\Delta y} - (\rho q)_y\right] + \left[(\rho q)_{z+\Delta z} - (\rho q)_z\right]\right\}\Delta t = \left[(n\rho)_t - (n\rho)_{t+\Delta t}\right]\Delta x\Delta y\Delta z \tag{4}$$

Considering the possibility of a sink or source term (R) within the REV, equation 4 becomes:

$$\left\{\left[(\rho q)_{x+\Delta x}-(\rho q)_x\right]+\left[(\rho q)_{y+\Delta y}-(\rho q)_y\right]+\left[(\rho q)_{z+\Delta z}-(\rho q)_z\right]\right\}\Delta t + \\ +\rho R\Delta x\Delta y\Delta z=\left[(n\rho)_t-(n\rho)_{t+\Delta t}\right]\Delta x\Delta y\Delta z \tag{5}$$

R is the volumetric inflow rate (if negative, outflow rate) per unit volume [T^{-1}]. Dividing the terms of equation 5 by -ΔxΔyΔzΔt:

$$-\frac{(\rho q)_{x+\Delta x}-(\rho q)_x}{\Delta x\Delta y\Delta z}-\frac{(\rho q)_{y+\Delta y}-(\rho q)_y}{\Delta x\Delta y\Delta z}-\frac{(\rho q)_{z+\Delta z}-(\rho q)_z}{\Delta x\Delta y\Delta z}+\rho R=\frac{(n\rho)_{t+\Delta t}-(n\rho)_t}{\Delta t} \tag{6}$$

Up to now it has been employed the law of conservation for mass. To obtain the governing equation of saturated groundwater flow also the law of conservation of energy is needed. This law can be described by Darcy equations (see Domenico and Schwartz 1990, for details):

$$v_x=-k_{xx}\frac{\partial H}{\partial x}$$
$$v_y=-k_{yy}\frac{\partial H}{\partial y} \tag{7}$$
$$v_z=-k_{zz}\frac{\partial H}{\partial z}$$

where H is the hydraulic head [L], v_x, v_y and v_z are the components of Darcy's velocity [LT^{-1}] and k_{xx}, k_{yy} and k_{zz} are the principal components of the hydraulic conductivity tensor. The hydraulic conductivity tensor has nine components in anisotropic material (see expression 8), but in equations 7 it is assumed that the principal directions of anisotropy coincide with x, y and z directions of the coordinate axis. For this case the tensor is reduced to the three components k_{xx}, k_{yy} and k_{zz}, while the other components of the tensor 8 are equal to zero.

$$\begin{bmatrix} k_{xx} & k_{xy} & k_{xz} \\ k_{yx} & k_{yy} & k_{yz} \\ k_{zx} & k_{zy} & k_{zz} \end{bmatrix} \tag{8}$$

The Darcy's velocity v is defined as the flow volume across the element faces divided by the area of the face. The components of Darcy's velocity are:

$$v_x = \frac{q_x}{\Delta y \Delta z}$$

$$v_y = \frac{q_y}{\Delta x \Delta z} \tag{9}$$

$$v_z = \frac{q_z}{\Delta x \Delta y}$$

Substitution of equations 9 in equation 6, using the definition of derivative and choosing smaller and smaller values of Δx, Δy, Δz and Δt, gives:

$$-\frac{\partial(\rho v_x)}{\partial x} - \frac{\partial(\rho v_y)}{\partial y} - \frac{\partial(\rho v_z)}{\partial z} + \rho R = \frac{\partial(n\rho)}{\partial t} \tag{10}$$

The right side of equation 10 represents the mass rate of water due to fluid compressibility and aquifer compressibility and it can be written as a function of hydraulic head and of the specific storage S_S [L^{-1}] (see, for example, Tindall and Kunkel, 1999):

$$\frac{\partial(\rho n)}{\partial t} = \rho S_S \frac{\partial H}{\partial t} \tag{11}$$

Using equation 11, equation 10 becomes:

$$-\frac{\partial q_x}{\partial x} - \frac{\partial q_y}{\partial y} - \frac{\partial q_z}{\partial z} + R = S_S \frac{\partial H}{\partial t} \tag{12}$$

Finally, substitution of Darcy's law (equations 7) in equation 12 gives:

$$-\frac{\partial}{\partial x}\left(k_{xx}\frac{\partial H}{\partial x}\right) - \frac{\partial}{\partial y}\left(k_{yy}\frac{\partial H}{\partial y}\right) - \frac{\partial}{\partial z}\left(k_{zz}\frac{\partial H}{\partial z}\right) + R = S_S \frac{\partial H}{\partial t} \tag{13}$$

Equation 13 can be written also in the form:

$$\overline{\nabla} \cdot \overline{\overline{k}} \cdot \overline{\nabla} H + R = S_S \frac{\partial H}{\partial t} \tag{14}$$

Where $\overline{\overline{k}}$ is the matrix of equation 8 with only the principal components in the diagonal (as the other components are equal to zero).

5.2 Groundwater flow simulation software

MODFLOW is a modular three-dimensional, cell-centred, finite difference groundwater flow code developed by McDonald and Harbaugh (1988) for the United States Geological Survey. The modular structure of MODFLOW consists of a Main Program and a series of highly-independent subroutines called modules. The modules are grouped in packages and each package performs a specific task. Some of these tasks are always required for a simulation and some are optional (McDonald and Harbaugh, 1988).

The Groundwater Modelling System (GMS) graphical user environment has been chosen. The entire GMS system consists of a graphical user interface (the GMS program) and a number of analysis codes (including MODFLOW).

5.2.1 Mathematical background

As MODFLOW is a block-centred, finite difference code, the aquifer system is divided into cells with rectangular faces and nodes that lie in the centre of these cells. These cells form rows, columns and layers. Figure 29 shows cell i,j,k and six adjacent aquifer cell, where i is referred to the row index, j to the column index and k to the layer index.

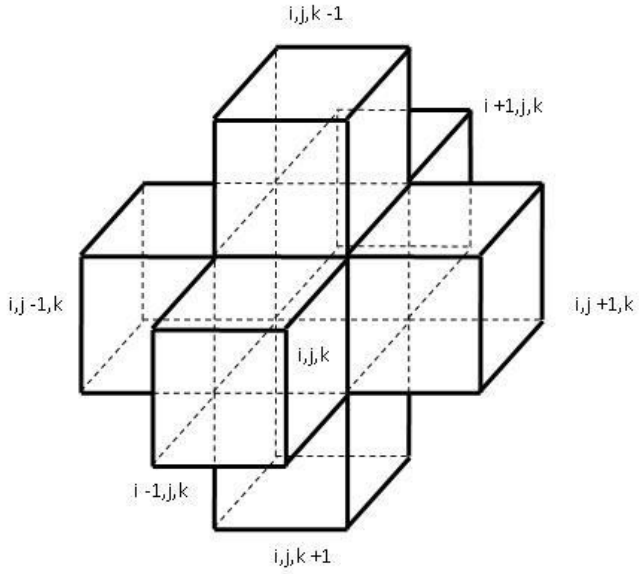

Figure 29. Three dimensional discretization in MODFLOW (McDonald and Harbaugh, 1988).

MODFLOW computes the flow from a cell to the neighboring ones with Darcy's law. Considering the flow between two cells in the row direction (Figure 30), the discrete form of equation 7 multiplied with the cell face gives:

$$q_{i,j-1/2,k} = kR_{i,j-1/2,k}\Delta c_i \Delta v_k \frac{\left(H_{i,j-1,k} - H_{i,j,k}\right)}{\Delta r_{j-1/2}} \qquad (15)$$

where:

$q_{i,j-1/2,}k$ volumetric fluid discharge through the face between cells i,j,k and i,j-1,k [L^3T^{-1}];

$kR_{i,j-1/2,k}$ hydraulic conductivity along the row between node i,j,k and node i,j-1,k [LT^{-1}];

Δc_i width of cells along columns [L];

Δv_k width of cells along rows [L];

$\Delta r_{j-1/2}$ distance between nodes i,j,k and i,j-1,k [L];

$H_{i,j-1,k}$ hydraulic head in cell i,j-1,k [L];

$H_{i,j,k}$ hydraulic head in cell i,j,k [L].

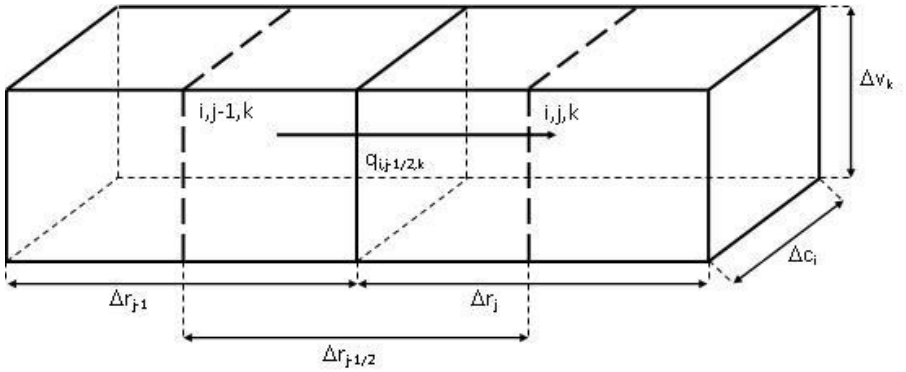

Figure 30. Flow from cell i,j-1,k into cell i,j,k (McDonald and Harbaugh, 1988).

In equation 15 the grid dimensions (Δc_i, Δv_k and $\Delta r_{j-1/2}$) and the hydraulic conductivity ($kR_{i,j-1/2,k}$) are constant and can be combined into a single constant called conductance:

$$CR_{i,j-1/2,k} = kR_{i,j-1/2,k}\frac{\Delta c_i \Delta v_k}{\Delta r_{j-1/2}} \tag{16}$$

Equations 15 and 16 can be rewritten also for the column and layer directions as to obtain similar expression for the conductance along column $CC_{i-1/2,j,k}$ and along layer $CV_{i,j,k-1/2}$. The vertical conductance, however, is calculated using these equations if both cells are saturated. In this case MODFLOW computes the vertical flow using equation 15 written for the vertical direction:

$$q_{i,j,k+1/2} = CV_{i,j,k+1/2}\left(H^m_{i,j,k+1} - H^m_{i,j,k}\right) \tag{17}$$

As mentioned before, MODFLOW solves equation 13 using the finite difference method and for each node the finite difference equation is written:

$$CR_{i,j-1/2,k}\left(H^m_{i,j-1,k} - H^m_{i,j,k}\right) + CR_{i,j+1/2,k}\left(H^m_{i,j+1,k} - H^m_{i,j,k}\right) +$$

$$CC_{i-1/2,j,k}\left(H^m_{i-1,j,k}-H^m_{i,j,k}\right)+CC_{i+1/2,j,k}\left(H^m_{i+1,j,k}-H^m_{i,j,k}\right)+$$
$$CV_{i,j,k-1/2}\left(H^m_{i,j,k-1}-H^m_{i,j,k}\right)+CV_{i,j,k+1/2}\left(H^m_{i,j,k+1}-H^m_{i,j,k}\right)+$$
$$P_{i,j,k}h^m_{i,j,k}+Q_{i,j,k}=S_{Si,j,k}\left(\Delta r_j\Delta c_i\Delta v_k\right)\frac{\left(H^m_{i,j,k}-H^{m-1}_{i,j,k}\right)}{t_m-t_{m-1}} \tag{18}$$

where:

$CR_{i,j-1/2,k}$ conductance in row i and layer k between nodes i,j-1,k and i,j,k [L^2T^{-1}];

$CC_{i-1/2,j,k}$ conductance in column j and layer k between nodes i-1,j,k and i,j,k [L^2T^{-1}];

$CV_{i,j,k-1/2}$ conductance in row i and column j between nodes i,j,k-1 and i,j,k [L^2T^{-1}];

t_{m-1} beginning of the time interval [T];

t_m end of the time interval [T];

$\Delta r_i\Delta c_j\Delta v_k$ cell volume [L^3];

$H^m_{i,j,k}$ head in node i,j,k at time m [L];

$P_{i,j,k}$ sum of head-dependent source and sink terms [L^2T^{-1}];

$Q_{i,j,k}$ sum of constants source and sink terms [L^3T^{-1}];

$S_{Si,j,k}$ specific storage [L^{-1}];

Equation 18 can be rewritten as:

$$-\left[CR_{i,j-1/2,k}+CR_{i,j+1/2,k}+CR_{i-1/2,j,k}+CR_{i+1/2,j,k}+CR_{i,j,k-1/2}+CR_{i,j,k+1/2}+P_{i,j,k}+S_{Si,j,k}\frac{\left(\Delta r_j\Delta c_i\Delta v_k\right)}{t_m-t_{m-1}}\right]H^m_{i,j,k}+$$
$$+CR_{i,j-1/2,k}H^m_{i,j-1,k}+CR_{i,j+1/2,k}H^m_{i,j+1,k}+CC_{i-1/2,j,k}H^m_{i-1,j,k}+CC_{i+1/2,j,k}H^m_{i+1,j,k}+CV_{i,j,k-1/2}H^m_{i,j,k-1}+$$
$$+CV_{i,j,k+1/2}H^m_{i,j,k+1}=-Q_{i,j,k}-S_{Si,j,k}\frac{\left(\Delta r_j\Delta c_i\Delta v_k\right)}{t_m-t_{m-1}}H^{m-1}_{i,j,k} \tag{19}$$

Equation 19 applies to an arbitrary node i,j,k and it involves the head at the node itself and the heads at the six neighboring nodes. Therefore writing an equation similar to 19 for each node results in N equations with N unknown head values to be determined, where N is the total number of nodes. The general form of these equations, written in matrix form is:

$$\overline{\overline{A}}\,\overline{H}=\overline{q} \tag{20}$$

where:

$\overline{\overline{A}}$ matrix containing coefficients related to grid spacing (Δci, Δvk and Δrj) and to aquifer properties (S_{Sijk}, CR , CC and CV);

$\overline{H}$ vector of head (dependent variable to be determined);

$\overline{q}$ vector of the terms constant during Δt that are written for all nodes in the mesh;

MODFLOW solves this equations numerically with an iterative method: the head is calculated by iterating for all nodes until an error criterion is attained. Once this criterion is met, calculations for the next time step t_m are initiated and the final head values computed for the time step t_{m-1} then become the fixed-head values in the storage term used to calculate heads at time step t_m.

5.2.2 Used Packages

A package is a group of modules that deals with a single aspect of the simulation. The packages that are always required for a simulation are the Basic Package, the flow Package and a solver Package, while the others are optional. The package used in this study, described in the followings, are:

- the Basic Package;
- the LPF flow Package;
- the PCG2 solver Package;
- the Recharge Package
- the Well Package;

The Basic Package handles the administrative tasks for the model. Among these tasks are computational time intervals (time steps), spatial discretization, specification of initial and boundary conditions and of the packages to be used, budget calculations and control of the output results.

The Layer Property Flow Package (LPF) performs the cell by cell flow (see Figure 30). The vertical and horizontal hydraulic conductivity are defined as input data for each layer of the model and then this package computes the celle by cell conductance using the k values and the layer geometry. Moreover, also anisotropy values can be entered on a cell by cell basis. Two layer types can be used: confined and convertible. A convertible layer can be either confined or unconfined depending on the elevation of the computed water table.

The Preconditioned Conjugate Gradient (PCG2) solver Package was used. The Solver Package takes the data from the other packages and solves iteratively equations 20 as to obtain hydraulic head and groundwater flow at each node. This solver uses the preconditioned conjugate-gradient method to solve equations.

The Recharge Package is used to simulate a spatially-distribute recharge to the aquifer due to rainfall and infiltration. The recharge is expressed in terms of flow rate per unit area, then the volumetric rate of flow into a cell is given by the following equation:

$$Q_{R_{i,j}} = I_{i,j} \cdot \Delta r_j \cdot \Delta c_i \tag{25}$$

where:

$Q_{R_{i,j}}$ recharge flow rate applied to the model at cell i,j [L^3T^{-1}];

$I_{i,j}$ recharge flux in cell i,j [LT^{-1}];

$\Delta r_j \cdot \Delta c_i$ area of cell i,j [L^2];

The well module simulates volumetric rate discharge (or recharge) from (or to) a cell of the aquifer. This flow is not head-dependent but it is specified by the user. The only input required is the column, row, layer and rate of discharge in L^3T^{-1} for each stress period. A negative rate indicates withdrawal and will result in drawdown, while a positive value indicates a recharging well. As the rate is not affected by the head in the aquifer or by the cell area, the recharge rate is added to the term $Q_{i,j,k}$ of the finite-difference equation (equation 17) as an external source.

5.2.3 Karst modeling

As described before, MODFLOW mathematical theory is based on Darcy equations governing groundwater flow in a porous medium, therefore the code seems not suitable to simulate flow in fractures and karst.

Darcy law based mathematical model can be used as a reliable tool to simulate groundwater flow in fractured media whether it is possible to assume that homogeneous properties occur on a sufficiently large scale and then the average behavior of the aquifer can be represented. In this case, the weathered and fractured rock layer may be modeled as an equivalent porous media and the hydraulic conductivity set in the model represents the bulk properties of the fractured rock.

Whereas, if local scale groundwater flow in fractures or karst conducts has to be modeled, the previous approach cannot be used. Therefore, other models that take into account flow theory suitable to this case should be used. Usually, code developed to simulate also fracture and karst flow are based on finite element method, that can be more appropriate to represent the system complexity.

Nevertheless, the purpose of this study is to simulate aquifer behavior at a large scale without claiming to represent flow at fracture or conduit detail. Therefore, some equivalent method can be used to simulate fracture and karst conduits behavior to overcome the limitations of the Darcy law based code MODFLOW. For example, high conductive cells or the drain package can be used, reminding that detailed characteristics of flow within fractures or conduits cannot be simulated using this approach.

5.3 Model Description

The hydrogeological model was built by using the "conceptual model approach" provided by GMS interface. This tool leads to implement a groundwater model by using a GIS environment to develop a conceptual model where layer parameters distribution, model boundaries, source and sinks and all other data needed for the simulation can be defined at the conceptual model level by creating features objects. Once the conceptual model is completed, the grid is generated and the all data defined previously are assigned automatically to each cell of the grid. Moreover, feature objects needed to create the model can be imported as shape files using GIS module.

Sometimes, numerical modeling is used to identify the best among a set of alternative conceptual models (Poeter et al., 2005 and Wondzell et al., 2008). As already mentioned in paragraph 4.7, this is the purpose of the aquifer mathematical modeling performed. Taking into account uncertainly in aquifer conceptualization, especially regarding inflow from western Nurra, two different conceptual models were developed and their results were compared.

Therefore, two different models were simulated that have in common the same input data except for the boundary conditions:

- conceptual model n. 1 (CM1) doesn't simulate any inflow from Easter Nurra;
- conceptual model n. 2 (CM2) simulates inflow from Western Nurra.

Boundary conditions set for the CM1 are:

- first type or Dirichlet boundary condition (fixed hydraulic head) on the North side, simulating the limit of the model corresponding to the coastline and assuming a constant head of 0 m a.m.s.l.;
- second type or Neumann boundary condition (fixed flux) on the remaining limits of the study area, simulating a no flow limit corresponding to flow line or to impermeable border.

The CM2 boundary conditions were the same of the CM2, except for Eastern limit of the model, where a stretch of the limit was simulated with a fixed flow entering the model domain.

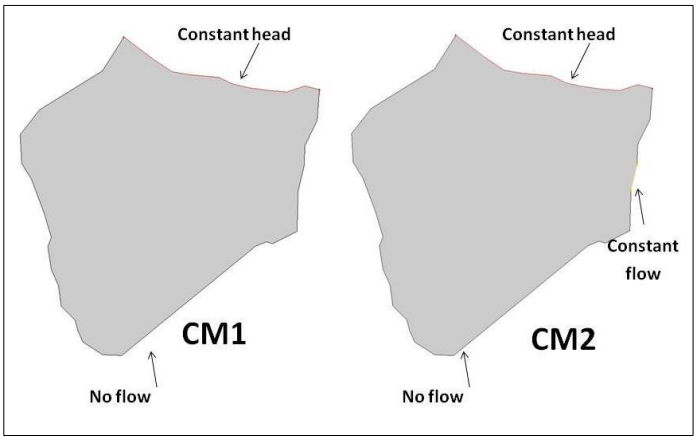

Figure 31. Boundary conditions for conceptual models 1 and 2.

A tree-dimensional grid was used to represent the aquifer system. The model domain consists of three layers (z-direction), 69 columns (x-direction) and 74 rows (y-direction). The grid space is uniform and it is equal to 100 meters both in x and y directions. All layers were simulated as convertible between confined and unconfined.

The upper domain boundary was defined by topographic data interpolating the gound surface to the MODFLOW grid, while lower boundary was taken at -200 m b.m.s.l..

The constant flow boundary condition of CM2 was assigned to the lower layer as to simulate deep groundwater inflow to the model domain.

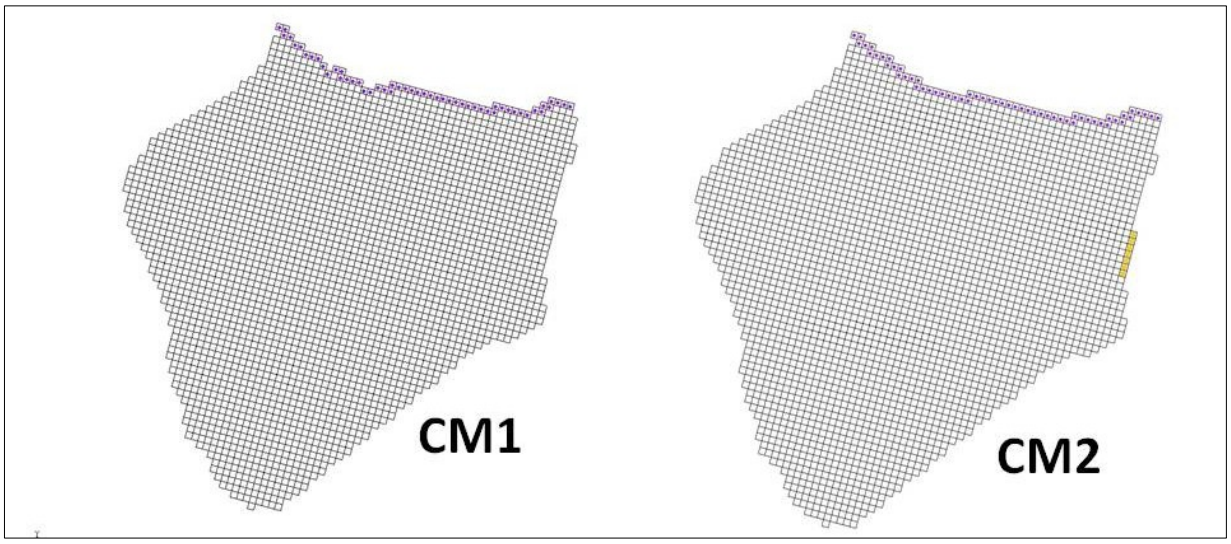

Figure 32. Model grid for conceptual models 1 and 2.

Hydraulic conductivity was assigned to layers cells considering the lithostratigraphic information coming from the three-dimensional schematization of aquifer domain performed in GMS. The values assigned are (Ghiglieri et al., 2006):

- K= 10^{-4} m/s for the Jurassic complex;
- K= 10^{-6} m/s for the Triassic complex;
- K= 10^{-6} m/s for the Miocene carbonate complex;
- K= 10^{-8} m/s for the Oligo-Miocene volcanic complex;
- K= 10^{-8} m/s for the Miocene clay.

Fractures and karst conduit flow were simulated using high conductivity cells, two orders of magnitude higher than Jurassic complex (10^{-2} m/s).

Aquifer high conductive cells simulated were placed from the constant flow boundary condition to the Fiumesanto springs trough the Triassic outcrops located on the South of the industrial zone. In fact, this is the aquifer sector assumed to be characterized by high amount of groundwater flow.

Recharge rate was applied to the upper layer and its amount was calculated based on meteorological data and on infiltration coefficient of different lithological formations (see paragraphs 1.1 and 6.3).

5.4 Model simulation and calibration

Groundwater flow simulation was run under steady state conditions. Therefore, the model was calibrated to reproduce the average water level conditions.

Measurement data available to calibrate the model were:

- piezometric head measurements acquired during the RIADE project (Ghiglieri et al., 2006) concerning only the Southern part of the study area for the period September-December 2004 (see Appendix C);
- piezometric head measured in July 2008 at industrial zone and surrounding areas (RAS);
- piezometric head measured at Fiumesanto power station for the purposes of this work (January 2007 and February 2008, see appendix C);
- discharge values of Fiumesanto springs recorded by Fiumesanto power station company during 1978-1971.

In order to provide some assurance that the model reflects the behavior of the flow system, calibration procedure is performed matching model results to observed data. As a piezometric head measurements covering the whole study area is not available, model resulted from calibration may be not enough reliable to correctly represent the aquifer system. Therefore, calibration procedure was done using both piezometric head to reproduce the aquifer behavior and spring discharge values to verify aquifer outputs.

Model calibration was performed using trial and error method. Thus, hydraulic conductivity was altered (within reasonable ranges typical of lithological formation present at the study area) based on pezometric map as to obtain a good agreement between the computed and measured behavior of the system. Finally, water balance was calculated for cells at the mouth of Fiumesanto stream as to compare the outflow of the model with the rate discharge typical of Fiumesanto springs.

The contour lines simulated by MODFLOW for CM1 are shown in Figure 33. Results are referred to the carbonate aquifer and reflect the assumption that the main discharge area of the aquifer corresponds to the Fiumesanto mouth area.

Water balance resulted from CM1 model simulation was computed both for the entire model and for local cell groups as to compare outputs with measured data.

The total recharge rate entering the model domain is $6.2 \cdot 10^6$ m^3/year and the outflow computed by the model at the Fiumesanto mouth is about $3.1\ 10^6$ m^3/year. Therefore, as discharge rates at Fiumesanto springs that in seventies had an average of about 130 l/s, corresponding approximately to $4.1\ 10^6$ m^3/year, it can be subtracted that, although the model was set to simulate the higher discharge rate to Fiumesanto mouth, discharge values were not achived by model simulation.

Moreover, quantifying abstraction discharge authorized from industrial wells leads to a total amount of water of about $21.4\ 10^6$ m^3/year showing that water abstracted is rather higher than water infiltrated. Therefore, the comparison made for model results and measured data evidences that an inflow should occur from adjacent aquifer sectors as to justify groundwater outflows.

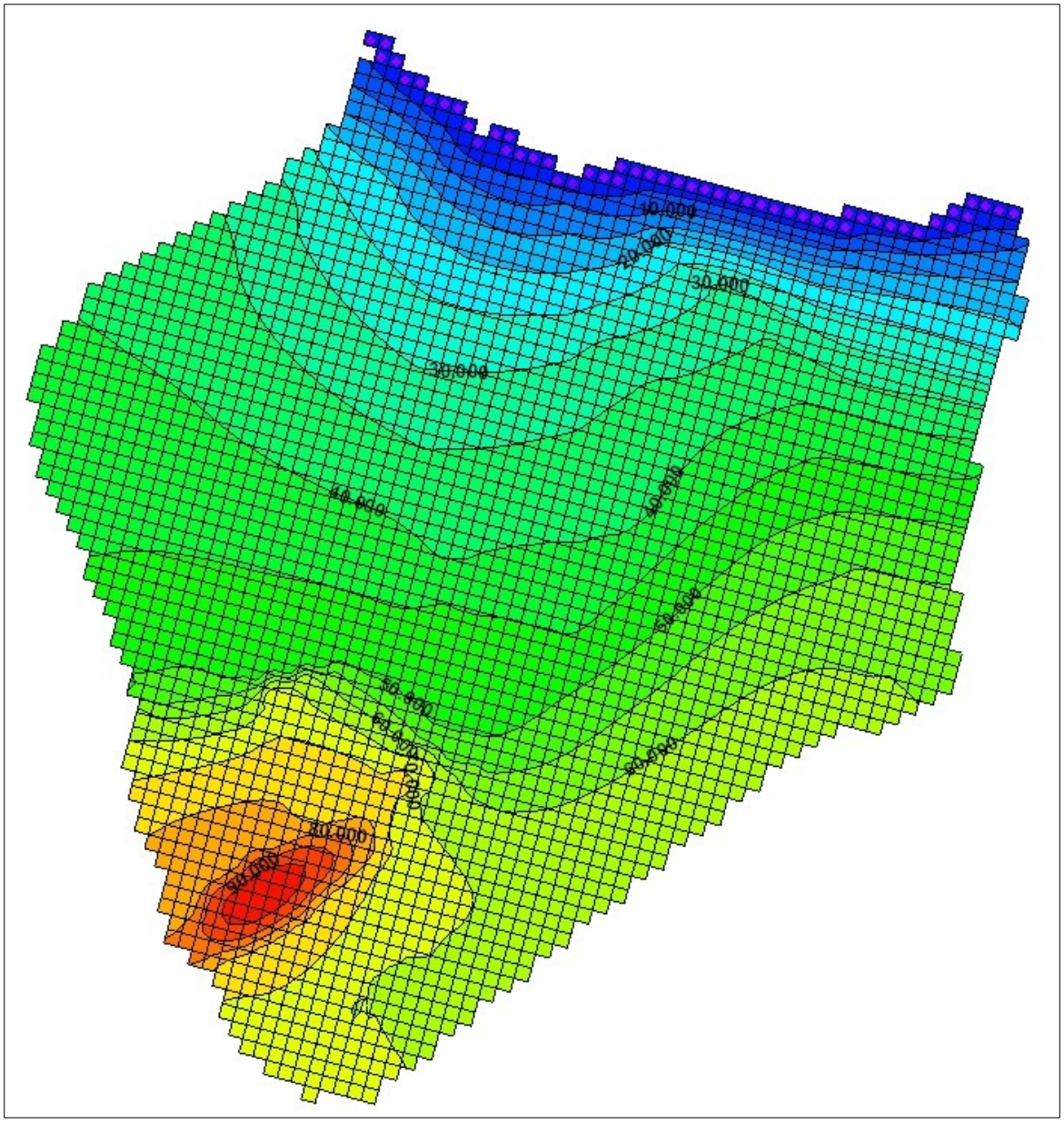

Figure 33. Simulated groundwater level for CM1 (meters).

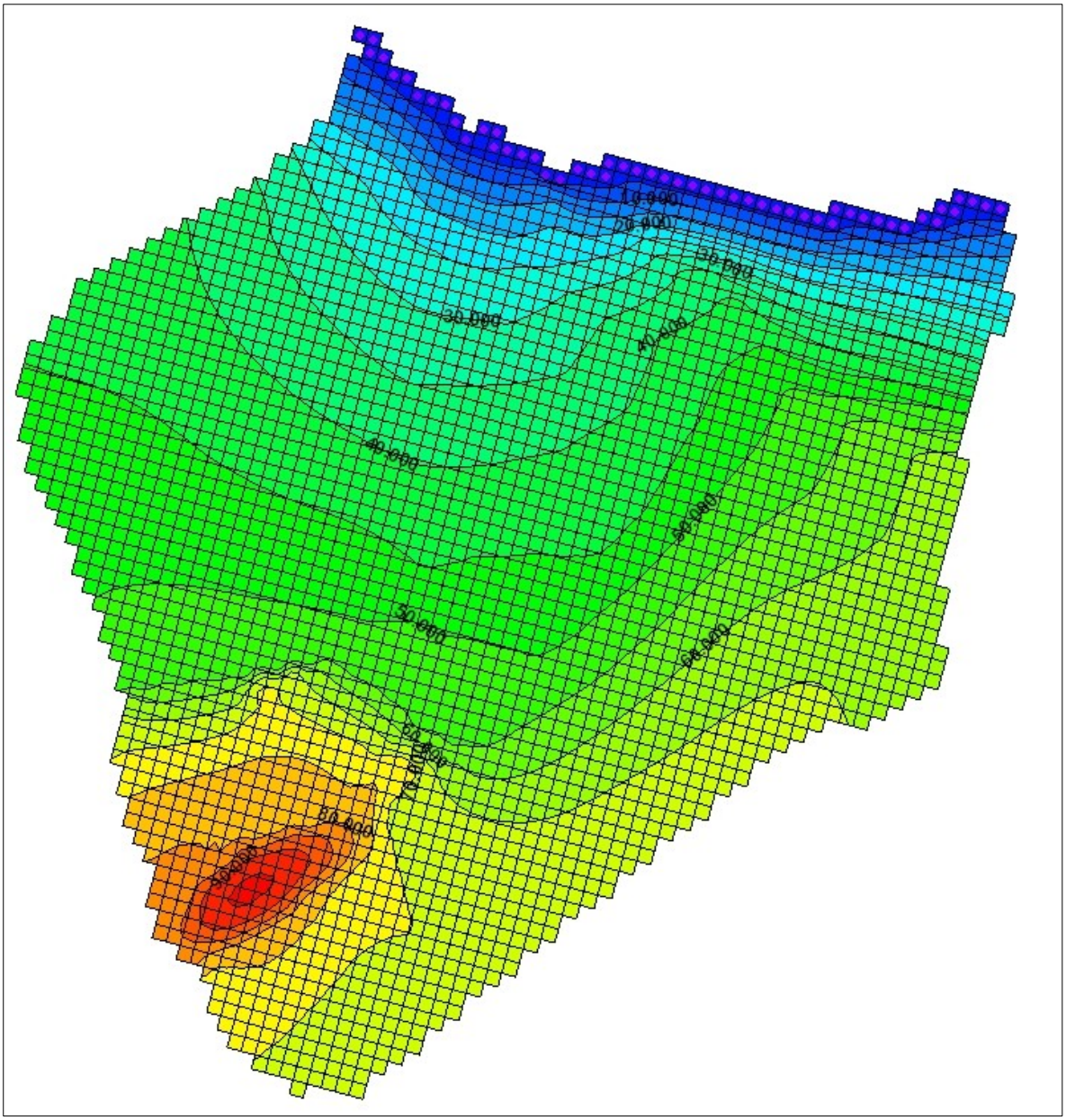

Figure 34. Simulated groundwater level for CM2 (meters).

Consequently, CM2 model was set as to simulate an inflow rate that best fits water balance data.

CM2 piezometric head simulated is shown in Figure 34. This model was run setting an inflow rate at the Eastern boundary (modeled as constant flow boundary condition) of 13.1 10^6 m^3/year.

Contour lines simulated for CM2 show higher values particularly for North-Eastern where it is assumed to occur the inflow to the model. The main groundwater movement flows North-Westward in the Northern and Eastern part of the model and Northward in the Southern part.

Water balance computation related to Fiumesanto mouth resulting from CM2 model outputs gives a groundwater discharge of about 4 m^3/year, that can be representative of the average values for this aquifer sector.

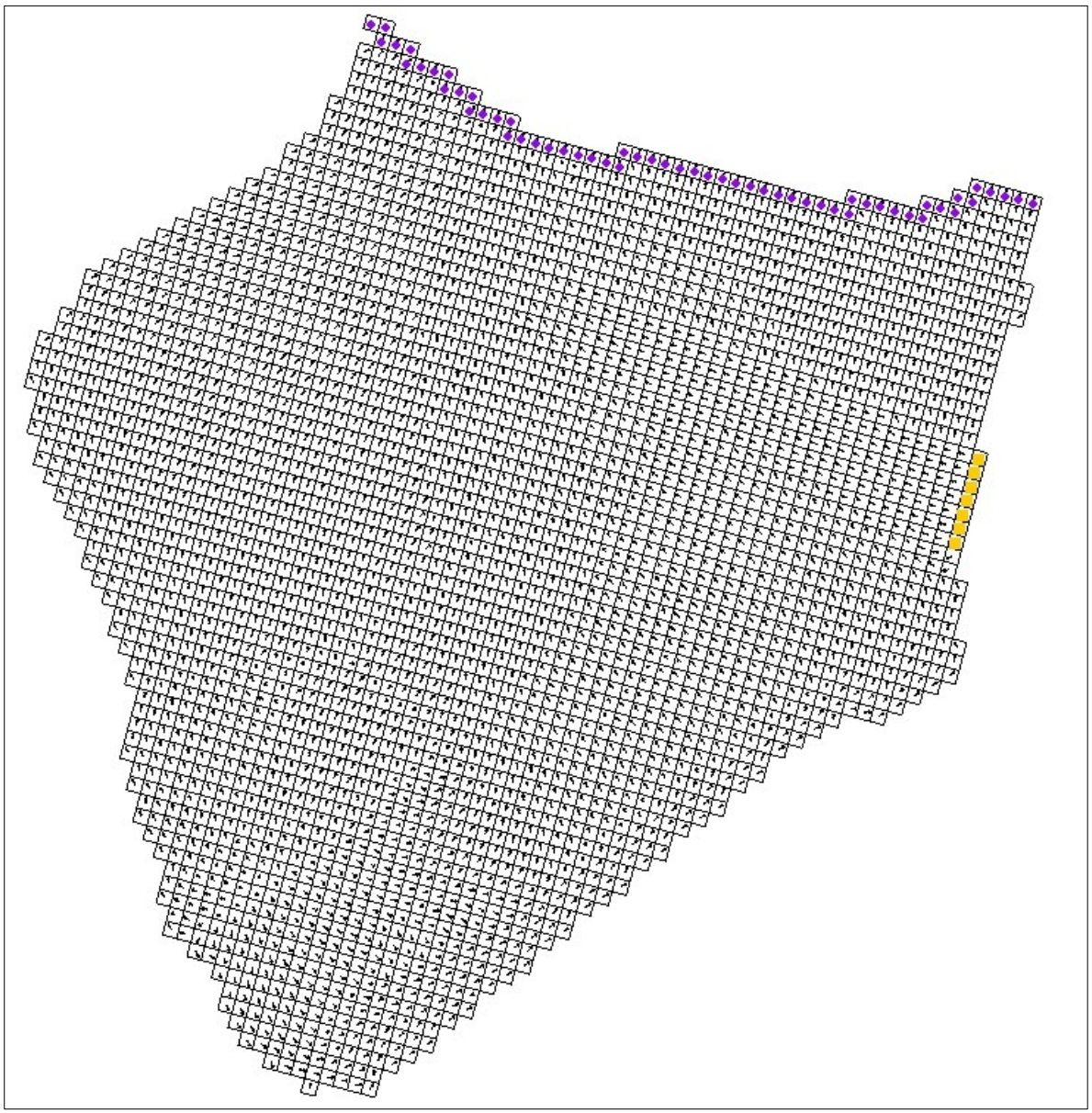

Figure 35. Flow direction simulated by CM2 model.

In conclusion, groundwater model performed doesn't claim to simulate detailed aquifer system but anyway was useful:

- to confirm that the more reliable aquifer system supposes a water inflow from East and to estimate this amount of water;
- to reproduce a piezometric map that best approximate the average values needed for vulnerability assessment;
- to reproduce flow map, therefore direction and magnitude of flow are given for each cell. This is useful as input data for vulnerability assessment purposes, representing high conductive pathways useful to estimate karst aquifer characteristics and factors;
- to define hydraulic conductivity that best reflects groundwater behavior, obtained through calibration, that can be used for related SINTACS parameter evaluation.

Moreover, the simulation and water balance analysis let arise some limitations of the model and highlight possible improvement of the groundwater model implemented. In particular, data that should be better evaluated as to improve groundwater simulation reliability are:

- infiltration rate may be evaluated more detailed, as to take into account karst aspects that influence the amount of water evaporated and the amount of effective infiltration;
- hydraulic head monitoring regarding the whole area, for both wet and dry season, would be useful to perform more detailed calibration procedures;
- pumping test needed to evaluate aquifer hydraulic parameters;
- kast conduits and fractures setting.

6 Vulnerability Assessment

6.1 Method

Intrinsic aquifer vulnerability is defined as the specific susceptibility of aquifer system, in their various parts and in the various geometric and hydrodynamic settings, to ingest and diffuse fluid and/or hydro-vectored contaminants whose impact on the groundwater quality is a function of space and time (Civita, 1987).

Intrinsic vulnerability assessment and cartography are instruments useful to inform groundwater protection strategies. Within this study, vulnerability assessment is used to highlights the exposure degree of the study area.

SINTACS method (Civita et al., 1997) was chosen to evaluate the intrinsic vulnerability to pollution of the Mesozoic aquifer in the study area. SINTACS parameters datasets were evaluated using GIS tools and results coming from groundwater modeling.

All layers needed to perform vulnerability assessment were represented using raster maps where the pixel dimension is related to the EFQ element of the SINTACS method. The pixel dimension was set as 10 meters, in order to have a good degree of precision in distributed parameters representation.

Parameters used to assess vulnerability and relative SINTACS acronyms are:

- groundwater depth (Soggiacenza);
- effective infiltration (Infiltrazione efficace);
- unsaturated zone (Non saturo);
- soil/overburden (Tipologia copertura);
- hydrogeological characteristics of the aquifer (Acquifero);
- hydraulic conductivity (Conducibilità idraulica);
- topographic slope (Superficie topografica).

A rating (from 1 to 10) should be assigned to each parameter for each EFQ as a function of its attenuation capacity with regard to contamination. A rating of 1 correspond to the highest attenuation capacity and a rating of 10 to the lowest attenuation capacity.

The SINTACS vulnerability index, calculated for each EFQ, is given by the sum of the different parameter rating multiplied by a weight given to each parameter as function of its importance in defining vulnerability:

$$I_{SINTACS} = \sum_{i=1}^{7} P_J \, W_J$$

Where P is the parameter rating and W is the weight assigned to each parameter. The weights given to the different parameters are function of the possible scenarios and SINTACS offer 5 weight string. Vulnerability degree of the study area was evaluated using three weight strings, one for each hydrogeological and impacting situations present:

- string one (normal impact scenario), was used for South-Western sector of study area;

- string two (relevant impact) was used for the industrial zone;
- string three (karst) was used for karst areas outcropping.

String one and two describe low topographic slope setting. The first case refers to areas where anthropization is scarce while the second string is related to intensive land use. String three refers to karst areas.

PARAMETER	NORMAL IMPACT	RELEVANT IMPACT	KARST
S	5	5	2
I	4	5	5
N	5	4	1
T	4	5	3
A	3	3	5
C	3	2	5
S	2	2	5

Table 2. Strings of weights for SINTACS parameters (CIVITA et al., 1997).

Vulnerability evaluation degree is done by map algebra procedures in GIS environment using raster datasets of different SINTACS parameters.

The raw score of vulnerability degree ranges between 26 and 260 and six classes are defined by SINTACS method:

- “Bb“ class (score between 26 and 80), very low vulnerability degree;
- “B“ class (score between 80 and 105), low vulnerability degree;
- “M“ class (score between 105 and 140), medium vulnerability degree;
- “A“ class (score between 140 and 186), high vulnerability degree;
- “E“ class (score between 186 and 210), very high vulnerability degree;
- “Ee“ class (score between 210 and 260), extremely high vulnerability degree.

6.2 Groundwater depth

Depth to groundwater is defined as the depth of the piezometric level in comparison with the ground surface and it is of great significance in vulnerability assessment because its absolute value, together with the unsaturated zone characteristics determine the time travel of hydrovectores or fluid contaminants and the time needed for the attenuation process through unsaturated zone. The SINTACS ratings of depth to groundwater therefore decrease together with an increase of depth.

Groundwater depth parameter was evaluated from piezometric head computed by MODFLOW model. The piezometric map simulated was used to compute groundwater depth by subtraction to ground elevation map. The main advantage of using groundwater head simulated by MODFLOW is that piezometric values used are calculated for each cell of the aquifer domain whereas the distribution map of this parameter derives usually by spatial interpolation between measured values.

This procedures was done only for unconfined sectors of the aquifer. Groundwater depth in confined sectors was calculated as the depth of the impervious layer bed by importing data elevation interpolated by three-dimensional schematization in GMS.

The parameter rating is given as function of groundwater depth as shown in Figure 36 and related map is given in Figure 37.

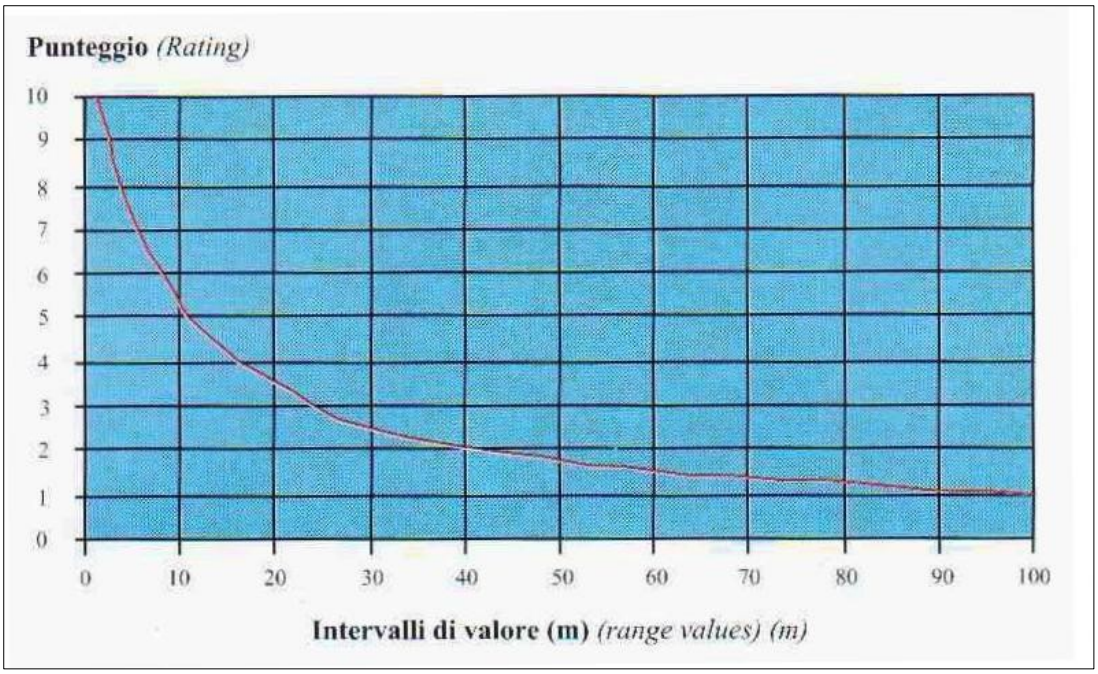

Figure 36. Groundwater depth range values and ratings (Civita et al., 1997).

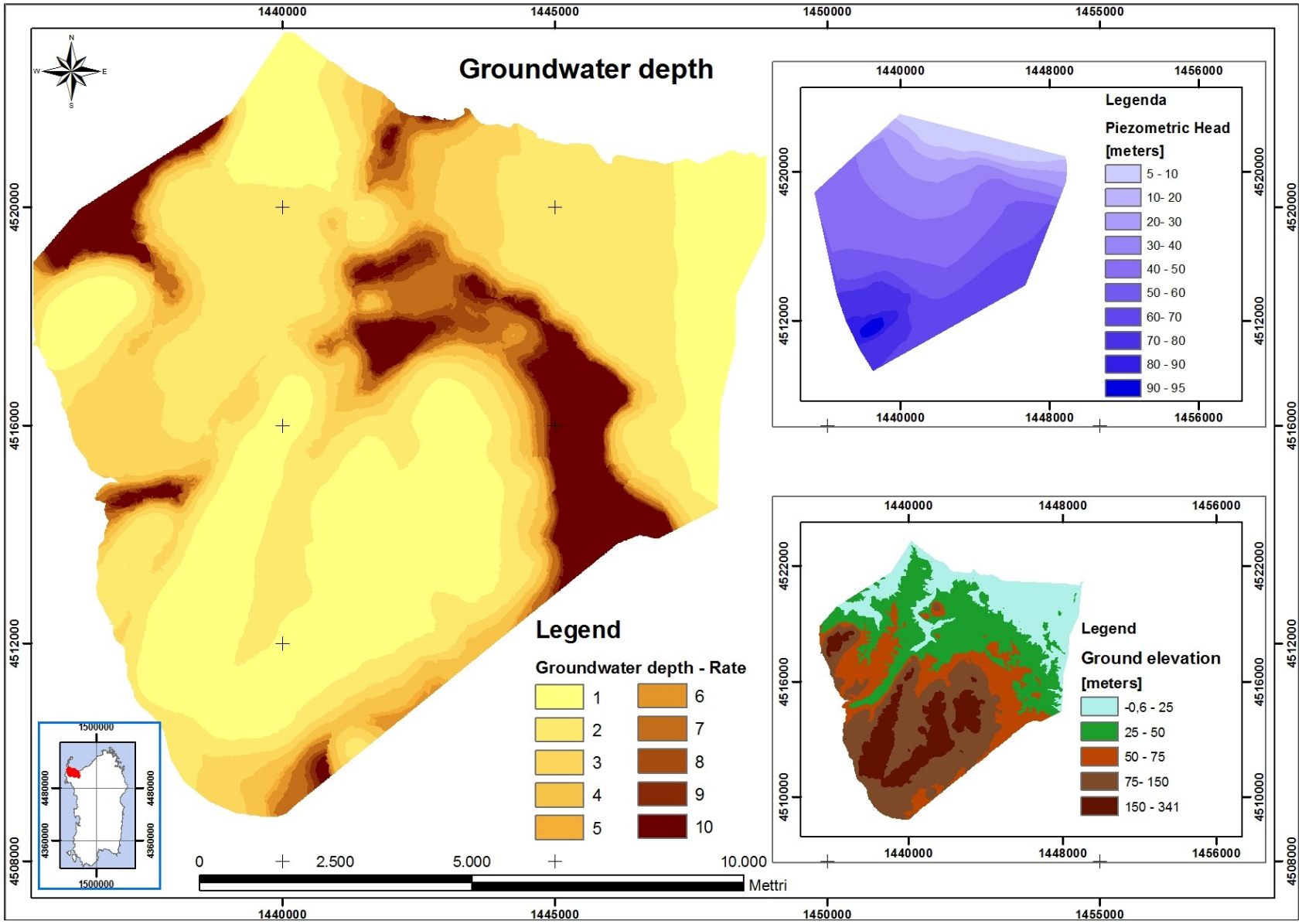

Figure 37. Groundwater depth rating.

6.3 Infiltration

Infiltration is the amount of rainfall which enters the ground surface and reaches the water table. It is important in vulnerability assessment as it represents the vehicle for transporting pollutants to groundwater. Moreover, infiltration rate is related to contamination dilution both in unsaturated and in saturated zone (Civita et al., 1997).

Infiltration rate estimation was evaluated by a simplification of the reverse groundwater balance technique, which is a distributed parameter approach that was implemented using GIS tools. The procedure used to evaluate infiltration rate for each grid cell (EFQ) can be summarize in the following steps (Civita et al., 1997):

- meteorological stations were localized and georeferenced;
- hydrological data needed (temperature and rainfall) were collected and historical series were analyzed and data homogeneity was tested;
- the mean monthly and annual values of temperature and rainfall were computed by taking the 72-year mean of the monthly means;
- correlations between rainfall and elevation, and between temperature and elevation were evaluated, then the relationships found were used to compute parameters values for each EFQ;
- mean elevations, rainfall, evapotranspiration and effective rainfall were computed for each EFQ;
- potential infiltration coefficient was defined based on study area parameters, like lithology, topographic slope, fractures and karst;
- effective infiltration was computed.

Identification and georeferencing of meteorological stations that are representative of the study area (see Figure 5) and hydrological historical series analysis are given in paragraph 3.2.

As the purpose of this evaluation is to obtain a raster dataset of effective infiltration, for each meteorological station, mean annual values of temperatures and rainfall were calculated (see Table 3).

Meteo station	Ground elevation [m s.l.m.]	P[mm]	T[°C]
Sassari	224	583.2	16.2
Olmedo	52	622.1	-
Porto Torres	2	508.9	-
Bancali (ex Macciadosa)	74	630.9	-
Stintino	9	507.6	-
Alghero	7	650.8	16.4

Table 3. Mean annual values of temperatures and rainfall.

Correlations between mean temperature and ground elevation (T=T(q)) and between rainfall and ground elevation (P=P(q)) were estimated and the relationships found were used

to elaborate the raster datasets that give a calculated value of temperature and rainfall for each EFQ. As it is known that temperature value is dependent on precipitation values, "corrected temperature" T_c was calculated using mean monthly values of temperature and precipitation available in those gauge station were both parameters were observed (Alghero and Sassari). The equation used to compute the corrected temperature for each meteorological station is:

$$T_c = \frac{\sum P_i \cdot T_i}{\sum P_i}$$

Where:

- P_i is the mean monthly precipitation;
- T_i is the mean monthly temperature.

Corrected temperatures values were estimated equal to 14,2 °C in Alghero station and 13,8 °C in Sassari station. These values, together with mean annual precipitations were used to compute the relationship between these parameters and ground elevation, as shown in Figure 38 and in Figure 39. The relationships shown are modeled using linear regression function.

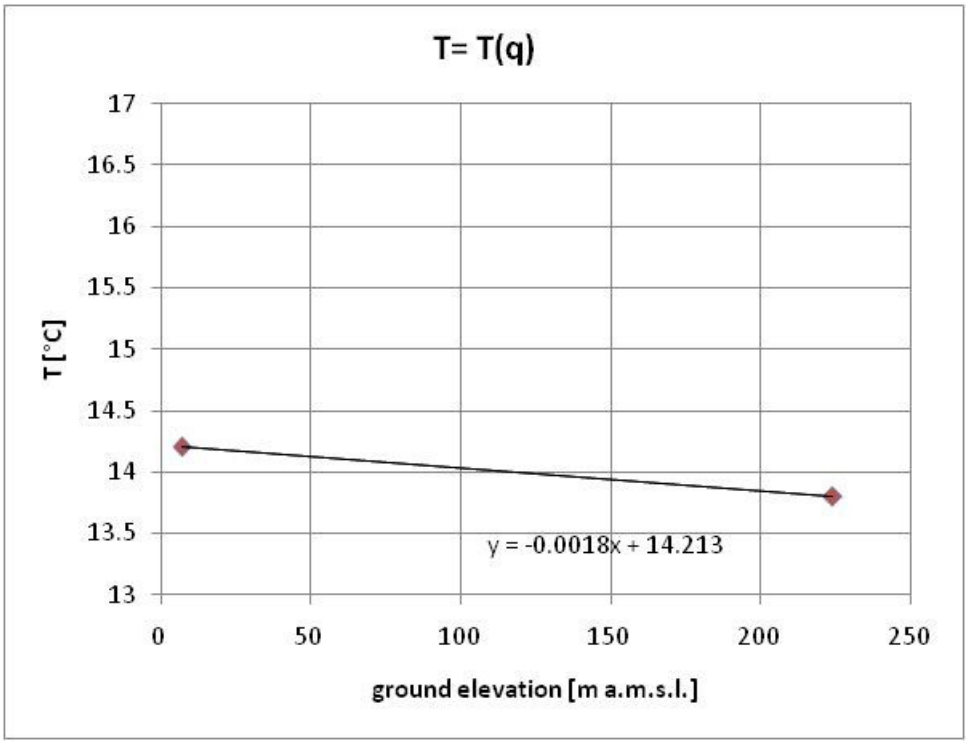

Figure 38. Relationship between temperature and ground elevation.

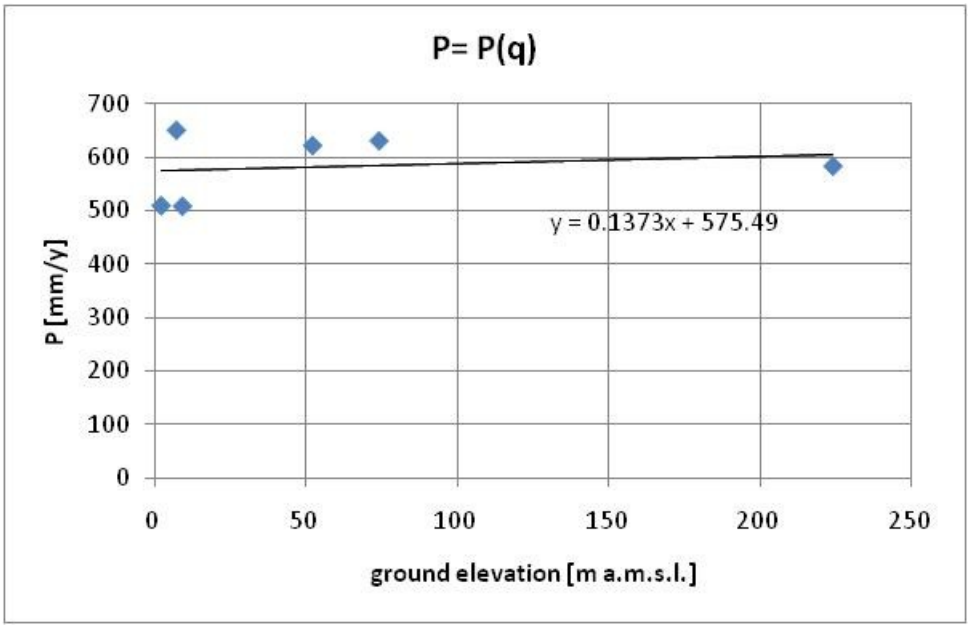

Figure 39. Relationship between precipitation and ground elevation.

Starting from these relationships found, raster datasets of corrected temperature and precipitation were obtained and were used to calculate the mean annual effective evapotranspiration (ET_r) dataset, using the equation proposed by Turc (1954) subsequently modified by Santoro (1970):

$$ET_r = \frac{P}{\sqrt{0.9 + (\frac{P}{L})^2}}$$

Where:

- P is the mean annual precipitation;
- L is the evaporating power of the air.

Evaporating power of the air is computed using the equation modified by Santoro (1970):

$$L=586-10T_c+0.05T_c^3$$

Where T_c is the corrected temperature.

Then, to evaluate SINTACS infiltration parameter, two different approaches are available, according to two different field situations: rock outcropping or thick soil cover.

Under rock outcropping (or limited soil cover) conditions, the amount of effective precipitation Q is calculated:

$$Q=P-ET_r$$

The obtained value is multiplied by the potential infiltration index χ:

$$I=Q\cdot\chi$$

While in the second case, under thick soil cover conditions, the whole value of precipitation is multiplied by the potential infiltration index:

$$I=P\cdot\chi$$

The potential infiltration index is assessed on the basis of the following parameters (Civita et al., 1997):

- surficial lithology (rock outcropping or thick soil cover);
- the hydraulic characteristics of the soil (if it is thicker than 0.5 m);
- the surface slope;
- the relative permeability type of outcropping medium (porous, fractured or karst), that can be expressed by the prevalent grain size, the fracture index or the karst index;
- other refining data that depend on the depth to groundwater, land use, shape and density of surficial draining network.

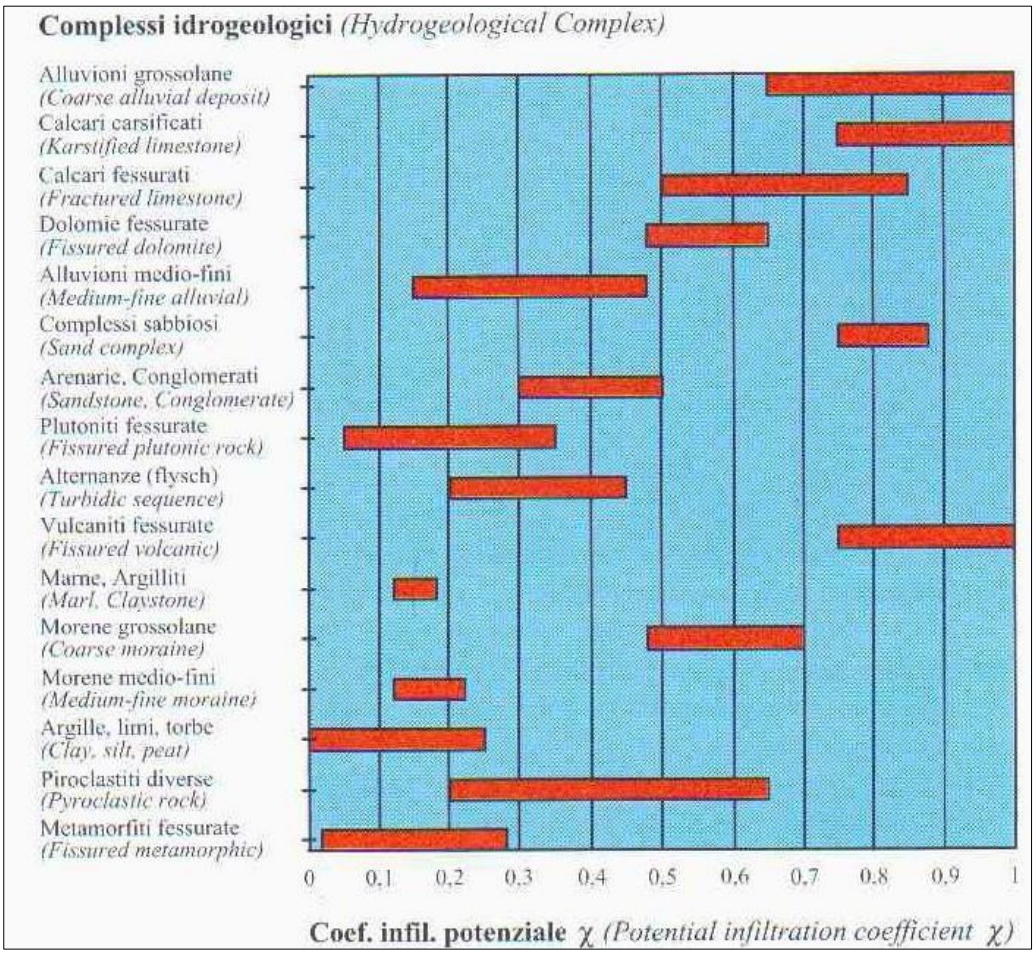

Figure 40. Graph for evaluation of infiltration coefficient for outcropping or lightly overburden rocks (Civita et al., 1997).

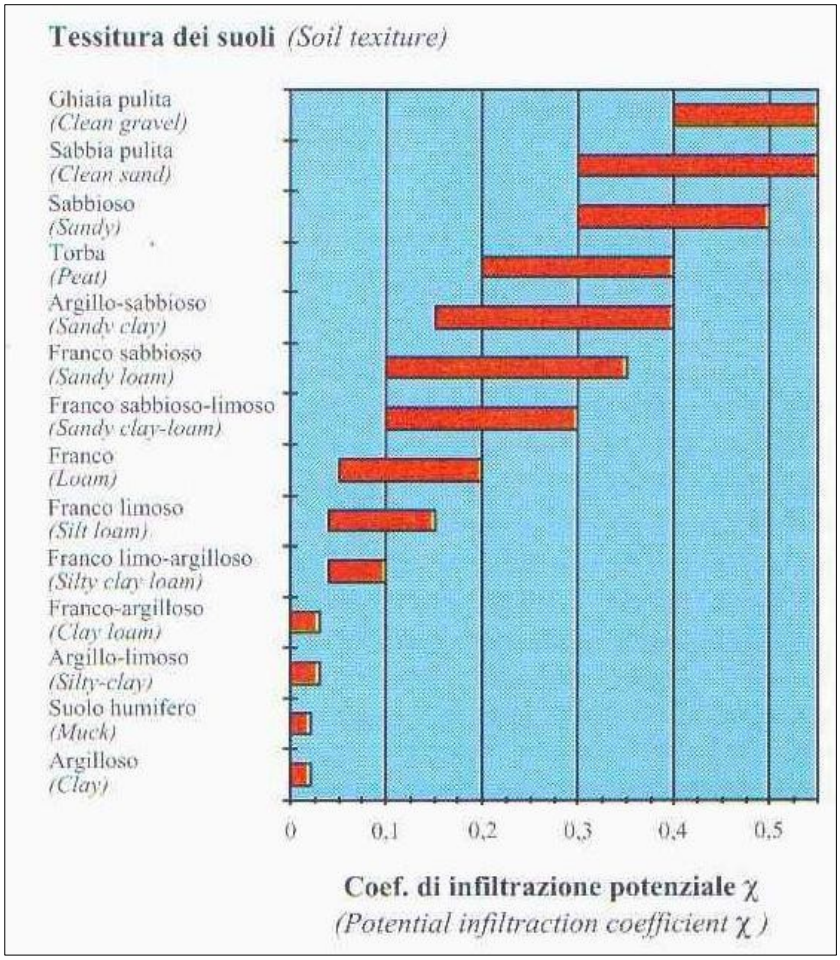

Figure 41. Graph for evaluation of infiltration coefficient for thick soils (Civita et al., 1997).

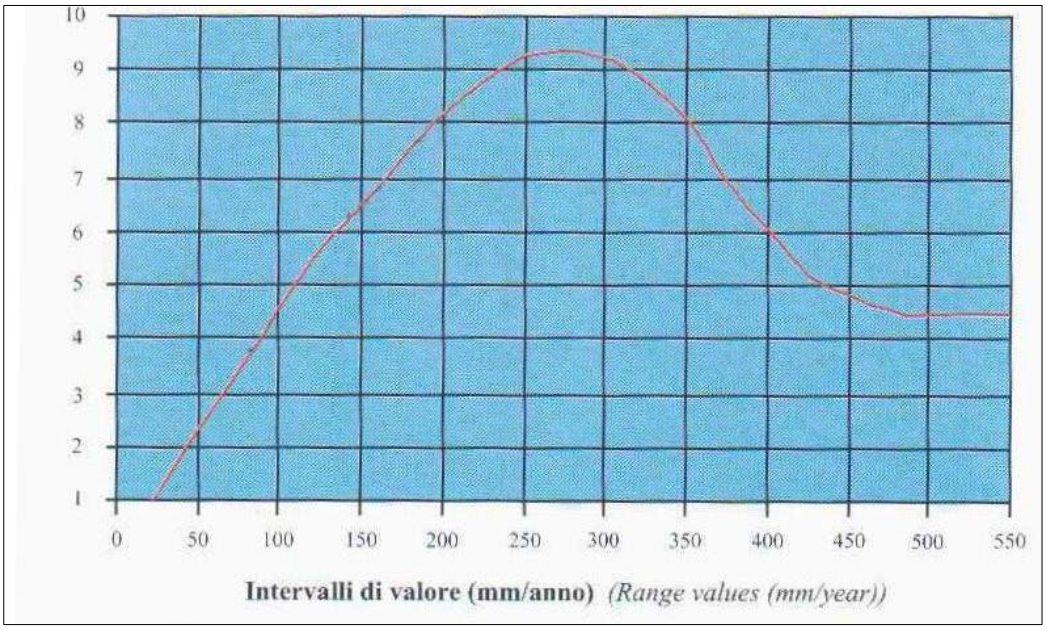

Figure 42. Infiltration range values and ratings (Civita et al., 1997).

Taking into account the parameters described before, the values defined in RIADE project for the same hydrogeological complex (Ghiglieri et al., 2006), and on the basis of range values of Figure 40 and Figure 41 given for the different outcrop formations or soils texture, the values assigned to the potential infiltration index are shown in Figure 25.

Infiltration rating map, computed using the procedure described and on the basis of rating values suggested by SINTACS method (Figure 42), is given in Figure 43.

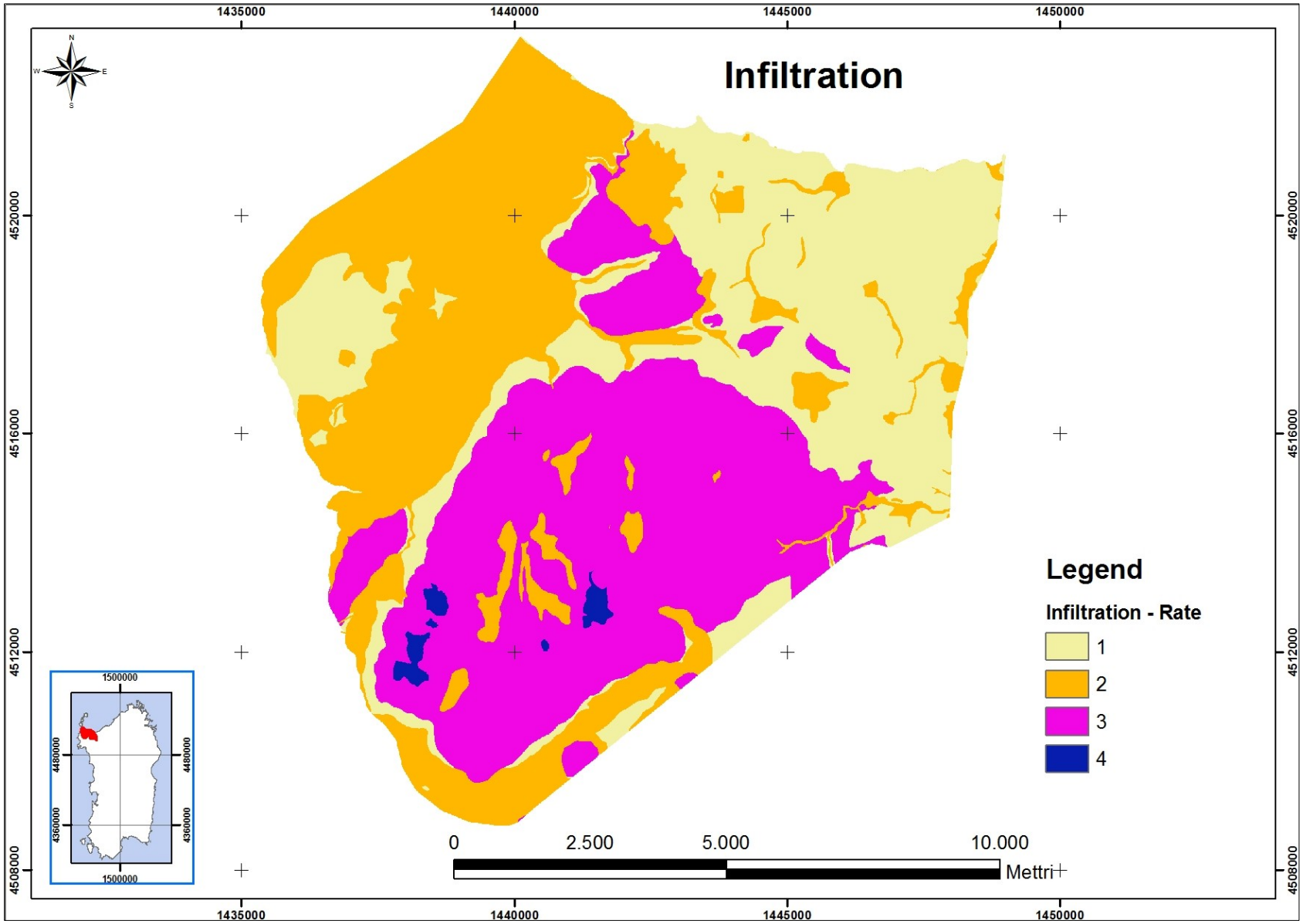

Figure 43. Infiltration rating.

6.4 Unsaturated zone attenuation capacity

Unsaturated zone (or vadose zone) is the subsurface zone of soil or rock that extends from the top of the ground surface to the water table. In unsaturated zone water mainly flows downwards and it is bordered on the bottom by the phreatic surface. Whereas, in confined aquifer, unsaturated zone bottom is taken equal to the confined layer bottom. Consequently, unsaturated zone thickness varies as function of groundwater level in unconfined aquifer.

After soil, unsaturated zone in the second defense line of aquifer system against contamination and it plays an important role in attenuation processes because of physical and chemical processes that take place there. Among these processes the most important are (Civita et al., 1997):

- filtration and dispersion, that depend mainly by grain properties and by thickness and diagenesis of rock medium;
- chemical reactivity of minerals that has an important role in different processes like cations exchange, acid-base reaction, adsorption and desorption;
- biodegradation and volatilization processes, mostly influenced by unsaturated zone thickness.

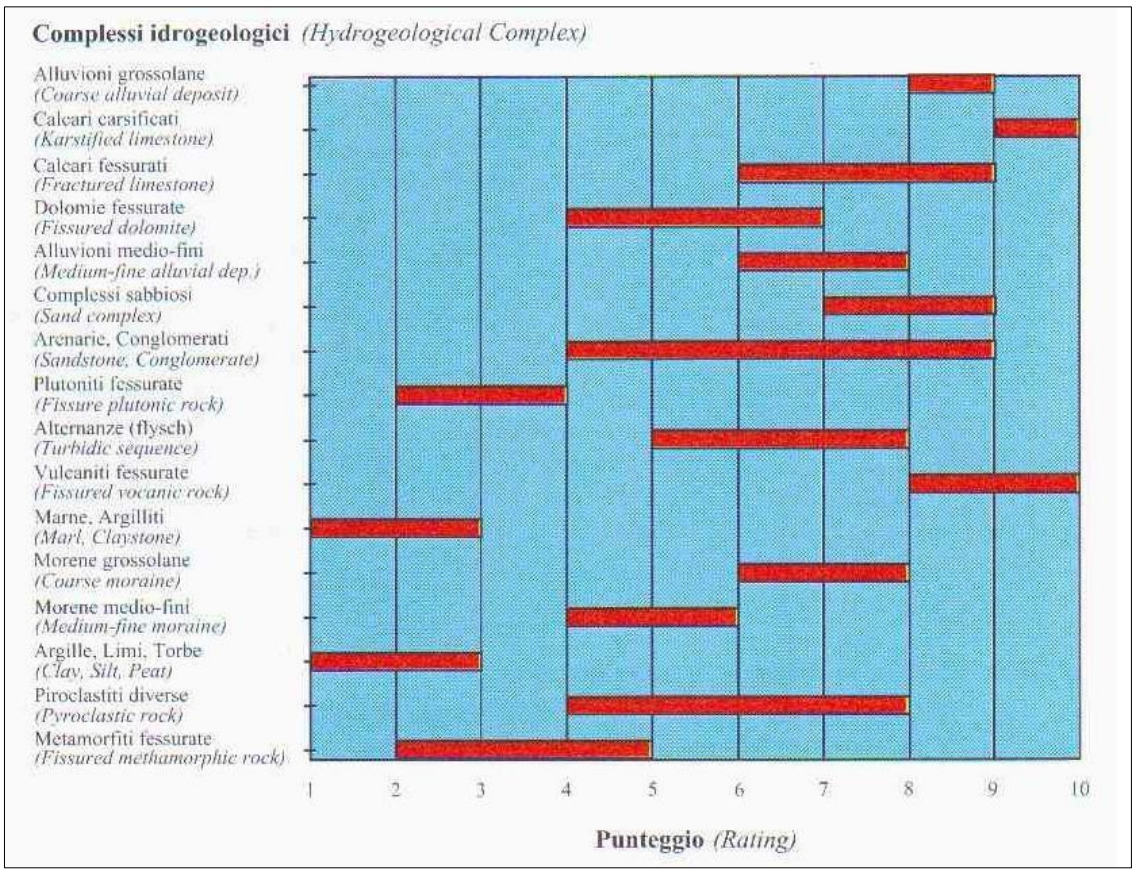

Figure 44. Attenuation capacity of rock media in the unsaturated zone and ratings (Civita et al., 1997).

All these factors are quite easy to be evaluated in soil matrix, whereas unsaturated zone attenuation is harder to be estimated in rock matrix. In the latter case, it can be important to analyze spacing, size, orientation, density and interconnection of fractures.

Fractured rock chemical reaction can be low or nothing, depending on the nature of the rock. Generally magmatites and metamorphic rocks show a lower chemical reaction, while carbonate rock are characterized by higher reaction. It can be important to take into account the possible presence of fracture filling material in carbonate rock that can indeed change the effect of attenuation in unsaturated zone.

Therefore, unsaturated zone attenuation capacity is computed based on the factors and parameters described previously and using range values of rating proposed by SINTACS methodology (see Figure 44) as function of unsaturated lithology (see Figure 45).

When the aquifer is confined, the rating must be 1. The same rating must be given to semiconfined no storage aquitard groundwater bodies whereas if the aquitard has its own storage, it should be considered as part of the unsaturated thickness above the aquifer (Civita et al., 1997).

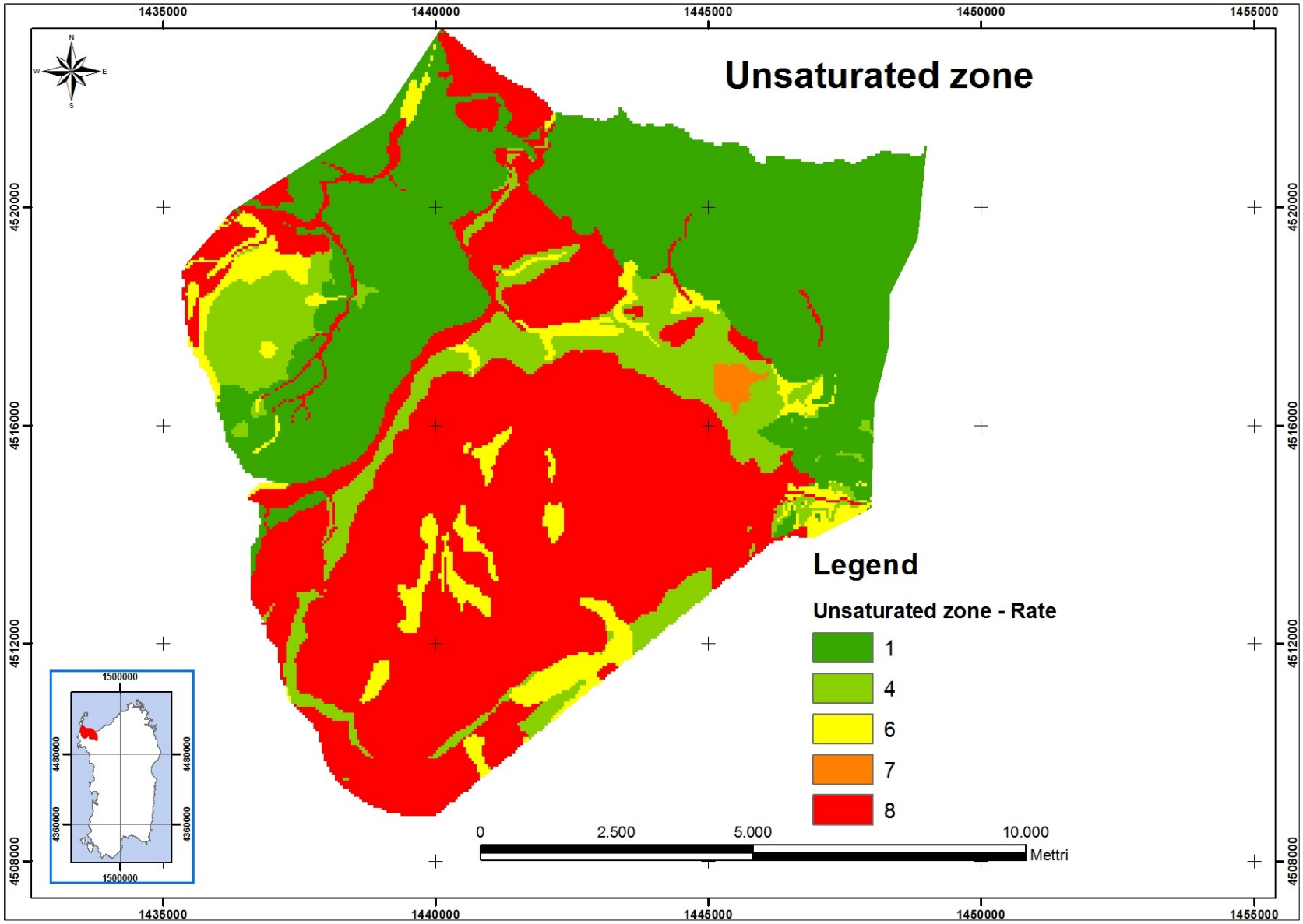

Figure 45. Unsaturated zone rating.

6.5 Soil/overburden attenuation capacity

Overburden type, especially soil, plays an important role in attenuation processes and in groundwater vulnerability assessment. It can be considered the first defense line of the hydrogeological system since important processes related to attenuation capacity take place in it. Soil can be considered as an open, three-phasic accumulator and transformer of matter and energy sub-system that is formed from particles of bedrock lithotypes altered by chemical and physical processes including weathering and erosion (Civita et ali., 1997).

In soil attenuation evaluation it is necessary to take into account two groups of pedologic parameters. The first parameter group are in charge of the effective physic setting and its characteristics, while the second group gathers those parameters that directly affect the soil/water adsorption coefficient K_d.

The first parameters group controls processes like adsorption, filtration, drainage capacity, water content, infiltration velocity, and include grain size, texture, effective depth, bulk density, total porosity, available water content and hydraulic conductivity of the soil.

The second group parameters controls soil adsorption level of a chemical compound and are pH, cationic exchange capacity, organic matter content and clay content.

SINTACS method gives a soil texture and grain size diagram to evaluate attenuation capacity rating (see Figure 46). Therefore, based on this diagram and on parameter previously discussed, rating values assessed for soil of study area are given in Figure 47.

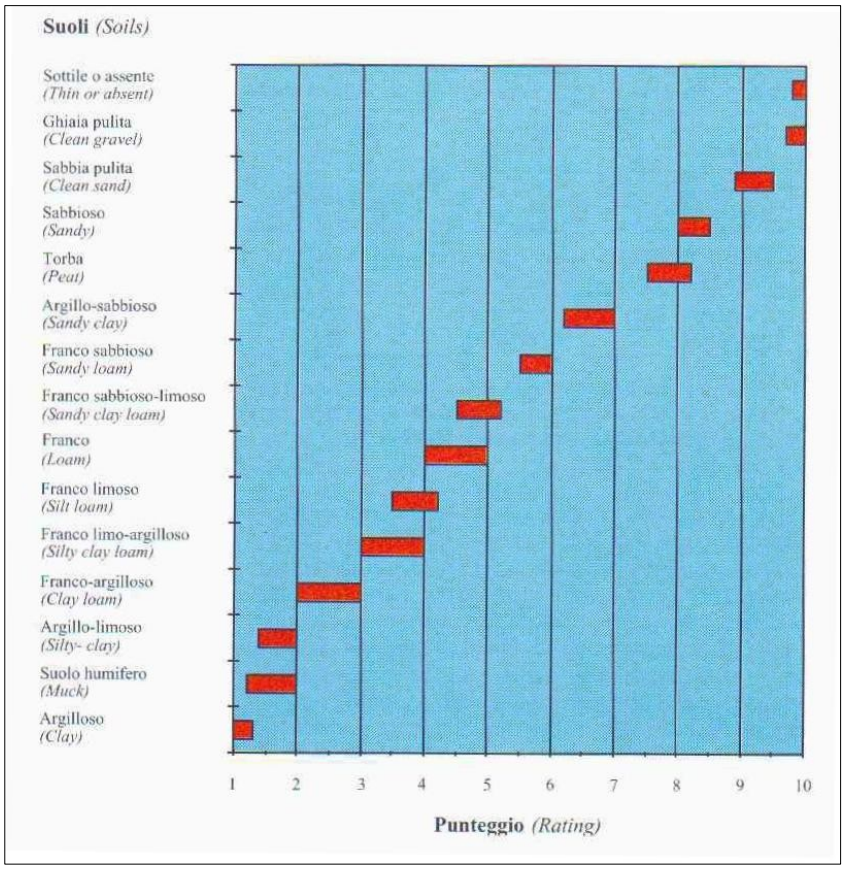

Figure 46. Soil textures and ratings to evaluate the attenuation capacity of soil and overburden (Civita et al., 1997).

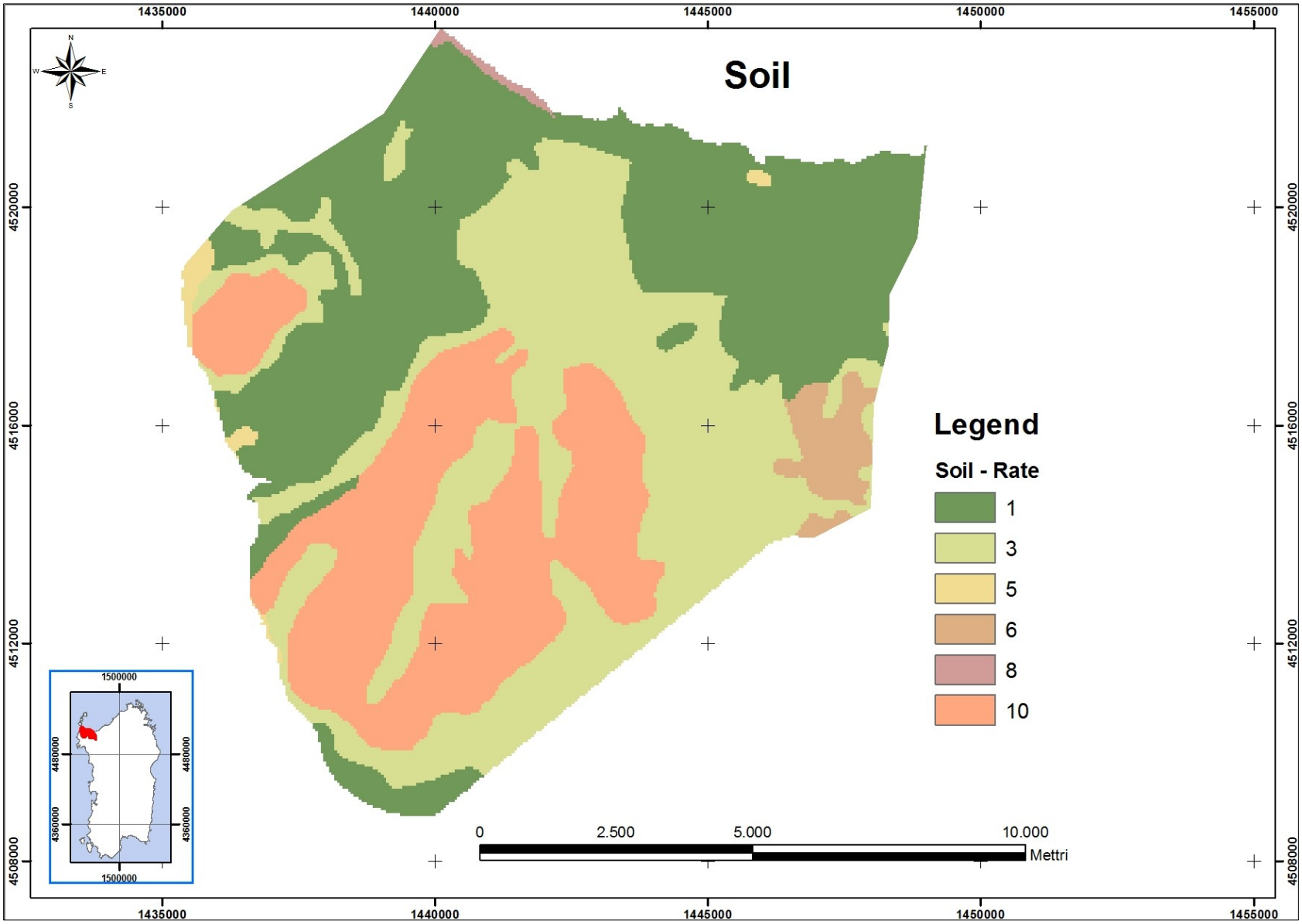

Figure 47. Soil rating.

6.6 Aquifer hydrogeologic characteristics

The aquifer is the saturated zone inside the hydrogeological complex. This parameter take into account attenuation processes in saturated zone, when contaminants mix with water after having lost a part of them passing through the soil and unsaturated zone.

The main processes that occur in saturated zone are molecular and kinematic dispersion, dilution, sorption and chemical reactions between the rock and contaminant. Kinematic dispersion depends mostly on path length and tortuosity of network in the aquifer. In porous media this process is function of grain size and of compaction while in fractured and karst aquifer it depends on fractures and conduits system. Dilution is related to aquifer specific discharge, aquifer recharge, effective groundwater flow velocity. Adsorption depends mainly by rock chemical composition and its reactivity with pollutants.

Therefore, lithology, aquifer structure, fracture and karst settings are the basic data that were assessed, moreover aquifer type (confined, unconfined or semiconfined), flow direction, groundwater divides positions, potential interflows between aquifers belonging to the same system and aquifer discharge were analyzed to define the aquifer characteristics parameter.

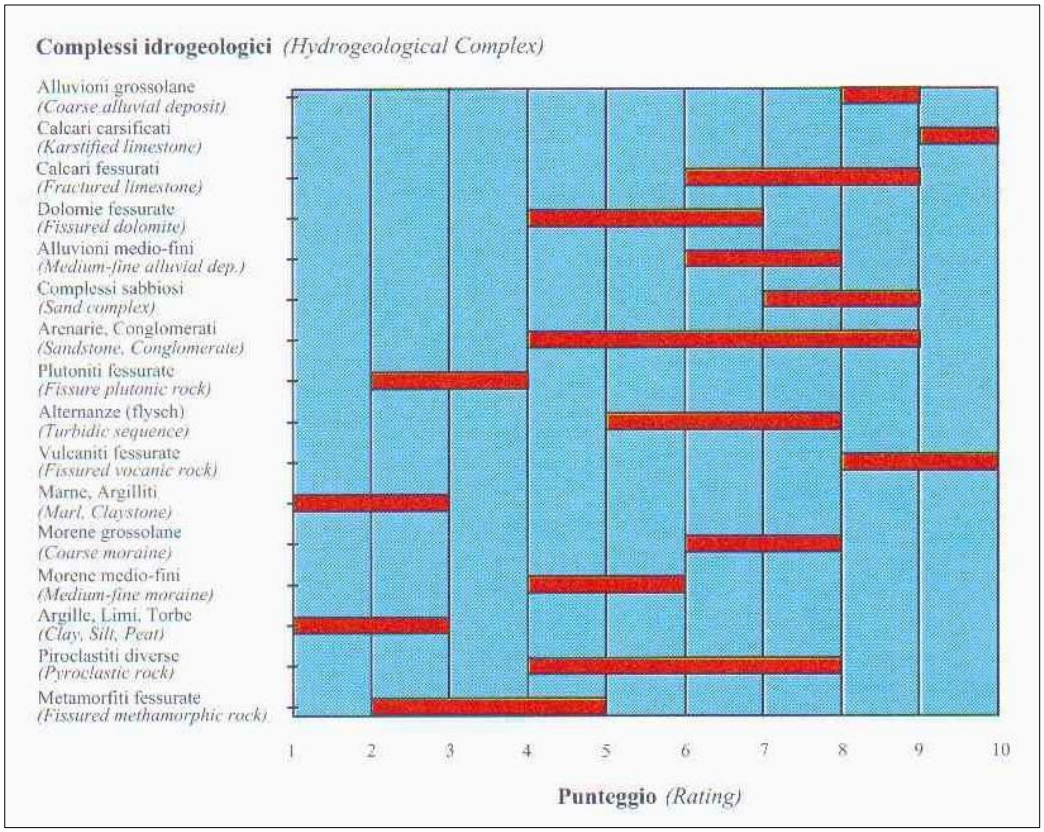

Figure 48. Aquifer characteristics and ratings (Civita et al., 1997).

MODFLOW simulation outputs were helpful in aquifer characteristic parameter evaluation, in particular piezometric head and flow direction map simulated. In fact, using this information, direction and magnitude of flow was defined for the different aquifer sectors and therefore the most important factors that influence the rating values could be evaluated.

Taking into account these factors evaluated and on the basis of range values given by Civita (1997) and shown in Figure 48 for the different Hydrogeological complex, the ratings given to aquifer characteristic parameter are shown in Figure 49

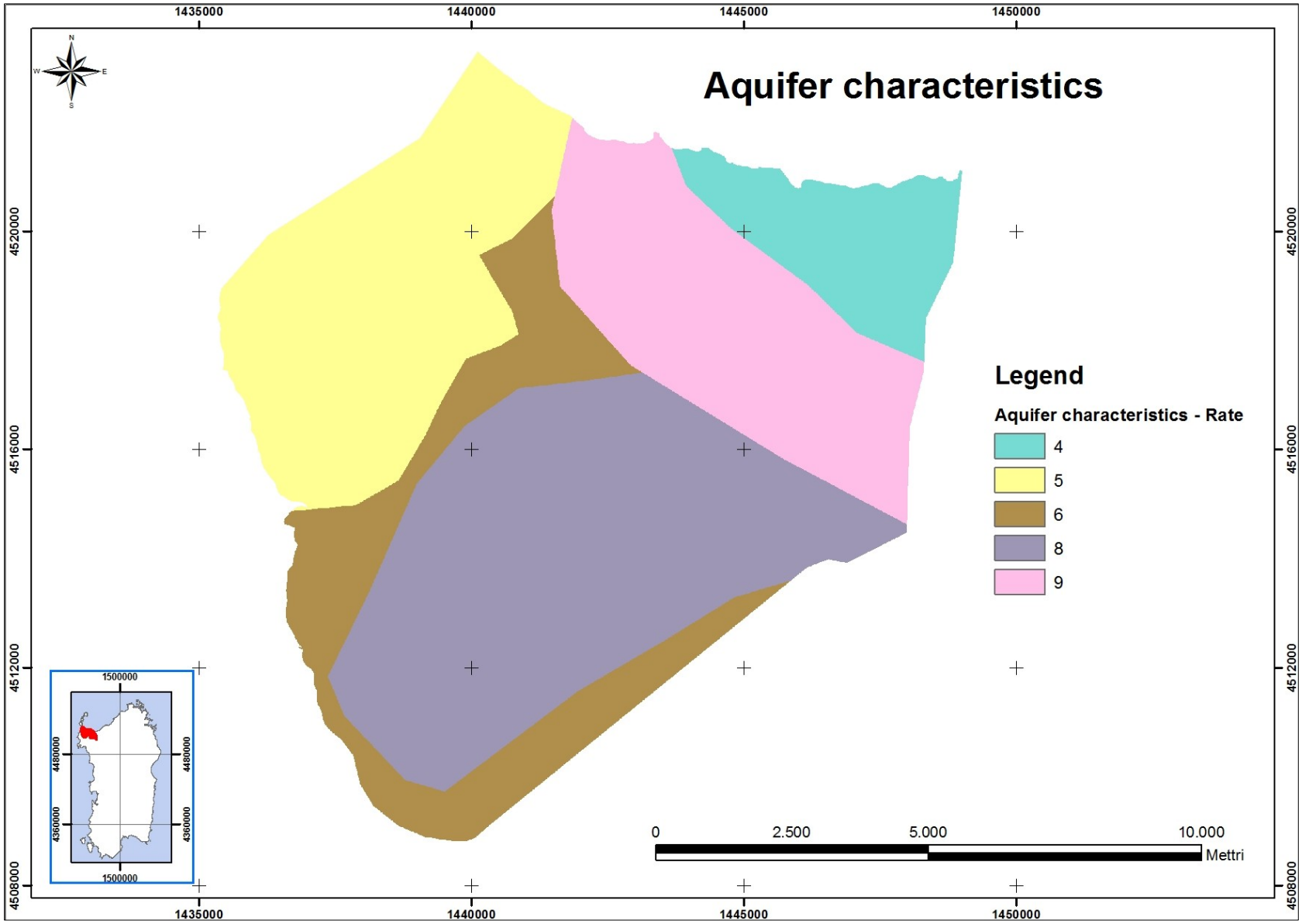

Figure 49. Aquifer characteristics rating.

6.7 Hydraulic conductivity

Hydraulic conductivity represents groundwater mobility capacity and consequently characterizes the mobility of a hydrovectored contaminant or of a contaminant that has almost the same viscosity and density of water.

The hydraulic conductivity average values for the study area aquifer are (Ghiglieri et al., 2006):

- K= 10^{-4} m/s for the Jurassic complex;
- K= 10^{-6} m/s for the Triassic complex;
- K= 10^{-6} m/s for the Miocene carbonate complex;

During mathematical model calibration the hydraulic conductivity spatial distribution was set as to match as close as possible piezometric head observed values. The parameter distribution obtained by model calibration was useful to evaluate SINTACS parameter.

The rating values for this parameter were determined using the diagram given by SINTACS methodology (see Figure 50), and are shown in Figure 51.

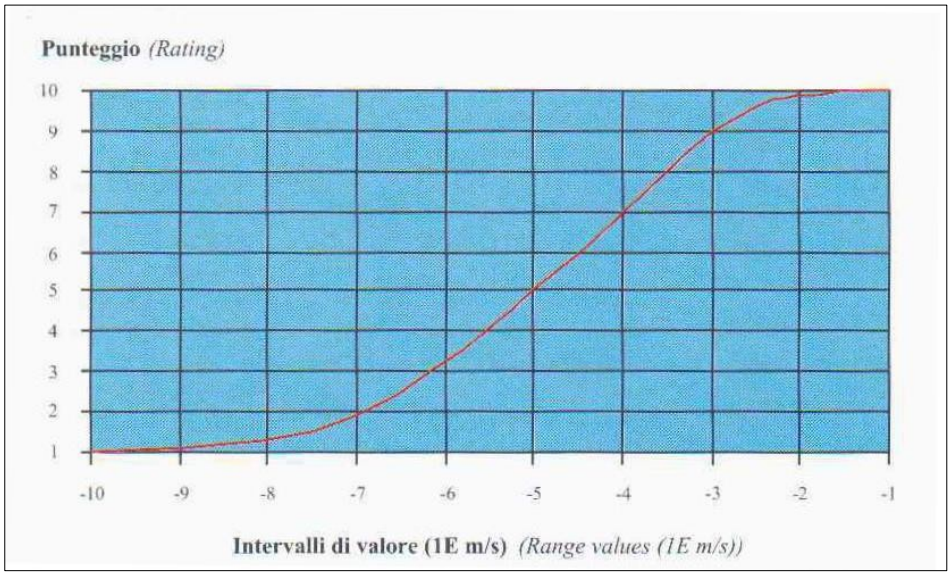

Figure 50. Hydraulic conductivity values and ratings (Civita et al., 1997).

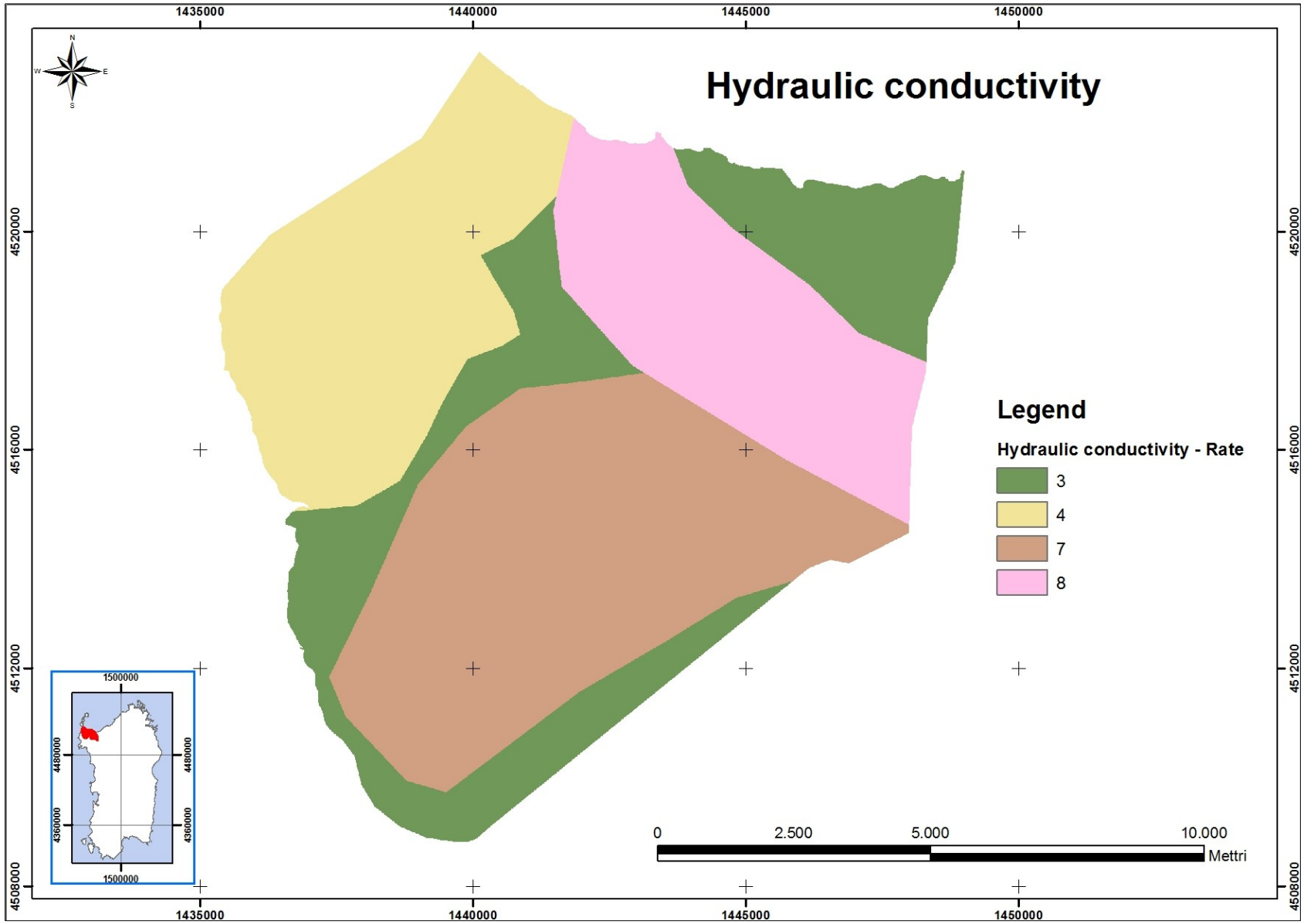

Figure 51. Hydraulic conductivity rating.

6.8 Topographic slope

Topographic slope is important in vulnerability assessment as it controls the amount of surface runoff and its velocity. Therefore it was assigned an higher rating to slighter slopes since in flat areas water stagnation leads to increasing percolation.

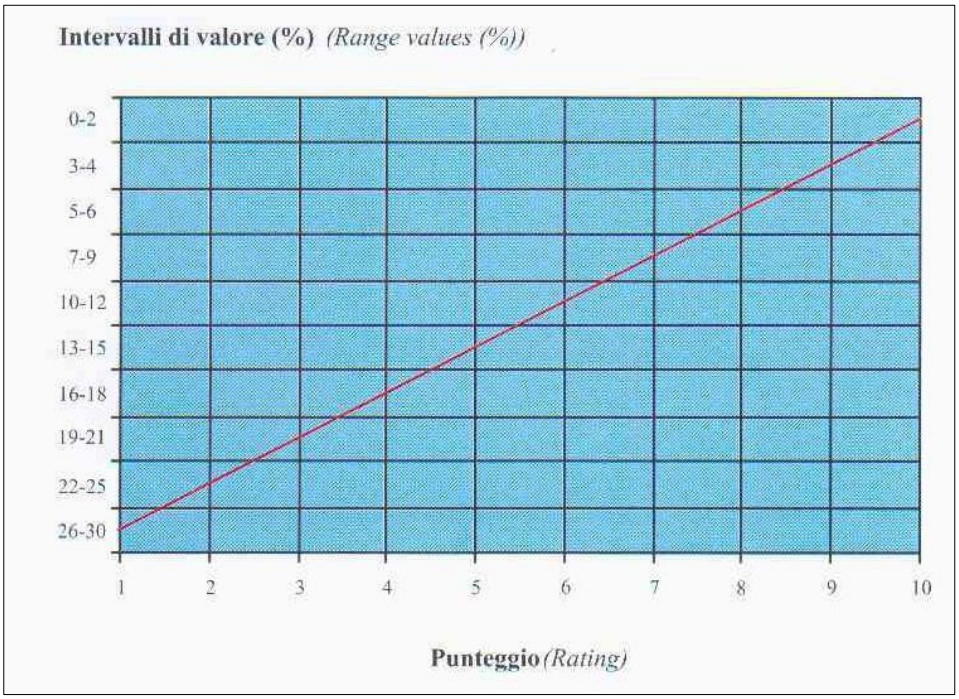

Figure 52. Slope ranges and ratings (Civita et al., 1997).

Slope rating values are derived from diagram in Figure 52 and represented in Figure 53.

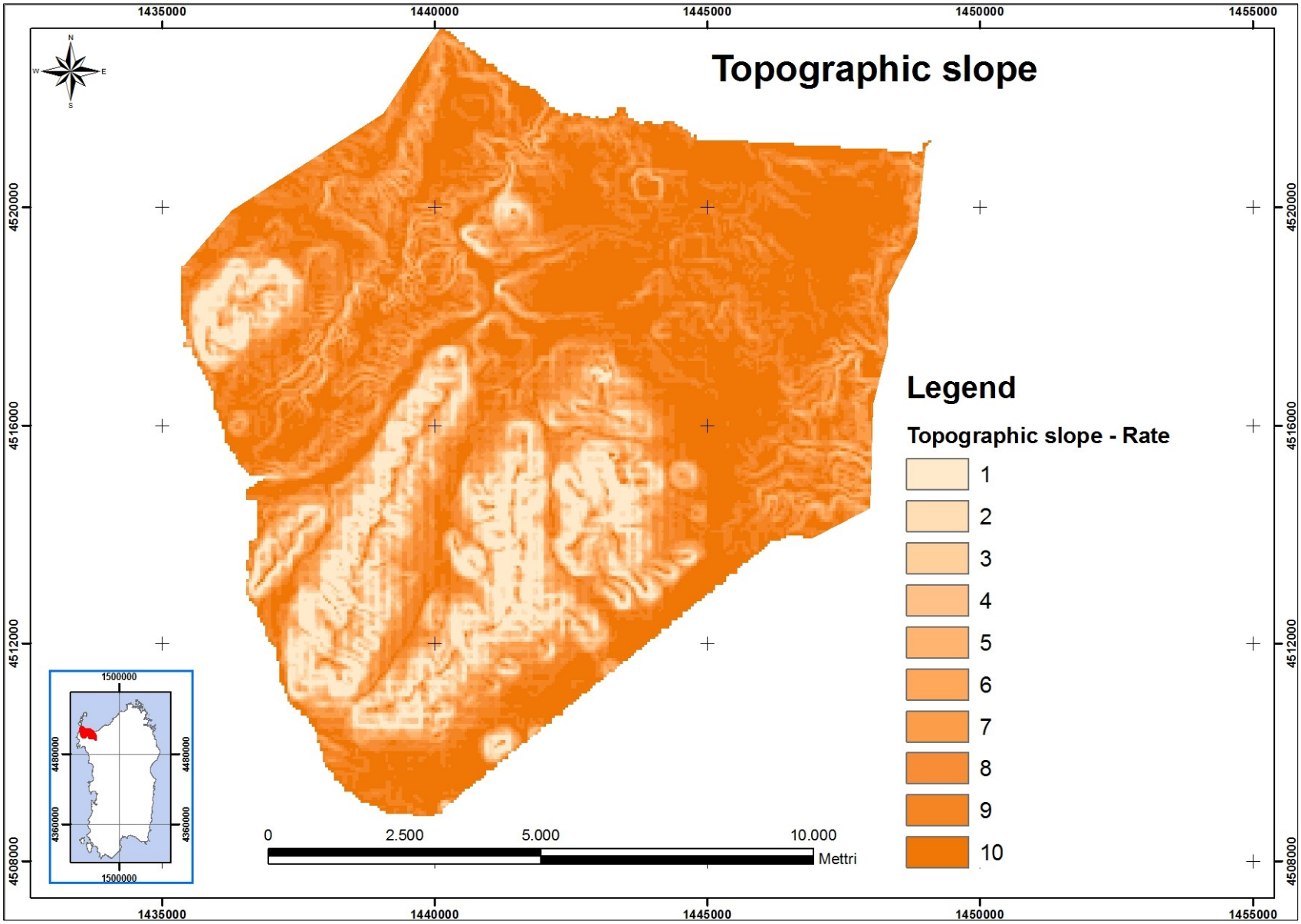

Figure 53. Topogrphic slope rating.

6.9 Results

Vulnerability degree map (shown in Figure 54) evidences that less vulnerable part of the Mesozoic aquifer corresponds to the sector confined by Fiumesanto formation and to the Eastern part of industrial zone. Highest vulnerable areas are karst outcrops, especially those corresponding with Jurassic formations, that are characterized by higher infiltration rates and by higher hydraulic conductivity values.

SINTACS vulnerability degree was evaluated using, as already said, different strings of parameters weights.

Over karst areas, results are strongly influenced by infiltration, aquifer characteristics, hydraulic conductivity and topographic slope that have the highest weights. Among these parameters, aquifer characteristics and hydraulic conductivity ratings derives from results of groundwater modeling. In particular, aquifer domain sectors assumed to be characterized by significant karstification degree and thus with lower attenuation capacity were defined by high rating in aquifer characteristics and hydraulic conductivity parameter.

Moreover, groundwater modeling permits to improve vulnerability assessment detail, by giving other outputs useful for defining SINTACS parameters, like hydraulic conductivity derived by mathematical model calibration and simulated groundwater depth.

Industrial zone is not vulnerable, except for areas in the nearness of Fiumesanto springs, where karst outcrops and the main aquifer outflows occur. This may lead to the conclusion that, regarding natural (or intrinsic) aquifer vulnerability, areas where industrial zone raised are not characterized by high vulnerability degree and therefore are suitable for this use.

However, it should be remarked that SINTACS procedure is referred only to aquifer vulnerability and therefore it doesn't take into account, for example, of the close presence of the sea as receptor of contamination. Anyway, the task to entirely evaluate all environmental issues in land planning is handled by other disciplines and procedures. Moreover, it is known that very impacting activities have been carried out in the industrial zone since the past, when appropriate rules on environmental protection were not yet in force. Therefore, also in areas where the intrinsic vulnerability is low, the presence for example of leaking wells that cross over the confining unit, could definitely be cause for an increase of vulnerability degree. However, the vulnerability map shown in Figure 54 is aimed to evaluate only natural vulnerability, without taking into account man-made impacts on the environmental system.

It is interesting to observe that, among Petrochemical plant area, Western sectors have an higher degree of vulnerability to aquifer contamination, mainly due to a shallower karst aquifer and to aquifer characteristics and conductivity that are modeled as increasing toward Fiumesanto springs.

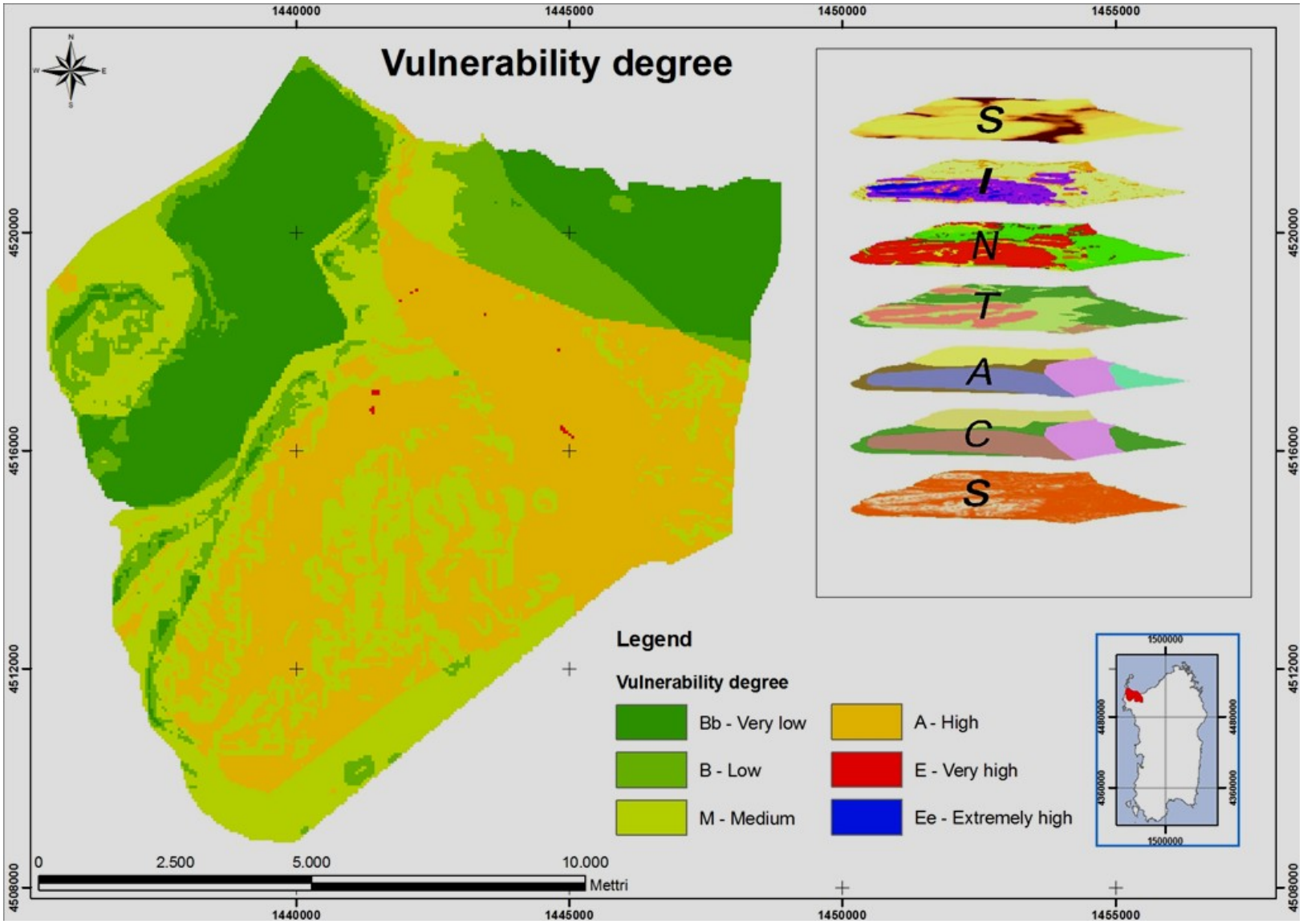

Figure 54. Vulnerability degree map of Mesozoic aquifer.

7 Conclusions

This work was finalized to develop an integrated technique of GIS and groundwater modeling program to improve hydrogeological system understanding of Porto Torres industrial zone and to perform intrinsic vulnerability evaluation of the aquifer to contamination.

To reach this aim, GIS capabilities let to implement geographic data more efficiently for hydrogeological analysis, management and modeling. Moreover, GIS interfaced to the hydrogeological software GMS, permits to manage a wide range of geographical information and data efficiently.

Hydrogeological conceptual model understanding of the study area results to be quite difficult due to aquifer complexity, hosted in a karst medium. To overcome this difficulty, all the available data were managed in GIS and GMS environments as to define a tree-dimensional schematization of aquifer domain both of Fiumesanto power plant site and of Mesozoic system at the aquifer basin scale.

The Miocene-Quaternary covers schematization at the Fiumesanto power station shows an high heterogeneity and spatial variability of sedimentary covers, that consist mainly of a stratified clay/silt, with sand and gravel layers intercalated. Moreover, sand and gravel layers are not continuous and act as permeable lenses included into impermeable sediments. Aquifers hosted in these permeable layers are generally not under pressure and, on the contrary, show a small saturated thickness suggesting to be scarcely fed. However, some permeable lenses are located on the eastern part of the power station site, close to the Fiumesanto mouth (where those sediments enter into contact with the underlying Mesozoic carbonate formations) and consequently are under pressure.

Mesozoic aquifer schematization evidences that the main groundwater reservoir of the study area basin occur in the syncline on the South of the industrial zone located in the Campu Chelvaggiu area, where more recent Mesozoic deposits constituted by Dogger formation widely outcrop; whereas syncline fold limbs are present on the boundary of Dogger outcrops and are given by Keuper and Muschelkalk formations.

The Fiumesanto formation constitutes the confining unit of Mesozoic aquifer Western sector (where it consists mainly by Traissic rocks since Dogger formation has been almost totally eroded) and its thickness increases in the North direction and decreases in the West and South direction.

In the petrochemical industrial area, Mesozoic aquifer lies under Miocene sediments, whose thickness increases in the East direction, varying between few meters on the West of Minciaredda area to one hundred meters near Rio Mannu mouth. Miocene deposits are divided from Mesozoic carbonate by the volcanic formation that acts as an impermeable layer.

Both diffuse infiltration and internal runoff take place in Mesozoic outcropping inside the study area, where also sinkhole are present (like vertical shafts or sub-superficial caves).

The most important springs are located near Fiumesanto mouth, which in seventies years could guarantee an high amount of discharge (average of 134 l/s), while nowadays are almost completely dried out because of groundwater abstraction. Moreover, an high amount

of groundwater abstraction for industrial uses is currently authorized (authorized discharge of 678 l/s).

According to piezometric measurements and to three-dimensional schematization, the main amount of groundwater of the study area flows from the recharge zone in Campu Chelvaggiu syncline to the Fiumesanto Spring; part of aquifer flow is directed also to the petrochemical zone and part to the Western sector of karst aquifer.

Unfortunately, karst conduits and fractures distribution and geometry are not well known. Anyway, the presence of very high productive wells, drilled for industrial uses in seventies years, let to assume the localization of higher conductive zone in kast aquifer.

The most uncertain element of hydrogeological conceptual model is given by the difficulties to dismiss hypothesis regarding a possible inflow to the study area coming from Eastern Nurra. A support to the possibility of an inflow from East is inferred by discharge amounts of industrial wells and by discharge values of Fiumesanto springs, foregoing the industrial utilization, that seem not comprehensible whether inflow to the aquifer came only by infiltration evaluated inside the study area. Therefore, numerical modeling was finalized to provide proof to support or dismiss assumptions made on conceptual model implementation and, based on water balance information, two different conceptual models were tested by simulating groundwater system both with and without East inflow and thus comparing water flow balance.

The groundwater simulation code used to perform mathematical modeling is MODFLOW GMS, whose mathematical theory is based on Darcy equations governing groundwater flow in a porous medium, therefore the code seems not suitable to simulate flow in fractures and karst. In fact, Darcy law based mathematical model can be used as a reliable tool to simulate groundwater flow whether it is possible to assume that fracture permeability has homogeneous properties on a sufficiently large scale and then the weathered and fractured rock layer may be modeled as an equivalent porous media and the hydraulic conductivity set in the model represent the bulk properties of the fractured rock.

As the purpose of this study is to simulate groundwater flow at a large scale without claiming to represent flow at fracture or conduit scale, some equivalent method can be used to simulate fracture and karst conduits behavior. Therefore, to overcome the limitations of the finite difference code MODFLOW fractures and conduits effect was simulated using high conductive cells.

The two conceptual model simulated by MODFLOW have almost the same input data, except for Eastern limit of the model, that in one case was simulated with a fixed flow entering the model domain from the East. The model sets to simulate the inflow rate to the aquifer domain best fits water balance data and contour lines shows that the main groundwater movement flows North-Westward in the Northern and Eastern part of the model and Northward in the Southern part.

Groundwater model performed doesn't claim to simulate detailed aquifer system but anyway was useful to confirm that the more reliable aquifer system supposes a water inflow from East and leads to estimate this amount of water. Moreover, aquifer modeling gives some outputs that helps the subsequent estimation of aquifer vulnerability (piezometric map, flow vectors map and hydraulic conductivity distribution derived from calibration procedure).

Moreover, the simulation and water balance analysis let arise some limitations of the model and highlight possible improvement of groundwater modeling of the study area. In particular, data that should be better evaluated as to improve groundwater simulation reliability are:

- infiltration rate may be evaluated more detailed, as to take into account karst aspects that influence the amount of water evaporated and the amount of effective infiltration;
- hydraulic head monitoring regarding the whole area, for both wet and dry season, would be useful to perform more detailed calibration procedures;
- pumping test needed to evaluate aquifer hydraulic parameters;
- kast conduits and fractures setting.

SINTACS method applied to evaluate vulnerability degree of the Mesozoic aquifer evidences that less vulnerable areas correspond to the sector confined by Fiumesanto formation and to Eastern part of industrial zone. Highest vulnerable areas are karst outcrops, especially those corresponding with Jurassic formations, that are characterized by higher infiltration rates and by higher hydraulic conductivity values.

In karst areas results are strongly influenced by infiltration, aquifer characteristics, hydraulic conductivity and topographic slope that have the highest weights. Therefore, groundwater modeling permits to improve vulnerability assessment detail, by giving outputs useful for defining most important parameters.

Industrial zone is not vulnerable, except for areas in the nearness of Fiumesanto springs, where karst outcrops and the main aquifer outflows occur. This can led to the conclusion that, regarding natural (or intrinsic) aquifer vulnerability, areas where industrial zone raised are not characterized by high vulnerability degree and therefore are suitable for this use.

First of all, it should be remarked that SINTACS procedure is referred only to aquifer vulnerability and therefore it doesn't take into account, for example, of the close presence of the sea as receptor of contamination. Anyway, the task to entirely evaluate all environmental issues in land planning is handled by other disciplines and procedures. Moreover, it is known that very impacting activities has been carried out in the industrial zone since the past, when appropriate rules on environmental protection were not yet in force. Therefore, also in areas where the intrinsic vulnerability is low, the presence for example of leaking wells that cross over the confining unit, is definitely cause for vulnerability degree increase. However, the vulnerability map shown in Figure 54 is aimed to evaluate only natural vulnerability, without taking into account man-made impacts on the environmental system.

It is interesting to observe that, among Petrochemical plant area, Western sectors have an higher degree of vulnerability to aquifer contamination, mainly due to a shallower karst aquifer and to aquifer characteristics and conductivity that are modeled as increasing toward Fiumesanto springs.

8 Bibliography

ANDERSON, M.P., WOESSNER W.W. – Applied groundwater modeling" – Academic Press, San Diego, 1992.

BARCA S., CHERCHI A. – "Sardinian Paleozoic Basement and its Meso-Cainozoic covers (Italy)" – 32th International Geological Congress, Vol. n. 5. Florence – Italy, 2004

BEAR J., TSANG C., DE MARSILY G. – "Flow and contaminant transport in fractured rock" – Academic Press, 1993.

CABOI R., CIDU R., PALA A., PECORINI G. – "Le acque fredde della Sardegna – Lineamenti idrogeologici e idrogeochimici" Ricerche Geotermiche in Sardegna, Pisa, 1982.

CARMIGNANI L., OGGIANO G., BARCA S., CONTI P., ELTRUDIS A., FUNEDDA A., PASCI S., SALVADORI I. – "Geologia della Sardegna – Note illustrative della Carta Geologica della Sardegna a scala 1:200.000" – Istituto Poligrafico e Zecca dello Stato, Roma, 2001.

CARRERA, J., NEUMAN S.P. – "Estimation of aquifer parameters under transient and steady state conditions: 1. Maximum likelihood method incorporating prior information" – Water Resource Research Vol. 22 n.2, 1986.

CIVITA M. – "Idrogeologia applicata e ambientale" – Casa Editrice Ambrosiana, 2005.

CIVITA M., DE MAIO M. – "SINTACS – Un sistema parametrico per la valutazione e la cartografia della vulnerabilità degli acquiferi all'inquinamento" – Pitagora Editrice Bologna, 1997.

DETTORI B. – "Studio geo-idrologico della Sardegna Settentrionale. Memoria n.4. I bacini ad Ovest e ad Est del Rio Mannu di Porto Torres" – Gallizzi, Sassari, 1972.

DETTORI B., ZANZARI A.R., ZUDDAS P. – "Le acque termali della Sardegna" – Ricerche Geotermiche in Sardegna, Pisa, 1982.

DI MOLFETTA A. – "Ingegneria degli acquiferi" – POLITEKO EDIZIONI, 2002.

ENEL – “Studio geologico e idrogeologico della zona della centrale termoelettrica di Fiume Santo (SS)”, 1985.

FETTER C.W. – “Applied hydrogeology” – Prentice Hall, 2001.

GHIGLIERI G., BARBIERI G., VERNIER A. – “Studio sulla gestione sostenibile delle risorse idriche: dall’analisi conoscitiva alle strategie di salvaguardia e tutela” – ENEA, 2006.

GHIGLIERI G., OGGIANO G., FIDELIBUS M.D., ALEMAYEHU T., BARBIERI G., VERNIER A. – “Hydrogeology of the Nurra Region, Sardinia (Italy): basement-cover influences on groundwater occurrence and hydrogeochemistry” – Hydrogeology Journal n.17, 2008.

HARBAUGH A. W. AND MCDONALD M. G. – “User's Documentation for MODFLOW-96, an update to the U.S. Geological Survey Modular Finite-Difference Ground-Water Flow Model” U.S. Geological Survey, Open-File Report, 1996.

MARTINEZ-LANDA L., CARRERA J. – “A methodology to interpret cross-hole tests in a granite block” – Journal of Hydrology 325, 2006.

MERCER J.W., FAUST C.R. – “Ground-water modeling” – National Water Well Association, 1981.

MUCEDDA M. – “Grotte e pozzi della Nurra di Sassari e Porto Torres” - Bollettino del Gruppo Speleologico Sassarese N. 17 del 1998.

MUCEDDA M. – “Il pozzo di Monte Alvaro” - Bollettino del Gruppo Speleologico Sassarese N. 6 del 1980-1981.

OGGIANO G., SANNA G., TEMUSSI I. – “Caractéres géologiques et géochemiques de la bauxite de la region de la Nurra (Geological and geochemical feature of Nurra bauxite)” – Groupe Frnçais du Crétacé, Sardinia, 24-29 May, 1987.

PIETRACAPRINA A. – “Studio geo-idrologico relativo all’approvvigionamento idrico del complesso industriale S.I.R. di Porto Torres (Sardegna)” – Aziende Tipografiche Eredi Dott. G. Bardi, Roma, 1971.

PINNA M. – “L’atmosfera e il clima” – UTET, Collana il nostro universo, 1978.

POETER E., ANDERSON D. – “Multimodel ranking and inference in groundwater modeling” – Ground Water Vol. 43 n. 4, 2005.

RAS, EAF – “Nuovo SISS – Nuovo Studio dell’Idrologia Superficiale della Sardegna”, 1998.

SAR – CHESSA P.A., DELITALA A. – “Il Clima della Sardegna” – Note tecniche di agrometeorologia per la Sardegna, Sassari, 1997.

SGI – “Progetto CARG - Carta Geologica d’Italia 1:50.000 – Catalogo delle formazioni” – website: www.apat.gov.it, date of access: 13/02/2010.

WHITE B.W. – “Conceptual models for karstic aquifers” – Speleogenesis and evolution of karst aquifers – The virtual Scientific Journal”, 1 January 2003.

WONDZELL S.M., LANIER J., HAGGERTY R. – “Evaluation of alternative groundwater flow models for simulating hyporheic exchange in a small mountain steam” – Journal of Hydrology Vol. 364, 2009.

APPENDIX A

Temperature

Alghero temperature [°C]

Year	Jan	Feb	Mar	Apr	May	Jun	Jul	Aug	Sep	Oct	Nov	Dec
1922	-	-	-	-	-	-	-	-	-	-	-	-
1923	-	-	-	-	-	-	-	-	-	-	-	-
1924	8.7	8.7	11.4	14.1	18.5	21.2	23.9	22	22.2	18.2	14.8	10.9
1925	9.3	9.4	9	13.7	17	21.4	22.8	22.8	20.7	18.4	13.5	10.5
1926	9.9	12.4	12.6	13.7	16.1	20.7	22.2	23.8	22.6	18.5	14.8	10.8
1927	9	9.2	12.2	15.1	18.6	22.1	23.9	23.4	21.7	17.7	15.1	11.3
1928	10.1	10	10.9	14.3	15.5	22.5	23.6	25.5	22.1	19.3	13.8	10.3
1929	7.4	6.9	11.1	14	17.7	21.6	24.1	22.8	22.6	17.9	14	11.8
1930	10.4	8.9	12	13.7	16.6	22.1	23.1	23.5	21.6	18	14.7	11.5
1931	9.7	7.6	12.3	13.7	17.4	21.1	23.7	25.5	20.2	18.2	15.4	9.7
1932	9.8	7.7	11.5	13.7	17.3	20.2	21.2	22.9	22.7	20.1	14.6	12.7
1933	8.9	9.1	11.4	14.7	16.5	19.8	25.3	25.8	21.9	18.3	13.2	10.4
1934	7.9	7.8	11.5	15	18.9	22.2	23.9	23.6	21.4	16.6	13.3	12.8
1935	7	10.2	10.9	14.1	16.3	21.1	24.1	23.4	21.5	18.1	14.7	12
1936	12.3	11.4	13.2	14	16.3	20.2	22.5	22.5	22	16.3	14	10.7
1937	10.4	11.6	11.8	13.7	17.6	21.7	23.2	22.3	21.4	19	15.6	10.5
1938	10	8.5	11.7	13	15.9	21.4	23.1	22.8	21.4	18.9	15.4	10.9
1939	12	11.3	10	14.8	15.4	20.1	23.1	23.5	22.2	19.2	15	11.2
1940	10.2	12.1	12	14.1	17.2	20.1	22.9	22.5	20.7	18.3	14.3	8.8
1941	10.6	11.1	12.3	14	15.9	21	23.5	22.8	20.1	17.3	13.1	9.6
1942	8.2	9.3	13.6	15.3	18.2	21.8	22.6	22.8	22.5	19.5	13.5	12.6
1943	10.6	10.4	12.1	15.6	18.2	21.2	23.3	22.9	22.9	19.5	13.4	11.9
1944	9.3	7.3	9.6	14.6	17.9	20.5	22.7	24.9	22.1	17.2	14.1	9.5
1945	6.9	9.7	11	14.9	19.4	23	24.1	24.4	21.2	17.4	12.5	10.3
1946	9	10.4	11.1	15.8	17.5	20.4	23.2	23.9	22.6	18.4	13.9	8.5
1947	8.5	11	13.4	14.2	18.2	22.3	25.5	25.7	23	19	15.7	8.4
1948	11.1	11	12.3	14.5	18.7	20.1	21.2	23.5	20.7	19.2	14.3	11.1
1949	8.8	9.9	9.9	15.4	17	21.6	24.3	23.9	25	19.9	14	10.9
1950	9.7	11.3	10.8	12.8	18.4	23	25.6	25.1	21.5	18.6	14.4	9.7
1951	9.1	11	11.6	14.2	17	21.6	23.5	24.4	22.7	16.3	14.8	9.9
1952	9.4	9.1	12.2	14.7	17	22.2	24.7	24.8	21.5	18.3	13.1	10.6
1953	7.4	8.7	10.2	14.1	17.2	19.1	23.1	23	22.3	18.5	13.9	12.7
1954	8.5	9.6	12.6	12.9	15.5	20.6	20.6	21.4	21.9	17.3	14	12.1
1955	12	12.2	11	13.3	17.2	20.8	23.3	22.5	20.4	16.5	13.1	13.1
1956	11.1	4.3	10.6	13.1	16.6	17.9	21.2	23	22.5	16.2	12.1	10
1957	8.7	11.7	11.7	13.2	15.4	20.2	21.8	22.5	20	18	14.5	10.5
1958	9.6	10.8	11.8	13	17.7	20.8	22.6	24.2	24.2	19.8	14.6	12.8
1959	9.4	11.3	13.6	14.7	17.1	20.9	23.9	23.6	22.8	17.7	13.5	12.5
1960	10.8	11.6	13.2	13.7	17.7	22.2	22.8	24.5	20.9	19	15.7	11.3
1961	10.2	11.2	12.2	16.3	18.1	21.5	23.2	23.3	23	18.9	15.4	12.7
1962	11.4	9.9	11.5	14.3	17.2	19.8	23.8	23.9	22.6	19.3	13.7	10

Year	Jan	Feb	Mar	Apr	May	Jun	Jul	Aug	Sep	Oct	Nov	Dec
1963	9	9.2	11.2	14.6	16.1	20.9	24.2	23.6	22.1	17	16.8	11.6
1964	9.5	11.2	12.8	14.8	17.8	22.3	23.9	23.8	22.3	17.4	15.2	11.3
1965	10.5	7.7	11.8	13.2	16.4	21.2	23.7	23.5	20.9	19.1	16	12.7
1966	11.3	12.9	11.1	15.6	17.9	21.8	22	22.7	21.8	21	14	12
1967	10.8	11.2	12.7	14.5	18.2	20.8	25	25.1	22	20.4	17	11.8
1968	10	12	12.7	15.8	18.5	20.7	23.9	22.3	21.4	19.1	15.5	12.3
1969	10.7	12	13.3	14.9	20	21.4	22.9	25.6	21.6	19.6	15.6	11.6
1970	11	10.2	11.2	13.9	16.4	21.8	23.7	24.4	21.9	18.3	14	11
1971	9.8	9.9	10	15	17.5	20.4	24.5	25.7	21.8	18	11.8	10.4
1972	9.8	11	13	13.6	16.2	21.4	23	23.6	20.5	17.3	14.2	11
1973	9.7	8.3	12.4	14	18.2	22.7	24.8	25.9	21.7	17.1	10.6	9.6
1974	9.3	9.4	11	11.9	16.5	21.3	25.2	25.3	21.1	14.1	8.9	8.6
1975	11.1	10.6	11.2	14	17	20.7	24.4	23.7	22.2	17.3	12.8	10.7
1976	8.5	7.2	9.4	10.8	15.2	22.7	25	25.1	20.9	17.9	13.8	11.9
1977	10.1	9.6	11.6	15.5	19.8	24.4	24.5	24.1	23.3	18.8	13.4	10.4
1978	8.5	10.1	11.5	12.8	15.8	21.2	22.9	22.7	20.7	16.7	11.5	11.5
1979	10	10.7	11.9	12.9	17	21.9	23.7	23.4	21.1	19	11.1	10.9
1980	9.7	10.9	11.4	12.7	15.5	20.7	22.6	21.8	21.6	17.2	13.7	9.4
1981	7.7	9	12.3	14.6	16.8	21.3	22.5	23	21.9	19.1	11.9	11.7
1982	11.2	10.5	10.6	13.4	17.4	22.1	25.5	23.4	22.3	17.8	15	10.7
1983	9.8	8.5	11	14.3	17.6	21.7	25.8	23.1	21.5	18.6	15.3	10.8
1984	9.7	8.8	10.5	13.2	15.6	20.8	24.3	23.6	20.8	17.5	15.6	10.5
1985	7.7	11.6	10.6	14.5	16.9	21.7	25	23.8	21.6	18.6	13.3	10.7
1986	9.6	9.3	12	13.8	19.3	20.9	23.8	24	22.2	19.9	14.5	10.8
1987	9.5	10.6	10.8	15	17	21.5	24.8	23.3	22.5	20.5	13.9	11.6
1988	11.2	10.2	11.8	14.5	17.9	21.4	24.2	23	21.4	20.6	13.5	10.3
1989	9.6	11	14.2	14.8	18.5	21.6	24.9	14.4	22.5	18.1	15.7	11.9
1990	11.5	14.2	12.3	13.1	18	21.1	23.7	24.5	22.2	20.9	14	8.5
1991	10	9.9	13.8	12.6	14.5	20.2	23.9	24.5	23.1	17.9	13.2	9.7
1992	9.8	9.9	11.9	13.8	18.2	21.1	23.1	25.5	22.7	18.6	15.3	11.8

Sassari temperature [°C]

Year	Jan	Feb	Mar	Apr	May	Jun	Jul	Aug	Sep	Oct	Nov	Dec
1922	-	-	-	-	-	-	-	-	-	-	-	-
1923	-	-	-	-	-	-	-	-	-	-	-	-
1924	7.3	7.6	10.5	14.1	19.8	21.3	24.6	21.7	22.1	17	14.9	10.4
1925	8.3	8.5	6.9	13	16.7	21.9	23	23.7	19.2	17	12.1	8.8
1926	8.5	11.7	11.9	13.9	15.6	19.1	21.9	23.3	23.3	20.1	15.6	9.2
1927	8.5	8.7	11.3	14.1	18.5	21.9	24	24.5	21.5	16.8	14.5	10.4
1928	9.4	9.8	10.9	14.2	15.3	22.5	24.4	26.6	22.1	17.6	12.6	8.4
1929	5.8	6	10.7	13.2	17.1	22.6	24.9	23.6	23.1	17.1	12.7	10.1
1930	10.3	8.3	11.8	13.4	16.2	23	23.8	23.8	22	17.2	14.6	10.5
1931	9.2	6.8	12.1	12.6	18.5	24.9	24.4	24.7	18.4	17.5	13.7	7.9
1932	9.1	6.8	11.6	12	17.1	18.7	21	25.3	23.1	16.3	13.5	12
1933	7	6.9	12.2	18.6	19.2	20.6	27.5	28.3	23	18.3	12.2	9.7
1934	8.4	9.6	11.1	14.7	18.5	21.8	24.9	23.5	21.4	17.4	13	12.1
1935	6.8	9.7	10.9	13.9	15.8	23	25.3	24.6	23.5	18.5	15	10.3
1936	10.7	10.5	11.9	13	15.8	19.5	23	23	22	14.5	12.7	9.5
1937	10.1	10.8	11	12.7	17.9	22.6	24.1	23.7	21.2	18.1	14.1	8.8
1938	8.5	7.9	11.7	12.3	15.2	22.3	23.7	23.9	20.9	17.6	14.9	9.8
1939	11	11.3	9.7	14.6	14.9	20.8	24.2	23.6	20.1	17.6	13.4	9.9
1940	8.3	11.3	12.1	13.8	16.7	19.7	23.3	22.3	20.4	15.5	11.4	5.3
1941	8.5	9.3	11.1	12.6	14.5	21	24.3	23	20.9	16.5	12.7	8.5
1942	6.4	6.8	12.3	14.4	17.1	21.4	22.9	23.7	21.8	18.8	12.8	11
1943	9.9	9.6	11.7	14.7	17.2	20.1	23.2	24.2	24.9	18.5	12.4	11.6
1944	9.9	6.5	7.9	14	16.7	20.4	23.4	25.4	22.1	14.6	11.1	8.7
1945	5.8	7.8	10.4	15.2	11.9	18.4	24.6	24.8	22.4	15.8	13	9.3
1946	8.9	9.9	11	15.2	15.3	21.8	23.9	25.7	24.5	16.4	11	6
1947	4.7	9.1	12.4	14.8	18.5	18.9	25.5	26.6	23.7	20.3	15.9	8.2
1948	9.5	9.1	12.3	13.4	17.1	20.6	21.9	24.2	19.5	19	15.1	12.1
1949	8.8	11.2	10.1	18.2	16.7	21.6	25.1	25.1	25.8	19.5	12.9	11.4
1950	9.9	10.7	12	12	19	23.8	26.5	26.4	22	19	13.9	9
1951	10.2	10.1	11.3	13.6	16.6	21.6	23.8	24.8	22.2	17.8	14.8	10.3
1952	8	8.2	12.5	15.4	18.2	24.5	26.1	25.7	20.9	17.6	12.4	10.1
1953	7	7.9	9.6	14.2	17.7	19.1	24	23.7	22.5	18.6	18.2	13.7
1954	6.6	8.2	12.6	14.1	16.3	23.6	21.9	22.5	22.8	17.6	13.5	11.7
1955	11	10.8	11	14.1	18.3	21.5	24.8	24.3	20.7	17.2	12.8	12.4
1956	11	4.1	10.3	12.6	17.3	19.2	23.2	25.7	23.5	16.5	11.6	10.2
1957	8.9	11.3	12.8	14	15.3	21.1	23.4	24.1	21.5	18.4	14.3	10.1
1958	9.3	10.8	10.3	11.7	19.4	21.2	23.2	25.3	23.7	18.7	13.8	11.7
1959	9	11.8	13.6	14.6	17.1	21.7	24.8	24	23.3	17.5	12.3	10.9
1960	9.9	10.9	12.1	13.3	19.1	22.5	23.4	24.4	21.1	17.6	14.1	10.2
1961	9.2	11.7	12.7	16	17.8	21.7	26	25	23.9	18.9	14.3	11.4
1962	11.7	9.6	9.1	14.8	17.1	20.2	23.6	25.1	22.5	19	11.6	8.9

Year	Jan	Feb	Mar	Apr	May	Jun	Jul	Aug	Sep	Oct	Nov	Dec
1963	6.9	7.4	10.5	16.9	16.5	20.9	25.6	23.7	21.4	17.3	16.5	10.8
1964	10.1	10.4	12	14.1	19.2	22.9	25.1	24.4	22.6	16.4	14.3	10
1965	9.3	7.3	11.3	12.6	17.3	22.4	24.8	23.7	20.4	19.8	14.1	11.8
1966	9.5	12.5	10.5	14.6	17.9	22.4	22.1	23.5	21.8	18.5	11.4	10
1967	9.2	10.6	12.7	14.2	18.9	21.2	27.1	26.2	21	19.7	15.1	10
1968	8.5	11.4	12.4	16.6	18.7	21.9	24.9	22.8	20.9	18.4	13.4	10.2
1969	9.5	8.8	11.5	14.5	18.8	19.5	24	24.1	21.1	18.4	13.5	8.5
1970	10.3	8.9	10	13.5	17	23.1	24.1	24.6	23	17.3	13.5	10.5
1971	9	9.2	8.5	15.4	18.9	20.9	25.8	27.6	21.8	17.6	11.7	10.7
1972	9.4	10.7	13.2	13.1	16.6	21.7	23.6	22.8	19.7	16.7	13.9	11.4
1973	10	9	10.3	12.6	19.7	23.9	25.3	25.7	22.3	17.2	12.3	9.6
1974	11.2	10.5	12.9	13.5	17.9	21.4	23.4	24.4	21.1	12.8	12	10.1
1975	10.3	9.7	10.2	14.2	17.6	20.7	25	24.2	21.9	15.2	11.5	10.1
1976	8.8	9.4	10.7	12.4	16.9	21.6	22.9	22.6	19.4	16	10.4	9.5
1977	9.5	10.7	12.6	13.5	17.1	20	23.1	21.8	19.2	17.9	12.3	9.8
1978	7.3	9.1	10.7	11.3	15.6	20.3	22.8	23	19.6	15	11.3	10.4
1979	8.8	9.6	11.3	12.6	17.2	21.6	24	23.9	21.1	18.7	12.6	10.3
1980	9.2	9.9	11	12.4	16.5	21	23.6	23.7	21.9	16.6	13.4	8.7
1981	7.2	8.5	12	14.3	17	21.6	23.8	24.4	22.1	18.2	12.8	10.1
1982	10.6	9.4	10.5	13.6	17.3	22.4	24.3	24.5	21.9	17.1	13.7	9.7
1983	8.8	8	11	14.3	17.4	21.5	24.5	24.2	22.3	17.7	13.8	10.3
1984	9.1	8.1	10.5	12.8	16.8	21	24	23.9	20.9	16.9	13.8	10.2
1985	7.2	10.8	10.5	14.2	17.2	21.7	24.6	24.4	22.6	17.6	13.2	10.7
1986	8	8.3	11	13.3	17.8	21.2	24.1	24.9	22.4	18	13.5	10.1
1987	8.3	9.5	10	14.2	17.1	21.4	24.3	24.9	23.9	18.8	13.3	11.3
1988	10.1	8.6	10.7	13.9	17.3	21.1	24.2	24.2	21.4	18.6	12.9	9.4
1989	8.9	9.8	12.5	12.6	17.3	21.1	23.9	24.4	20.9	16.6	13.3	11
1990	9.6	11.7	11.5	12.9	17.3	21.5	24.4	24.7	22.9	19.3	13.2	9.1
1991	10.3	10.1	12.6	13.6	16.8	21.7	24.6	25	22.6	18	13.4	9.7
1992	10.2	10.4	11.9	15.6	18	21.4	24.2	25.1	22.8	18.1	14.5	10.7

APPENDIX B

Rainfall

Alghero rainfall [mm]

Year	Jan	Feb	Mar	Apr	May	Jun	Jul	Aug	Sep	Oct	Nov	Dec
1922	122	45	57.5	49	12	3	0	3.5	122	102	34.2	135
1923	69.5	77.5	22	100.5	31.2	11	0	0	95	53.5	272.7	171.2
1924	68.5	226	70.5	42	7	0.7	7.2	3	30	105	57	179
1925	14	62.5	82.5	84	63.3	4.5	20	13	43.7	95.5	104	37.5
1926	80	11.4	71.5	122.5	66.3	1.5	11	0	20.5	74.5	190	158.7
1927	183.7	19.4	14.7	12.5	51	8	0	0	10.5	262	67.5	23.1
1928	118.5	2.5	127.7	84.5	75.5	0	10.2	0	48.5	90.2	191.5	96.2
1929	61.8	26	4.2	21.5	39.7	0	0	9.2	21	155.2	210.5	65
1930	68	179.3	86	88	33	18.5	0	0	33.5	51.2	27.5	99.2
1931	32.7	110.4	45.5	15.2	67	0	0	0.2	63	60.4	119.7	73.5
1932	7.2	89	56.5	60.5	32	14.9	9.4	29	71.7	166.9	71	134
1933	110.5	120	13.5	24	1.9	20.5	0	5.4	72.5	49	168.5	227.5
1934	53.5	98.5	72.5	90.5	10	0	0.5	22.5	41.7	26	192	146.5
1935	105.5	27.5	162.5	11.5	77	0	0	3	30	145.4	126.5	108.3
1936	74.4	79.6	96.8	115.3	107.5	14.6	1.5	13	26	62.1	39.5	43.4
1937	47.7	52.2	147.6	33.1	13.3	12	0	23.2	47.9	37.3	75.8	173.7
1938	39.3	39.8	15.2	24.4	101	4.2	1.9	24.4	90.9	91.9	82.8	250.3
1939	64	44.3	67.3	29.7	20.3	8.7	0	25.3	155.3	43.1	44.1	156.7
1940	147.8	22.1	8.3	31	73.7	43.3	0	0	14.8	205.6	109.2	90.4
1941	261.1	158.3	61.6	73.4	38.2	13.4	0	0.6	20.5	22.7	74.1	61.2
1942	143.4	198.6	20	52.4	7.4	35.4	0	0.2	94.1	55.5	60.9	101.1
1943	60.3	40	111.4	4.9	19.1	0	23	0	64	149.8	105.1	96.3
1944	8	62.5	53.4	72	13	0.5	0	0	44.9	116.3	39.2	44.6
1945	174.8	11	21.9	1	4.9	0	0	0.5	45	77.1	37.4	96.3
1946	27.3	0	77	66.5	45.2	3.4	0.1	10.5	0	172.4	308.4	128.5
1947	40.4	117.4	30.3	19.1	21.4	0	0	105.1	132.2	123.7	70.1	71.4
1948	130.4	74.8	0	63.5	87	8	3.4	0	53.2	82.6	12.6	47.6
1949	55.2	49.7	56.7	9.7	60.4	14.2	15.2	0	15	68.1	331.6	83.3
1950	33.3	38	75.9	140.2	1.6	11	0	0	51.2	65.4	49.2	173.2
1951	81.8	71.4	60.5	9.8	55.2	2.5	1.3	0	30.5	145.1	46.2	39.1
1952	78.9	56.6	17.3	32.8	22.6	0	14.1	22.6	131.2	61.2	41.4	139
1953	126.3	77.7	13.5	41.5	81.6	112	0	49	33.4	179.3	23.2	74.1
1954	85.4	109.7	52.3	53.1	30.5	61.2	19.4	32.8	2.6	19	96.4	60.1
1955	83.8	102.8	59.4	33.2	1.8	42.2	0.2	2.4	108	48	87.2	79.6
1956	77.8	84.2	62	55.6	16.8	5.4	0	0.8	23.8	73	146.6	99.8
1957	39.6	20	9	52.4	62.8	20.4	0	0	0	76.8	101.8	195.4
1958	55.6	23.6	89.6	81.2	23.4	5	3.2	0	1.6	76.8	93.6	113.6
1959	42.6	21.8	105.8	88	75.4	5.8	0	47.8	62	138.2	132.4	126.2
1960	111.2	42.8	84	46.8	6.4	4.6	0	0.2	54.6	130.6	106.2	231.8
1961	116.9	1	0.2	51.6	5.4	2.8	0	0	6.2	127.6	241.4	61.4
1962	16	76.6	58.8	28.4	17	7.4	0	0	123.9	43.6	382.4	80.6

Year	Jan	Feb	Mar	Apr	May	Jun	Jul	Aug	Sep	Oct	Nov	Dec
1963	77.2	177.4	30.8	60.4	20.8	16.8	17.4	12.2	70.4	52.2	62.4	126.4
1964	0.2	56.2	72	43.4	3.6	27.2	0	5	0	175.4	37.4	155.4
1965	100.4	91.2	109.6	17.6	11.6	3.4	0.4	0	63.9	52.8	115.8	21.2
1966	70	63.6	34.4	40.2	22.6	6.6	4.2	6.6	26.6	186.6	215.2	94.4
1967	70.2	19.8	45.4	51	21.4	4.4	0	0	33	72.2	109.8	113
1968	57.4	54.6	45.8	47.6	15.8	9.8	7.6	7	27.8	16	132.8	101.8
1969	40.4	78.8	91.6	22.8	44.2	20	1.8	1.2	80.9	36.2	94	104.2
1970	77.3	62.3	57.6	26.5	24.9	10.6	1.2	6.4	0	0.4	64.4	75.4
1971	93.6	29.9	61	23.7	55	0.6	0	0	17.4	39.5	150.4	50.8
1972	99.8	145	40.7	62	73.5	15.4	14.6	0.1	35.8	64.7	12.7	0
1973	73.4	62.1	45.4	25.6	7.2	11.2	1.2	10	92.6	28	12.9	39.5
1974	58.3	104.3	72.2	77.8	16.4	4.4	43.2	0	19	45.8	42.8	13.4
1975	27.2	71.4	100	64	47.2	28.6	0	51	4	55	148.2	60
1976	34.8	72.6	104	34	36.6	40.4	16.6	23.8	35.1	149.6	134.6	75.3
1977	81.3	37.8	30.5	13	44.7	26.4	4.3	33.2	37.4	70.5	67.8	106.6
1978	180.2	87.3	44	98.1	25.5	6.6	2	22.6	30.4	131.6	75.9	102.8
1979	90.3	73.9	41.5	115	0	6	0	11.9	23.4	101	44.9	63.6
1980	57.4	10.6	32.1	43	116	9.3	2.3	13.3	7	173.6	154.4	59.7
1981	43.8	45.8	26.1	75.6	33.4	9.4	9.9	0	40.8	131.6	0	94.3
1982	38.3	35.2	36.1	17.5	29.1	14.8	0.8	4.4	33.8	175	79.4	90.1
1983	29	83.2	60	20.2	10.4	20.6	1.1	28.5	37.2	68.7	71.2	87.2
1984	35	88	93.4	44	158.2	20.6	0	28	51.4	75.8	82.4	63.4
1985	100.2	23.2	97.4	30	50.6	0.2	0	0.2	14.4	55	108.6	12.6
1986	106.6	115.8	37	80.8	4	2.4	41.8	0	6.4	28.2	64.4	73
1987	85	62.8	30.4	15	18	10.6	0	0	3.2	69.8	200	89.2
1988	58.6	23.4	51.4	40.4	40	6.6	0	0.8	48.4	60.4	21.8	43
1989	27.4	68	15.2	94	27.8	1	1.4	0	43	14	106.4	53.2
1990	47.4	34.4	45.6	91.2	31	33	1.8	0.4	7	166	124.4	103.4
1991	9.4	22.8	57.4	122.2	75.4	4.4	0	0	96	196	132	3.8
1992	72	25	18.2	29	34	31	32.6	4	5	258.6	26	45

Bancali (ex Macciadosa) rainfall [mm]

Year	Jan	Feb	Mar	Apr	May	Jun	Jul	Aug	Sep	Oct	Nov	Dec
1922	80.9	42.7	83.5	58.2	16.1	9	1.1	8.7	81.7	68.9	77.8	92.8
1923	78.9	86.8	60.7	64.8	17.9	29.6	4.4	0	91.7	43.4	171.7	140
1924	52.4	118.6	85.4	27.9	17.2	3.8	2.6	1	15.9	102.4	33.3	106.2
1925	3.2	94.5	75.8	89.7	57.3	20.1	3.3	7.5	66.3	95.3	58.7	57.1
1926	62.3	22.4	47.1	72.4	46.5	16.5	2.9	3.3	26.3	43.5	114.8	105.5
1927	158.6	18.6	41.8	11	40	23.9	2.9	1.7	12.6	90.9	72.7	161.3
1928	49	27.6	109.4	52.9	50.1	3.8	25.2	0	73.8	63.9	168.6	115.7
1929	58.4	23	0	21	27	5	0	8	96	90	219	70
1930	86	99	105	101.2	39.5	4.1	0	0	51	42	43	116
1931	39	110	56	19	58	0	0	0	38.5	60.4	90.7	62.5
1932	32.6	82.6	64.2	39.9	18.7	12.7	26.4	15.9	65.9	97	59.5	44.9
1933	41.7	39.9	38	43.6	0	16.1	6.1	6.7	73.5	82	128.7	131.7
1934	64.6	32.2	78.2	79.3	57.4	17	0	23	10.6	35.9	147.7	147.1
1935	86.3	21.9	53	26.7	43.1	7.3	22.6	3.5	25.3	117.7	111.6	86.2
1936	79.2	51.7	123.7	81.5	51.5	46.2	1.6	0	36.8	96.6	92.2	38.4
1937	25.7	46.3	115.3	36	42.3	18.5	2.2	9.2	74.2	43.9	86.2	159.1
1938	27.6	50.4	22.2	30.6	86.8	5.1	2.6	0	103.9	106.9	54.1	123.5
1939	61.9	21.4	58.1	46.3	59.1	10.7	1.1	24.4	119.5	82.9	40.7	157.3
1940	198.2	30.7	12.3	29.3	44.1	27.3	2.4	0	58.8	191.3	108.1	45.5
1941	174.6	162	44	66.5	30.4	4	0	0	10.6	29.9	74.5	61
1942	199	158.5	38	58	26	22	0.5	6	126	41	37	55
1943	66.5	34	100	14	4.5	0	12	0	72.1	127.6	89.8	69.8
1944	1.6	53.4	39.4	57.3	1.8	0.2	0	1	46.3	150.8	49.6	39.4
1945	116.9	5	17.5	5.4	2.5	0	0	1	31	46.9	37	125
1946	53.5	5.5	61	68	99.5	4	2	15.3	0	234	305.5	192.8
1947	27.3	112.7	18.5	12.2	5.5	0	0	54	93.4	119.7	57.2	83.1
1948	67.8	61.2	0	69.8	20.1	0.2	9.1	0	73.7	78.5	28.5	17.5
1949	87	45.6	62	18	88	29	0	0	20	71	188	89
1950	22	38	61	166.5	2	11.5	0	0	111	54.5	75.9	202.7
1951	89.5	166	112.5	28.3	97.5	0	0	0	35	177	64.5	52
1952	107	42.5	18	48.5	40.5	0	3	18	185.1	117.1	57.5	160
1953	54	117	39	35	77.8	129.7	0	34.9	37.5	129.5	30.8	57.5
1954	95.5	140.9	61.9	76.4	29.4	70.8	11.2	20	0	15.7	75.3	51.5
1955	148.3	147.8	111.7	24.8	0	41	0	1.1	92.6	69.9	133.9	80.4
1956	123.2	163.5	79.2	123.9	44.2	27.3	0	3	33	65	71.2	77.5
1957	67.4	23	8.7	54.1	54	24.2	0	0.9	2.5	138.7	140.9	171.5
1958	87.8	20.2	110.8	93.8	20.4	4.8	3	0	0.5	102.1	113	100.3
1959	51.9	29.8	125.7	41.4	111.8	16.7	0	70.7	36.5	114.4	140.2	201.9
1960	103.7	58.4	107.6	46.8	9.1	5	0	0	75	139.9	93.4	228.7
1961	146.6	8	0	59.8	10.3	14.7	0	0	11.9	144.8	220.4	89.3
1962	19.1	60.3	69.9	18.4	18.5	8.5	3.5	0	63.5	82.4	301.8	62.6

Year	Jan	Feb	Mar	Apr	May	Jun	Jul	Aug	Sep	Oct	Nov	Dec
1963	38.6	138.8	39.8	35.2	15	46.8	7.8	27	43.6	46.1	65.4	130.2
1964	0	49.9	66.2	35.2	7	27.5	0	12.7	0	172.1	48.8	137.6
1965	70.3	46.3	88.6	11.4	24.7	6.4	1.3	1	74.2	73	104.3	30.3
1966	84.8	67.8	33.9	28.3	28	5.2	9.3	5.5	36	165.3	139.3	85.3
1967	71.9	12	33.3	24	16.8	4.8	0	0	70.1	22.3	97.3	94
1968	50	67.6	33.7	46.8	19.6	2.5	5.1	15	37.5	12.5	142.1	73.3
1969	41.6	68.3	75.4	32.9	76.1	12.8	0	0.5	160.4	10.5	69.3	111.9
1970	72.5	47.6	50	7.3	12.8	5.3	0	28.2	0	7	92	103.4
1971	70.7	30.2	68.5	13.5	74.8	0	0	5	32.2	8.7	124.9	29.3
1972	88.6	148.3	48.3	49.4	69.7	58.3	0.5	0	40.2	48.6	9.2	46.9
1973	86	53.6	42.4	22.5	8.7	10.8	3	3	96.7	20.4	13.7	70.5
1974	69.4	74.1	43.4	118.2	19.6	0	15	0	25	47.1	51.5	13.6
1975	16.8	51.5	101.1	36.8	35.4	16	0	96.5	15.4	44.5	167.8	52.5
1976	24.5	79.1	81	48.3	30	24.3	37	27	55.8	160.1	133.8	49.5
1977	85.8	39.5	19.5	37.2	31.5	38.5	7	62.5	36	82.1	58.7	130.1
1978	126.2	76.7	23.1	92.3	32.4	3	5	10	36	92.2	52.8	90.8
1979	85.8	57.4	36.8	48.7	0	6.8	0	3.2	71.2	66.1	76.4	91.8
1980	35.8	13.4	37.3	13.3	118.3	5.6	0	20.9	0.4	177.6	114.7	61.3
1981	31.6	45	38.6	48.2	25.6	0.4	38	0	25.4	108.6	0.4	129.6
1982	33.4	39.2	38.4	31	28.6	0.6	0	0.2	9.6	180.4	85.2	124
1983	6.4	73.4	54.6	23.2	2.8	3.4	0	48.6	21.6	38.8	86.2	98
1984	40	79.8	109.4	48	156	27	0	24.4	51.4	77.4	108.4	68.4
1985	78.6	19	114	6	57.2	12.6	0	0	16.4	33.8	119.2	14.2
1986	117.2	122	47.8	88	3.2	22.4	43.6	0	19.8	71.4	46.8	44
1987	75.6	60	31.8	9.2	23.6	10.4	0	0	6.2	89.4	195.8	99.4
1988	55.4	33.8	45	73.6	40.4	8.4	0.2	0.2	27.4	70	18.2	36.6
1989	18.8	77.4	35.2	133	3.4	1.2	3.8	0	45.8	29.2	87.8	64.2
1990	31.4	14.2	35.2	81.2	9.4	23.8	0	0	14	145	105.4	91.4
1991	15.4	22.8	65.8	117.4	84	3.8	1.2	13.4	90.4	141.6	86.4	5
1992	64.6	11.6	31.2	38.6	23	59	5.6	25.4	15.4	213.2	38	100.6

Olmedo rainfall [mm]

Year	Jan	Feb	Mar	Apr	May	Jun	Jul	Aug	Sep	Oct	Nov	Dec
1922	111.3	51.3	65.1	65	20.4	16.4	0	4	101.6	67.2	24.4	98.5
1923	71.6	80.3	38.8	126.3	30.9	25	0	0	97.2	55.1	258.9	225.8
1924	66.7	162.5	96.1	43.2	8.4	1	3.4	4	32.5	79.5	74.5	160
1925	6	69.5	94.5	98	95	4.5	25	9.5	61	97	131.5	50.5
1926	95.2	16	79.5	110	63	3	3.2	2	15	41	182	142
1927	164	35	24	14	27	17	3	0	18	177	104	185
1928	62	4	101	36	57	0	0	0	88	77	182	103
1929	86	21	9	31	33	0	0	16	40	131	174	74
1930	65	140	84	73	40	20	0	0	51	69	31	104.5
1931	28	104	62	14	60	0	0	0	28	72	137	77
1932	7	107	41	59	28	9	20.2	12	59	114	76	124
1933	77	90	28	27	1	7	0	2	63	48	175	176
1934	38	68	104	74	21	2	0	30	29	32	218	140
1935	95	31.3	144.8	10.6	58.2	0	0.2	41.4	11	122.9	115.8	102.4
1936	58	60.2	60.5	84.6	104.7	29.4	0.2	3.3	23.6	39.4	32	36
1937	31.1	64.4	137.7	29.7	10.5	9.2	0	28	52.6	55	49.6	152.8
1938	16	36	7	24.7	52	0	11	23	74	96	38	155.2
1939	51.5	24.5	58.5	34	20.3	3.2	0	18	137.5	37	37	156.7
1940	104.7	32	7	9.5	55	28	0	0	26.5	144	87.8	63.2
1941	252.4	114	36.1	37.2	22.9	6	0	0	20.5	14.6	59.7	59.2
1942	152.8	128.2	22	43	4.5	26.3	0	0	65.7	25	33	77.6
1943	80.2	34.3	85.7	28.6	22.3	0.7	3.6	1.7	65.4	98.7	121.1	78.7
1944	2.6	54.1	53.7	53.8	25	6.2	0.8	8.1	50.4	87	52.6	65.4
1945	139	13.9	28.6	63.2	8.1	8.7	0	1.6	32.2	46	42.9	93.5
1946	36.2	12.6	71.7	68.8	61.1	0	1.3	9.5	13	135.6	150.9	172.2
1947	64.5	70.6	48.1	29.4	24.9	4.6	0	17.1	42.3	131.7	59.9	74.5
1948	100.6	35.6	26.6	43	61.8	5.1	4.8	0.8	60.2	110.2	3	70.5
1949	34.6	31.8	41.6	25.1	58	15.7	3.6	4.1	14.3	84.2	215.2	95.2
1950	26.7	33.2	36.5	84	12.1	31.9	0	6.4	45.7	70	63.5	150.3
1951	82.5	83.8	69	39.1	78.5	21	2.2	10.3	40.6	182.1	88.2	54.5
1952	53.4	54.2	25.1	27.9	23	1.7	8.2	7.4	91.2	63	31.4	117.3
1953	67.7	62.4	29.9	38.2	57.3	89.2	0	5.2	10.9	140.3	22.5	67.1
1954	77.8	74.6	54.1	33.4	26.5	60.6	13	26.8	39	4	40.2	42.6
1955	85.6	99.1	70.5	38.3	0	15.7	20.3	0	130.9	48.1	60.2	58.5
1956	62.8	65.9	40.4	65.9	21.1	0	0	13.2	29.7	55.7	79.7	72.6
1957	40.6	12	8.9	32.9	33.3	15.7	0	0	0	184	102.6	194.3
1958	48.6	10.2	76	71.7	18	4.3	0	0	2	72.7	91.2	94
1959	38.6	26.8	88.5	70.1	78.8	2.4	0	26.3	42.9	118	99.3	147.5
1960	76.5	43.1	84.7	41.8	7.8	1.3	0	0	49.5	86.7	116.3	144.9
1961	99.2	0	0	58.6	5.8	2.8	0	0	9	118.4	192.1	53.8
1962	12.5	66.8	52	20	14.2	10	0	0	67.8	79.8	313	57.2

Year	Jan	Feb	Mar	Apr	May	Jun	Jul	Aug	Sep	Oct	Nov	Dec
1963	65	137.8	33.7	27.1	21.8	13	14.2	30.8	42.9	56.6	64.1	125.9
1964	0	59	58.7	33	2.9	51.9	0	20.5	0	230.2	30.1	130
1965	75.8	58.8	75.2	10.4	20	4.1	0	1	74.6	67.1	119.6	25.8
1966	52.9	75.1	30.3	29	15.2	2	5.7	6.5	32.5	151.7	141.5	95
1967	62.5	12.4	30	32.2	31.9	4	0	19.6	28.6	53.1	112.1	112.2
1968	51.9	45.6	29.1	58.7	22.1	33.1	1.8	11.5	18.8	38.4	146.7	127.1
1969	59.6	73.6	88	41.1	28.6	20.6	4.4	4.7	53.5	64.1	117	155
1970	63.6	57.3	40.6	27.3	19	9.2	0.1	3.6	26.5	38.4	77.2	94.9
1971	82.2	36.1	87.5	48.3	35.7	2.9	1.9	6.7	26	28.9	161.8	58.9
1972	76.3	116.1	56.1	53.3	54.8	7	2	9.5	25.8	57.7	42.4	112.6
1973	80	70.6	63.1	52.7	4.2	9	3.6	14.6	52.7	38.2	17.3	65.7
1974	52.1	87.3	57.9	64.8	11.5	11.3	4.7	14.3	25.9	76.6	59.3	30.6
1975	18.3	39.4	104.5	46.2	43.6	21.7	0	58.1	18.1	68.8	166.7	46.9
1976	25.5	73.1	87.6	41.5	20.5	28.5	11.9	24	31.3	144.9	113.2	64.7
1977	74.7	31.5	32.7	32.3	25.5	72.7	5.7	38.7	31.4	54.9	86.1	140.6
1978	149.4	110	36.2	102.9	39.3	6.2	3.8	4.1	31.5	77.1	64.5	71.3
1979	130	63.3	61.8	57.6	0	14	0	10	75.4	137.9	70.2	101.7
1980	60.3	16.2	34	35.9	118.8	11.3	0	12.2	0	175.1	112.2	47.4
1981	35.6	71	41.4	61.6	31.8	2	9.6	0	36.8	164.2	5.8	104
1982	51.4	39.8	44.4	45	23.4	4.2	0	0.8	18.4	151.4	89.6	126
1983	5	94.8	73.6	12.6	10.4	7.2	2.8	28.6	23.8	42.6	71.6	85.8
1984	42.4	92.2	127.2	49	167	25.2	0	37.6	58.6	85.6	114.4	100
1985	116.6	26.6	107.8	12.8	54.6	9.6	0	1.6	24	59.2	144.4	16
1986	125.2	148	51	96	5.4	15.6	44	0	28.4	68.2	76.8	59.4
1987	70.6	60	43.2	15.6	30.2	11	0.6	0	16.4	75.8	202.2	94.4
1988	63.6	42.4	51.4	79.2	38.8	20	0.6	4.8	73.4	58.2	27	45.2
1989	21	80	27.4	94	31.4	25.6	2.2	0.6	73	13	115.2	77.4
1990	41.4	32.2	39.2	73.6	14.2	25.2	0	0.8	12	175.2	113	115.6
1991	13.2	34.8	62.4	129.6	89.4	2.8	1.8	1.4	93.8	178.4	145.8	1.6
1992	73.4	32.2	29.6	34.6	12.4	55.6	6.6	14	18.4	247.2	27	81.2

Porto Torres rainfall [mm]

Year	Jan	Feb	Mar	Apr	May	Jun	Jul	Aug	Sep	Oct	Nov	Dec
1922	70	26.5	72	39	26.2	12.8	0	5	115.5	30	24	85
1923	79	72	33.5	37	21	6	0	0	15	19	221	178
1924	40.5	131	53	41	12	35.2	0	13	33	68.7	71.5	94.7
1925	9	62	62	53	49.7	0.5	29.5	16	33.5	44.5	70.7	45.4
1926	28.4	10	42.2	51.5	47.8	4.2	13.5	0.1	8.7	51.7	140	91.3
1927	119	41.5	21.5	12	26.5	8.4	0.5	0	4.3	118	90	228
1928	36.2	15	76.1	35.1	54	0	0.8	0.5	82.2	53.4	95.6	97.7
1929	59.3	14.5	6.5	13.8	11.1	0	0	0	6	109	190	40
1930	62	98	72	70	27	0.5	0	1	41	41	18	85
1931	28	54	48	12	46	1	0	3	28.7	30.2	117	69
1932	14	59	44.8	51.2	15.3	33.4	27.2	32.5	50.2	112.4	91.5	82.5
1933	76.8	68.4	18.2	37.4	2.3	9	0	0	58.8	46.3	157	139.3
1934	30.9	58.6	80.4	50	7.3	0	0	34	7	14	137	127.5
1935	52.8	37.5	74	20	57.5	0	0	92	29	242.5	88	69
1936	54	71.5	51.5	59	76	9	4	0	38	118	40.5	54
1937	34.5	42.5	140	15.5	15	1.5	0.5	21	48.5	86.2	15.4	154.7
1938	7	29	7	15.3	37.1	0	8	11	51.3	81.8	87.9	132.7
1939	43.9	20.4	43.8	24.5	24.1	3	0	15.2	49.7	20.8	1.5	34.1
1940	54.1	4.2	8.3	19.5	38	52	0	0	25	73	82	78
1941	100.5	88	19	35.6	14	1	0	1	15.8	27.8	38	20.2
1942	86.8	100.1	25.7	36.9	10.8	24	0.8	0	53.3	27.9	52.4	64.1
1943	63.5	28.2	61.9	7.1	34.4	3.8	5.2	2.2	73.8	98.3	77.3	60
1944	12.2	65.9	51.6	36.6	20.7	2.9	1	0	21.4	109.6	57.1	61
1945	71.7	0	20.4	0	0	0	0	1.2	20.4	34.6	41.6	80.3
1946	35.5	0.3	53.9	53.3	50.5	35.3	1.2	13	0	130	138	56
1947	24.5	60	15	35	18.3	0	0	35	45	126	68	54.5
1948	64	35	0	38	5	13	0	0	86	123	9	29
1949	57	61	46	16	112	62	0	0	3	78	160	74
1950	12	27	43	79	7	8	0	0	47	75	46	135
1951	91	99	86	33	70	2	6	8	44	96	31	16
1952	38	36	5	17	29	0	18	17	88	86	18	90
1953	45	115	19	26	32	123	0	15	12	104.6	3.6	6.3
1954	32.2	47.4	30.4	24	22	57	13	8	0	0	31	30
1955	83.6	64	53.8	11.9	0.2	10.2	0	0.2	45.4	29.1	49.2	55.4
1956	44.3	54.5	42.3	65.5	17.3	6	0	0	13.1	44.5	92.7	51.4
1957	45.3	10.6	14.7	49.1	32	49.2	0	0.2	0	59.6	62.1	114.2
1958	38.6	10.9	63.1	61.4	14.4	2.3	2.3	0	8.4	91.7	121.4	67.1
1959	41.6	21.9	89.8	26.8	68.9	66.2	0	45	50.4	114.5	97.1	56.2
1960	107.3	33.9	77.6	44.3	9.4	0.4	0.6	1.2	19.7	89.5	79.8	172.6
1961	93.9	0.7	0	28.8	5.4	4.7	0	0	15.8	59	171.4	63.2
1962	11.6	64.8	83.3	21.1	26.8	7.9	0.9	0.5	71	51.6	293.4	48.1

Year	Jan	Feb	Mar	Apr	May	Jun	Jul	Aug	Sep	Oct	Nov	Dec
1963	60.8	105.6	26.7	42.9	11.4	20.3	1.1	13.9	48.6	23.1	79.7	89.2
1964	0.5	35.8	58.7	26.3	0.8	8.6	0	9	0	230.6	36.2	127
1965	48.1	50.7	78.7	0	3.7	2.3	3	6.3	86.8	42.3	71	14.4
1966	41.5	57	25.1	17.7	32.8	2	6.6	10.4	13.2	171.1	105.9	82.6
1967	50.7	22.7	35.8	13.1	14.5	9.3	0	0	53.3	21.4	84.7	91.5
1968	39.2	44.6	29.1	30.9	12.8	4.8	12.5	5.3	13.5	7.6	129.2	82
1969	40.8	94.5	63	32.7	36.3	7.2	0	14.2	156.3	23	71.2	129
1970	88.9	36.7	48.6	5.7	13.3	5.5	0	6.9	0	4.3	30.9	91.6
1971	75.7	36.9	56.4	13.2	46.4	2	2.3	5.5	7.6	10.5	123	38.8
1972	84.1	131.3	83	49.9	53.9	14.3	0.4	0	51.3	61.6	5.4	50.1
1973	72.3	53	47	29.8	12	15.7	0	13.9	112.5	26.8	21.3	64.4
1974	45.9	81.1	46.7	98.1	21.2	1	5	0.5	57.7	43.7	43.5	10.6
1975	23.7	49.7	101.1	28.4	25.5	12	0	63.8	11.1	48	128.5	28.5
1976	23.4	79.4	77.8	44.4	35.8	60.9	34.6	32.7	68.9	156.8	137.1	61.8
1977	81.6	18.1	38.5	38.6	26.2	11.7	23.6	50.9	31.7	56.3	105	102.4
1978	113.3	50.7	24.4	81.3	41.5	10.8	8.5	2.1	46.9	115	42.5	79.2
1979	64.8	57.3	41.2	46.2	0	0.8	0	4.5	50.1	82.7	37.4	54.1
1980	59.8	8.4	44.6	23.6	122.8	12.3	0	41.6	0.5	125	160.7	44.5
1981	14.4	39.4	50.6	42	28.6	3.4	26.4	0	27.4	151.8	7.2	75
1982	43.8	40.4	22.4	39.4	22.6	3.6	0	0.6	16.8	188	77	85.8
1983	2	72.8	43.4	14.6	4.8	5.6	0	47	21.8	14.8	114	91
1984	17.6	85	86.2	30.6	112.6	25.2	0	18.2	93.2	70.4	92.8	54.2
1985	72.4	14	119.8	7	63.6	3.2	0	0	13.4	44.8	101.2	17.2
1986	77.6	113.2	43	49.6	10	8.8	1.4	0	16.2	49.2	28.8	27.8
1987	52.6	39.8	29	21.8	26	6.6	0.8	0	10.2	69.4	186.6	95.8
1988	46.8	26.6	41.4	44	32	5.4	0.8	2.2	9.2	74.2	26.6	32.2
1989	13	69.8	19.4	77	4.6	0.2	8	0.4	65.2	16.2	83.2	64
1990	39	6	33.6	64	8.4	23	0	5	13.8	149.4	118.6	69.4
1991	12.2	27.4	48	84.8	73.4	1.8	3	0	69.4	144.6	105.2	5
1992	30.3	16	31.7	30	24.4	29.2	2.6	3.8	4.2	161.5	24.4	59.6

Sassari rainfall [mm]

Year	Jan	Feb	Mar	Apr	May	Jun	Jul	Aug	Sep	Oct	Nov	Dec
1922	122	45	57.5	49	12	3	0	3.5	122	102	34.2	135
1923	69.5	77.5	22	100.5	31.2	11	0	0	95	53.5	272.7	171.2
1924	68.5	226	70.5	42	7	0.7	7.2	3	30	105	57	179
1925	14	62.5	82.5	84	63.3	4.5	20	13	43.7	95.5	104	37.5
1926	80	11.4	71.5	122.5	66.3	1.5	11	0	20.5	74.5	190	158.7
1927	183.7	19.4	14.7	12.5	51	8	0	0	10.5	262	67.5	23.1
1928	118.5	2.5	127.7	84.5	75.5	0	10.2	0	48.5	90.2	191.5	96.2
1929	61.8	26	4.2	21.5	39.7	0	0	9.2	21	155.2	210.5	65
1930	68	179.3	86	88	33	18.5	0	0	33.5	51.2	27.5	99.2
1931	32.7	110.4	45.5	15.2	67	0	0	0.2	63	60.4	119.7	73.5
1932	7.2	89	56.5	60.5	32	14.9	9.4	29	71.7	166.9	71	134
1933	110.5	120	13.5	24	1.9	20.5	0	5.4	72.5	49	168.5	227.5
1934	53.5	98.5	72.5	90.5	10	0	0.5	22.5	41.7	26	192	146.5
1935	105.5	27.5	162.5	11.5	77	0	0	3	30	145.4	126.5	108.3
1936	74.4	79.6	96.8	115.3	107.5	14.6	1.5	13	26	62.1	39.5	43.4
1937	47.7	52.2	147.6	33.1	13.3	12	0	23.2	47.9	37.3	75.8	173.7
1938	39.3	39.8	15.2	24.4	101	4.2	1.9	24.4	90.9	91.9	82.8	250.3
1939	64	44.3	67.3	29.7	20.3	8.7	0	25.3	155.3	43.1	44.1	156.7
1940	147.8	22.1	8.3	31	73.7	43.3	0	0	14.8	205.6	109.2	90.4
1941	261.1	158.3	61.6	73.4	38.2	13.4	0	0.6	20.5	22.7	74.1	61.2
1942	143.4	198.6	20	52.4	7.4	35.4	0	0.2	94.1	55.5	60.9	101.1
1943	60.3	40	111.4	4.9	19.1	0	23	0	64	149.8	105.1	96.3
1944	8	62.5	53.4	72	13	0.5	0	0	44.9	116.3	39.2	44.6
1945	174.8	11	21.9	1	4.9	0	0	0.5	45	77.1	37.4	96.3
1946	27.3	0	77	66.5	45.2	3.4	0.1	10.5	0	172.4	308.4	128.5
1947	40.4	117.4	30.3	19.1	21.4	0	0	105.1	132.2	123.7	70.1	71.4
1948	130.4	74.8	0	63.5	87	8	3.4	0	53.2	82.6	12.6	47.6
1949	55.2	49.7	56.7	9.7	60.4	14.2	15.2	0	15	68.1	331.6	83.3
1950	33.3	38	75.9	140.2	1.6	11	0	0	51.2	65.4	49.2	173.2
1951	81.8	71.4	60.5	9.8	55.2	2.5	1.3	0	30.5	145.1	46.2	39.1
1952	78.9	56.6	17.3	32.8	22.6	0	14.1	22.6	131.2	61.2	41.4	139
1953	126.3	77.7	13.5	41.5	81.6	112	0	49	33.4	179.3	23.2	74.1
1954	85.4	109.7	52.3	53.1	30.5	61.2	19.4	32.8	2.6	19	96.4	60.1
1955	83.8	102.8	59.4	33.2	1.8	42.2	0.2	2.4	108	48	87.2	79.6
1956	77.8	84.2	62	55.6	16.8	5.4	0	0.8	23.8	73	146.6	99.8
1957	39.6	20	9	52.4	62.8	20.4	0	0	0	76.8	101.8	195.4
1958	55.6	23.6	89.6	81.2	23.4	5	3.2	0	1.6	76.8	93.6	113.6
1959	42.6	21.8	105.8	88	75.4	5.8	0	47.8	62	138.2	132.4	126.2
1960	111.2	42.8	84	46.8	6.4	4.6	0	0.2	54.6	130.6	106.2	231.8
1961	116.9	1	0.2	51.6	5.4	2.8	0	0	6.2	127.6	241.4	61.4
1962	16	76.6	58.8	28.4	17	7.4	0	0	123.9	43.6	382.4	80.6

Year	Jan	Feb	Mar	Apr	May	Jun	Jul	Aug	Sep	Oct	Nov	Dec
1963	77.2	177.4	30.8	60.4	20.8	16.8	17.4	12.2	70.4	52.2	62.4	126.4
1964	0.2	56.2	72	43.4	3.6	27.2	0	5	0	175.4	37.4	155.4
1965	100.4	91.2	109.6	17.6	11.6	3.4	0.4	0	63.9	52.8	115.8	21.2
1966	70	63.6	34.4	40.2	22.6	6.6	4.2	6.6	26.6	186.6	215.2	94.4
1967	70.2	19.8	45.4	51	21.4	4.4	0	0	33	72.2	109.8	113
1968	57.4	54.6	45.8	47.6	15.8	9.8	7.6	7	27.8	16	132.8	101.8
1969	40.4	78.8	91.6	22.8	44.2	20	1.8	1.2	80.9	36.2	94	104.2
1970	77.3	62.3	57.6	26.5	24.9	10.6	1.2	6.4	0	0.4	64.4	75.4
1971	93.6	29.9	61	23.7	55	0.6	0	0	17.4	39.5	150.4	50.8
1972	99.8	145	40.7	62	73.5	15.4	14.6	0.1	35.8	64.7	12.7	0
1973	73.4	62.1	45.4	25.6	7.2	11.2	1.2	10	92.6	28	12.9	39.5
1974	58.3	104.3	72.2	77.8	16.4	4.4	43.2	0	19	45.8	42.8	13.4
1975	27.2	71.4	100	64	47.2	28.6	0	51	4	55	148.2	60
1976	34.8	72.6	104	34	36.6	40.4	16.6	23.8	35.1	149.6	134.6	75.3
1977	81.3	37.8	30.5	13	44.7	26.4	4.3	33.2	37.4	70.5	67.8	106.6
1978	180.2	87.3	44	98.1	25.5	6.6	2	22.6	30.4	131.6	75.9	102.8
1979	90.3	73.9	41.5	115	0	6	0	11.9	23.4	101	44.9	63.6
1980	57.4	10.6	32.1	43	116	9.3	2.3	13.3	7	173.6	154.4	59.7
1981	43.8	45.8	26.1	75.6	33.4	9.4	9.9	0	40.8	131.6	0	94.3
1982	38.3	35.2	36.1	17.5	29.1	14.8	0.8	4.4	33.8	175	79.4	90.1
1983	29	83.2	60	20.2	10.4	20.6	1.1	28.5	37.2	68.7	71.2	87.2
1984	35	88	93.4	44	158.2	20.6	0	28	51.4	75.8	82.4	63.4
1985	100.2	23.2	97.4	30	50.6	0.2	0	0.2	14.4	55	108.6	12.6
1986	106.6	115.8	37	80.8	4	2.4	41.8	0	6.4	28.2	64.4	73
1987	85	62.8	30.4	15	18	10.6	0	0	3.2	69.8	200	89.2
1988	58.6	23.4	51.4	40.4	40	6.6	0	0.8	48.4	60.4	21.8	43
1989	27.4	68	15.2	94	27.8	1	1.4	0	43	14	106.4	53.2
1990	47.4	34.4	45.6	91.2	31	33	1.8	0.4	7	166	124.4	103.4
1991	9.4	22.8	57.4	122.2	75.4	4.4	0	0	96	196	132	3.8
1992	72	25	18.2	29	34	31	32.6	4	5	258.6	26	45

Stintino rainfall [mm]

Year	Jan	Feb	Mar	Apr	May	Jun	Jul	Aug	Sep	Oct	Nov	Dec
1922	58.6	31.9	35.6	47	15.9	8.7	1.3	2.2	59.1	53.2	28.1	87.5
1923	76.9	95.9	43.8	46	14.9	20.1	0.8	0	91.6	43.5	150.2	132.7
1924	53.4	128.3	37.4	26.9	11.6	2.2	1.4	0.3	14.7	89.2	24	84.2
1925	13.5	65.8	44.5	38.2	38.6	19.7	0	12.2	34.5	63.9	82.8	77.8
1926	58.4	9.7	31.5	45.4	16.4	9.9	14.5	5.1	24.7	40.1	85.7	94.8
1927	103.1	34.3	21	8.6	16.4	12.2	4.8	0.7	19.2	63.8	49.9	103.8
1928	59	13.4	62.4	33.7	55.4	0	8	0	72.1	62.2	112.5	92.7
1929	79.7	43.8	34.3	22.3	7.6	6.9	0.8	8.7	39.6	67.5	98.7	42.6
1930	56.3	74	53.9	61.3	26.7	0	0	0	71.6	51.3	16.9	121.5
1931	39.2	53.3	59.4	22.5	26.8	0	1.2	0	24.3	79	110.2	58.4
1932	28.7	73.6	47.7	32.6	4.7	12.5	6.9	21.7	43.9	60.7	39	82.5
1933	57.2	57.2	35.1	35.2	0	8.5	0.7	0	40.8	70.8	141	101.7
1934	57	70.5	99.6	68.5	24	5	0	50	40	35	220.4	131.5
1935	78.9	52.3	95	14.9	65.7	0	0	16.4	3	163	93.8	76
1936	61.4	54.3	68.5	64.9	59.3	21.4	0	0	32.8	74.1	47.6	65.9
1937	27.4	26.4	88.5	26.5	6.6	3	0	27.5	44.4	65	22.5	155.7
1938	33.5	23.5	1.2	19	51.7	1.9	5	4	98.4	69.1	119	158.7
1939	51.8	18.8	78.5	24.9	13.3	21	0	25.2	105.5	21.7	19.4	131.1
1940	78.8	26.6	0	28.6	50.1	22.6	1.6	0	2.7	77.5	95.8	49.3
1941	84	129.9	39.8	43.9	24	2	0	0	6	37.7	65.6	44
1942	175.1	104	32.2	59.7	6.5	10	0	0	52.8	24.4	79.6	83.4
1943	38.8	13.5	63.9	2.4	7	0	2.9	0	38.5	176.8	72.5	79
1944	0.7	82.6	43.9	41.3	0	4.7	0	9.8	72.2	109.9	28	57.2
1945	85.5	1.5	13	2	1.5	0	0	0	42.7	64.2	58.1	131.5
1946	57.8	7.5	68	58.8	33	0	0	14.5	0	189.8	179.3	83.7
1947	23	97.4	28.3	16.6	17.3	0	4	6.5	23.3	114.5	49.6	70.4
1948	58.7	54.7	0	65	14.8	2.1	5	1.1	62	68.5	6	39.9
1949	45.5	31	45.8	18	91.8	23.8	0.2	0	10.6	71.3	174.1	91.4
1950	23	24.5	56.2	108.4	12	9.2	0	0.3	96.1	84.6	40.9	200.5
1951	134.3	99.1	85.2	25.2	53.2	3.9	4.3	2.1	37.8	126.9	46.7	38.3
1952	49.8	29.4	23.2	34.5	19.6	0	0.7	22	197.2	54.3	50.5	101.5
1953	61.7	114.2	55.7	47.9	53.2	158.8	0	14.4	29.4	104.7	27.6	49.7
1954	102.1	82.7	50.3	22.7	35.6	26.2	36.2	24.5	6.1	8	55	30.2
1955	91.9	69.9	50.8	19.7	1.1	29.4	0.2	1.1	21.2	12.8	108.3	58.2
1956	41.6	82.5	59	98.8	17.5	3	0.1	0	18.2	25.5	133.6	42.5
1957	50.6	11.6	9.2	44.2	28.3	28.7	0	0.1	4.6	117.6	87.1	156.5
1958	59.1	11.2	82.2	53.7	16	1	4.8	0.3	0.2	78.2	141.4	51.3
1959	35	21.5	87.2	27	38.5	1	0	39	21.6	166.6	90.8	88.7
1960	64.9	65	62.4	51.4	3.5	0.2	0	0	27.2	93.4	73.1	150.2
1961	105.2	0	0	0.3	1	0	0	0	5.6	89.8	266.7	52.6
1962	13.3	64.7	40.1	15.9	23.9	17.5	0	0.5	58.2	46.4	229.7	60.9

Year	Jan	Feb	Mar	Apr	May	Jun	Jul	Aug	Sep	Oct	Nov	Dec
1963	68	117.9	13.8	37	26.2	32.5	0	8.4	86.3	16.2	94.5	103.2
1964	1.3	33.7	57.9	19.1	0	17.4	0	0	0	192.6	27	124.2
1965	52.7	48.5	59.3	1.2	0	0	0	0	106.4	40.7	83.3	3.3
1966	53.6	41.6	38.2	26.3	15.3	0	7	14.5	24.6	139.2	124.3	36
1967	88.4	10.4	15.7	8.1	16	3.2	0	0	29	33.4	84.6	147.1
1968	27.2	21.9	42.4	32	6.7	0	0	5	5.4	5	79.5	76.1
1969	23.1	79.7	60	27	0	5	0	0	105	18.2	21.5	92.5
1970	45.8	14.5	53.3	4.2	1.4	0	0	12	0	27.7	18	108
1971	57.3	12.6	60.6	5.8	49.5	0	0	0	5	29	109.6	45.4
1972	108.2	117.6	32.5	53.3	25	28.5	0	0	86.5	27.5	9	30
1973	47.8	28	45.3	37.5	11.3	0	0	7	108.3	21.8	13.7	61.9
1974	41.9	88.2	43.2	113	2.6	0	5.4	0	21.9	29.5	24.7	11.3
1975	18	82	82.9	35.6	18.2	8.2	0	44.6	11.6	75.6	93.4	50.2
1976	22.8	95.1	57.7	46	26	37	59	34	39	115.8	157	62
1977	88.9	19.5	51	30	29	7.5	51	68.5	32	62	94	101.5
1978	81.6	58	36.6	67.5	28.4	10	4.6	0	42	135.8	17	101.5
1979	51.8	66.6	33.2	49.5	0	6	0	4	65.6	116.2	71.8	54.2
1980	83.6	6.8	29.2	21.2	112	11.6	0.2	12.8	1.4	85.2	97	37.8
1981	20.2	26.8	47	41.6	45.4	3.2	23	0	24.4	85.8	6.4	50.4
1982	27.8	24.6	27.6	23.4	21.8	10.4	0	3.6	6.4	88.2	82.4	122
1983	1	74.4	38	19.4	22.6	7.6	7	28	22.4	36	100.4	62.8
1984	17.6	87.2	89.6	30.8	95.6	27.4	0	28.8	55.6	102.2	98.2	88.2
1985	57.4	6.4	83	0.6	33	0	0	0.6	12.2	25	119.2	13
1986	126	106	31	62	16	7	62	0	12	39	27	36
1987	49.6	25.4	27	20.4	5.6	3.6	1.6	0	17.2	77.6	162	137
1988	44	19	15	12	2	0	0	0	6	62	41	0
1989	15	37	37	81	0	0	0	0	82	29	100	35
1990	56	15	18	52	0	0	0	0	14	134	127	131.2
1991	0	52	54	62	85	0	0	0	71	72	78	0
1992	62	0	35	20	19.4	34.6	1.5	1	35.2	100.6	60	20

APPENDIX C

Piezometric data

Piezometric map of September-December 2004 (Ghiglieri et al., 2006).

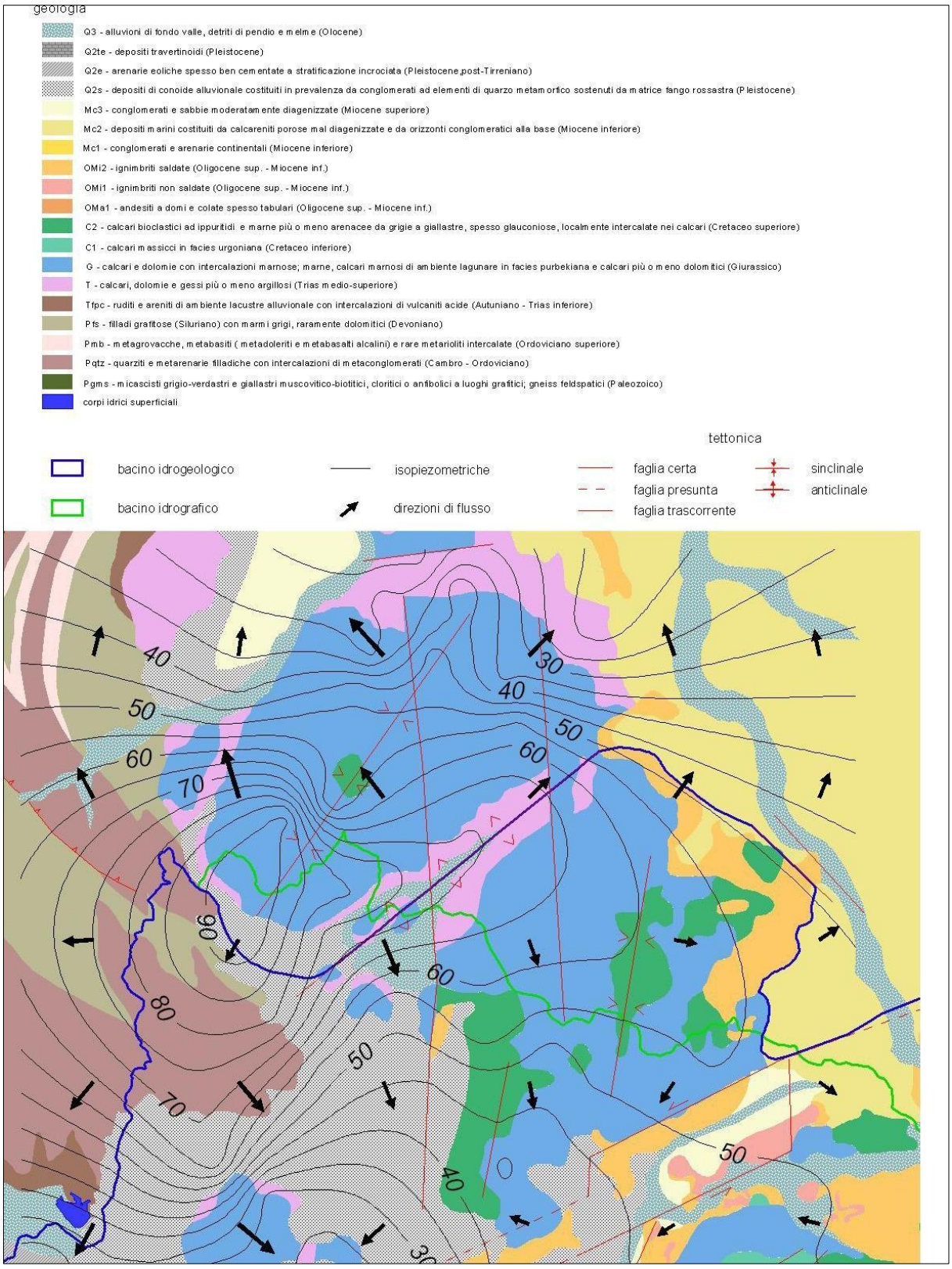

Piezometric head measurements at Fiumesanto power station

Well name	N coordinate	E coordinate	Ground elevation [m]	Piezometric head [m a.m.s.l.]	
				Jan 2007	Feb 2008
BH11PZ	4522426	1441162	7.71	0.20	0.06
BH12PZ	4522333	1441123	7.13	1.06	0.93
BH18PZ	4522378	1441237	7.34	0.39	0.34
BH36PZ	4522259	1441447	7.15	0.19	-0.15
BH36PZbis	4522164	1441340	7.40	1.65	1.55
BH40PZ	4522111	1441087	25.12	1.02	0.92
BH49PZ	4522144	1441690	4.08	0.24	0.15
BH52PZ	4522088	1441796	3.36	-	0.59
BH72PZ	4521978	1441840	3.47	0.11	0.27
BH81PZ	4521982	1441240	21.99	2.79	2.78
BH92PZ	4521868	1441897	7.09	0.24	0.29
BH95PZ	4521874	1441674	6.86	1.38	2.20
BH100PZ	4521821	1441396	6.91	4.41	4.41
BH138PZ	4521477	1441588	6.89	3.04	3.01
BH139PZ	4521429	1441302	19.39	11.10	10.44
BH143PZ	4521331	1441810	16.47	2.85	2.66
BH145PZ	4522050	1440312	34.03	2.03	1.68
BH148PZ	4522360	1440840	11.81	2.51	2.39
BH160PZ	4522494	1440365	29.77	14.76	14.44
BH161PZ	4522476	1440534	21.98	0.50	-
BH164PZ	4522479	1440679	17.78	8.53	8.20
BH169PZ	4522488	1441028	6.76	0.11	0.25
BH169PZbis	4522486	1441029	6.70	0.13	-0.04
BH177PZ	4522572	1440639	17.61	8.29	8.28
BH183PZ	4522583	1440974	2.36	0.07	0.06
BH186PZ	4522636	1440888	7.14	0.16	0.23
BH195PZ	4522677	1440657	14.76	4.33	3.92
BH212PZ	4522829	1440549	6.97	0.81	0.56
BH222PZ	4523082	1440325	6.68	0.42	0.27
BH225PZ	4523114	1440281	7.48	0.29	0.38
BH227PZ	4523102	1440122	8.63	0.52	0.48
BH234PZ	4521433	1440080	39.79	18.70	18.60
BH250PZ	4522353	1441011	7.68	1.60	1.44
BH252PZ	4522077	1441297	25.11	1.61	1.61
BH253PZ	4521834	1441304	13.33	4.75	5.03
BH254PZ	4521334	1441738	16.12	2.92	2.75
BH255PZ	4521450	1441924	7.62	2.10	2.04
BH256PZ	4521516	1441930	6.58	1.47	0.65

BH257PZ	4521476	1441167	25.43	7.55	7.53
BH258PZ	4521621	1441209	25.95	7.59	7.60
BH259PZ	4522145	1440715	31.81	9.65	9.32
BH260PZ	4522147	1440520	34.23	6.39	12.21
BH261PZ	4522254	1440292	32.58	13.08	-
BH262PZ	4522849	1440234	29.56	3.73	2.87
BH263PZ	4522734	1440244	28.97	8.09	7.32
BH264PZ	4522151	1440336	33.59	13.16	11.73
BH265PZ	4522656	1440387	29.52	13.66	13.27
BH266PZ	4522241	1440661	31.26	9.10	3.26
BH267PZ	4522105	1440919	28.01	2.51	2.86
BH268PZ	4521642	1441305	23.70	7.19	7.28
MW1	4522130	1441498	7.76	3.61	3.39
MW2	4522150	1441508	7.63	2.90	2.78
MW3	4522126	1441533	7.65	3.37	-
MW4	4522111	1441548	7.00	2.74	-0.90
MW5	4522099	1441561	7.15	2.96	2.95
MW6	4522083	1441581	6.78	2.63	2.53
MW7	4522016	1441575	6.80	2.85	2.78
MW8	4521972	1441537	7.00	3.31	3.20